UNIVERSITÀ DEGLI STUDI DI TRIESTE

XXXII CICLO DEL DOTTORATO DI RICERCA IN NANOTECNOLOGIE

Design of detection systems for the therapeutic drug monitoring of anticancer drugs

Settore scientifico-disciplinare: BIO/14

DOTTORANDO/A

Valentina Iacuzzi

COORDINATORE

Prof. Lucia Pasquato

SUPERVISORE DI TESI

Dott. Giuseppe Toffoli

CO-SUPERVISORI DI TESI

Prof. Federico Berti

Dott.ssa Elena Marangon

ANNO ACCADEMICO 2018/2019

Questo lavoro di tesi è stato svolto presso la Scuola di Dottorato in Nanotecnologie dell'Università degli Studi di Trieste, diretta dalla Prof.ssa Lucia Pasquato, in collaborazione con la Struttura Operativa Complessa di Farmacologia Sperimentale e Clinica del Centro di Riferimento Oncologico di Aviano, diretta dal Dott. Giuseppe Toffoli, il laboratorio del Prof. Federico Berti del Dipartimento di Scienze Chimiche Farmaceutiche dell'Università di Trieste e il Dipartimento di Chimica della Queen Mary University of London, diretto dalla Prof.ssa Marina Resmini.

SUMMARY

List of abbreviations

APCI: atmospheric-pressure chemical ionization

ATP: adenosine triphosphate

BRCA: breast related cancer antigens

C_{DBS}: concentration obtained from DBS measurement

C_{min}: through level

CDCL3: deuterated chloroform

CDKIs: cyclin-dependent kinase inhibitors

CE: collision energy

CI: chemical ionization

CID: collision-induced dissociation

CML: chronic myeloid leukaemia

CYP: cytochrome

CUR: curtain gas

CXP: collision exit potential

DBS: dried blood spot

DC: direct-current

DLS: dynamic light scattering

DMSO: dimethyl sulfoxide

DP: declustering potential

EBF: European Bioanalytical Forum

EI: electron ionization

EMA: European Medicines Agency

EP: entrance potential

ER: estrogen-receptor

ESI: electrospray ionization

ESMO: European Society of Medical Oncology

F_C: correlation factor

FDA: Food and Drug Administration

FM: functional monomer

GC: gas-chromatography

GI: gastro-intestinal

GIST: gastro-intestinal stromal tumours

Hct: haematocrit

HDRP: high dilution radical polymerization

HER2: human epidermal growth factor receptor 2

HPLC: high performance liquid chromatography

HR: hormone-receptor

ICCs: interstitial cells of Cajal

IF: imprinting factor

IMA: imatinib

IS: ion spray

ISR: incurred sample reanalysis

ISt: internal standard

LC: liquid chromatography

LETRO: letrozole

LLOQ: lower limit of quantification

m/z: mass to charge ratio

MAA: methacrylic acid

MALDI: matrix-assisted laser desorption ionization

MIP: molecularly imprinted polymer

MP: mobile phase

MRI: magnetic resonance imaging

MRM: multiple reaction monitoring

MS: mass-spectrometry

NCCN: national comprehensive cancer network

NIP: non-imprinted polymer

NMR: nuclear magnetic resonance

NP: normal phase

OS: overall survival

PALBO: palbociclib

PARA: paracetamol

PDGFRα: alpha platelet-derived growth factor

PFS: progression-free survival

PR: progesterone-receptor

PKs: pharmacokinetics

QC: quality control

Rb: retinoblastoma

RF: radiofrequency

RIBO: ribociclib

RP: reverse phase

RT: room temperature

SMR: selected reaction monitoring

SNR: signal to noise ratio

SP: stationary phase

STS: soft-tissue sarcomas

SUNI: sunitinib

TDM: therapeutic drug monitoring

TEM: turbo gas temperature

TFA: trifluoroacetic acid

TNBC: triple negative breast cancer

TTP: time to progression

TKIs: tyrosine kinase inhibitors

TOF: time-of-flight

ULOQ: upper limit of quantification

VEGFR: vascular endothelial growth factor receptors

WHO: World Health Organization

WT: wild-type

XIC: selected ion current

ABSTRACT

With roughly 9.5 million deaths annually, cancer is one of the leading causes of death worldwide. Many advances have recently been made in anticancer therapy, even transforming some previously deadly malignancies into chronically manageable conditions. However, the majority of these drugs is characterized by inter-individual variability in treatment outcome thus indicating the need of a personalized approach for anticancer therapy. On these bases, during this PhD project different techniques for therapeutic drug monitoring (TDM) of anticancer drugs were developed exploiting various strategies.

First, the work done was focused on imatinib (IMA), an oral potent tyrosine-kinase inhibitor indicated as first-line treatment for patients with inoperable, metastatic or recurrent gastrointestinal stromal tumours (GISTs). A relationship between IMA plasma-exposure and treatment efficacy has been already proposed (C_{min} >1100 ng/mL). In this context, a LC-MS/MS method for the simultaneous quantification of IMA and its active metabolite, norimatinib (norIMA), in GIST patients has been developed, validated and cross-validated. This method allowed to perform the quantification directly on a drop of blood, exploiting the dried blood spot (DBS) technique, reducing sampling time, costs and improving patients' compliance. Analytes were extracted from DBS samples by simply adding to 3 mm-discs 150 µL of acidified MeOH containing the internal standard, IMA-D8. The collected extract was then injected on a LC Nexera system in-house configured with a 2D chromatography for the on-line clean-up, coupled with an API-4000 QT. The developed method showed a good linearity (R^2>0,996) between 50-7500 ng/mL for IMA and 10-1500 ng/mL for norIMA. The method precision was confirmed by the intra- and inter-day CV ≤3.1% and ≤5.6% for IMA and ≤4.3% and ≤6.6% for norIMA. The intra- and inter-day accuracy was, respectively, between 88.9-106.2% and 98.9-104.3% for IMA and 92.9-112.8% and 95.7-101.0% for norIMA. Moreover, other variables that could specifically affect the DBS analysis were assessed and optimized like the analytes' extraction conditions from the filter paper, the influence of haematocrit (Hct), the sample homogeneity and the spot size. The correlation between finger-prick and venous collection (% diff in a range from -12 to 3.8%) and the DBSs stability up to 16 months (at RT in plastic envelopes containing a silica-gel drying bag) were also verified. After the validation, this method was applied to quantify 67 patients' finger-prick DBS samples.

Good agreement was obtained between IMA and norIMA concentrations found in DBS and plasma samples (quantified exploiting the reference LC-MS/MS method, internally validated), collected at the same time, applying the Hct normalization. Furthermore, the possibility to avoid the Hct normalization, simply multiplying the DBS concentration with a correction factor was demonstrated, not only for IMA but also for norIMA.

Despite the LC-MS/MS is considered the election technique for TDM analysis, it is quite expensive and it needs trained personnel. Thus, the development of a point of care device usable at the patients' bed side by non-specialized personnel could represent a turning point to operate TDM of anticancer drugs, such as IMA. For this reason, the synthesis of polymeric receptors (MIP) was performed, with the future goal of applying them as receptors in a system based on the IMA fluorometric detection. MIPs were synthesized, exploiting the non-covalent approach and the high dilution radical polymerization, and characterized using different techniques. Two methacrylic MIPs allowed to obtain nanoparticles (confirmed exploiting the DLS technique) in DMSO, using MBA (MIP4) and PBA (MIP7) as cross-linkers. The rebinding test showed that the polymers were able to bind IMA with good specificity compared to the corresponding non-template polymer (max IF_{MIP4}: 2.4 and IF_{MIP7}:1.7). Moreover, the polymers showed a good selectivity when compared to other drugs such as paracetamol and sunitinib.

Finally, in order to apply TDM approach to a new class of drugs used in breast cancer therapy, a LC-MS/MS method for the simultaneous quantification of ribociclib (RIBO), palbociclib (PALBO) and letrozole (LETRO) in human plasma was developed and validated (according to FDA and EMA guidelines). TDM recommendation for these drugs is currently only exploratory, based on limited exposure-response and -toxicity studies (PALBO and RIBO have been approved recently). RIBO and PALBO are small CDKIs indicated for the treatment of HR-positive, HER2-negative locally advanced or metastatic breast cancer in combination with an aromatase inhibitor, such as LETRO. The optimized method resulted to be suitable for the application in clinical practice due to the simple and fast sample preparation based on protein precipitation, the low amount of patient plasma necessary for the analysis (10 µL) and the total run time of 6.5 min. The linearity was assessed (R^2 within 0.9992-0.9983) over the concentration ranges of 0.3-250 ng/mL for PALBO, 10-10000 ng/mL for RIBO and 0.5-500 ng/mL for LETRO that properly cover the therapeutic

plasma concentrations. As related to intra-day precision and accuracy, the obtained values were, respectively, ≤ 3.6% and between 94.5-112.3% for all three analytes. At the same time, inter-day precision and accuracy were ≤ 7.3% and 94.5-112.9%, respectively.
The validated method was then applied for C_{min} quantification of PALBO, RIBO and LETRO in patients' plasma samples.
In conclusion, this PhD project led to develop, validate and cross-validate a LC-MS/MS method for the quantification of IMA and norIMA in DBSs samples, that has been successfully applied in samples of GIST patients. Moreover, new quantification strategies for IMA were investigated through the synthesis of MIPs which shown affinity, specificity and selectivity for IMA. Finally, a new LC-MS/MS method was developed for PALBO, RIBO and LETRO quantification in plasma samples, these drugs are used in breast cancer therapy. This method has been validated and applied in patient samples.
With the development of these strategies there is the hope to implement the application of TDM for anticancer drugs in the clinical practice.

Con circa 9,5 milioni di decessi ogni anno, il cancro è una delle principali cause di morte in tutto il mondo. Di recente sono stati fatti molti progressi nella terapia farmacologica antitumorale, trasformando alcune neoplasie precedentemente mortali in condizioni cronicamente gestibili. Tuttavia, la maggior parte di questi farmaci è caratterizzata da un'alta variabilità interindividuale nelle concentrazioni plasmatiche che si riflette poi sull'efficacia del trattamento. Questo indica, quindi, la necessità di un approccio personalizzato per la terapia antitumorale, per far sì che le concentrazioni plasmatiche di farmaco siano adeguate in ciascun paziente. Su queste basi, durante il progetto di dottorato qui presentato sono state sviluppate diverse tecniche per il monitoraggio terapeutico (TDM) di farmaci antitumorali sfruttando varie strategie.

In primo luogo, il lavoro svolto si è concentrato su imatinib (IMA), un potente inibitore delle tirosin-chinasi, con somministrazione orale, indicato nel trattamento adiuvante e di prima linea per pazienti con tumori stromali gastrointestinali (GIST). Nel caso di IMA, è stata descritta una relazione tra la concentrazione plasmatica e la risposta alla terapia (Cmin>1100 ng/mL). In questo contesto, è stato sviluppato, validato e cross-validato un metodo LC-MS/MS per la quantificazione di IMA e del suo metabolita attivo, norimatinib (norIMA), in pazienti affetti da GIST. Questo metodo è stato sviluppato sfruttando una tecnica di campionamento innovativa, quella del *dried blood spot* (DBS), che consente di eseguire la quantificazione direttamente su una goccia di sangue capillare, depositata su una cartina da filtro, riducendo sia i tempi di campionamento che i costi e migliorando la *compliance* dei pazienti. Gli analiti sono stati estratti dal DBS semplicemente aggiungendo 150 µL di metanolo (MeOH) acidificato contenente IMA deuterato come standard interno. L'estratto ottenuto è stato successivamente iniettato in un sistema LC Nexera internamente configurato con una cromatografia 2D (per la pulizia *on-line* del campione), accoppiato con uno spettrometro di massa API-4000QT. Il metodo sviluppato ha mostrato una buona linearità (R2> 0,996) nei range di 50-7500 ng/mL per IMA e 10-1500 ng/mL per norIMA. La precisione del metodo è stata confermata dai coefficienti di variazione (CV%) *intra-* e *inter-day*: ≤3,1% e ≤5,6% per IMA e ≤4,3% e ≤6,6% per norIMA, mentre l'accuratezza *intra-* e *inter-day* del metodo è risultata, rispettivamente, tra l'88,9-106,2% e il 98,9-104,3% per IMA e il 92,9-112,8% e il 95,7-101,0% per norIMA. Inoltre, sono state valutate e ottimizzate anche altre variabili che potrebbero influenzare specificamente

l'analisi dei DBSs, come le condizioni di estrazione degli analiti dalla carta da filtro, l'influenza dell'ematocrito (Hct), l'omogeneità del campione e l'influenza del volume depositato su carta. È stata altresì verificata sia la correlazione tra la quantità di farmaco derivante dal sangue capillare (dito) e dal sangue venoso (% di differenza tra -12 e 3,8%) sia la stabilità dei DBSs fino a 16 mesi a temperatura ambiente in foderi di plastica contenenti una bustina essicante. Dopo la validazione, questo metodo è stato applicato per quantificare 67 campioni DBSs di pazienti. È stata ottenuta una buona correlazione tra le concentrazioni trovate in DBS e quelle plasmatiche (quantificate sfruttando il metodo di riferimento LC-MS/MS, internamente validato) sia per IMA che per norIMA, applicando la normalizzazione per l'Hct. Inoltre, è stato anche identificato un fattore di correzione che consente, partendo dalle concentrazioni di IMA e norIMA trovate in DBS, di risalire alle loro concentrazioni plasmatiche, evitando la normalizzazione per Hct.

Nonostante l'LC-MS/MS sia considerata la tecnica di elezione per il TDM, risulta essere piuttosto costosa e necessita di personale qualificato. Pertanto, lo sviluppo di un dispositivo *point of care* utilizzabile al letto del paziente, da parte di personale non specializzato, potrebbe rappresentare un punto di svolta per l'applicazione del TDM per farmaci antitumorali, come IMA. Parte del lavoro di questo progetto di dottorato, quindi, è stata dedicata allo sviluppo di tali strategie alternative per la quantificazione di farmaci. In particolare, è stata eseguita la sintesi di recettori polimerici (*molecularly impronte polymers* - MIPs), con l'obiettivo futuro di applicarli come recettori in un sistema basato sul rilevamento fluorimetrico di IMA. I MIPs sono stati sintetizzati, sfruttando l'approccio non covalente e la polimerizzazione radicale ad alta diluizione, e caratterizzati utilizzando diverse tecniche. Due MIPs, sintetizzati in dimetilsofossido (DMSO), con acido metacrilico come monomero funzionale, hanno permesso di ottenere nanoparticelle (dati acquisiti tramite misure DLS), usando MBA (MIP4) e PBA (MIP7) come *cross-linkers*. Il test di *rebinding* ha dimostrato che i polimeri sono in grado di legare IMA con una buona specificità rispetto ai corrispondenti polimeri *non-imprinted* (IF_{MIP4}: 2.4 e IF_{MIP7}: 1.7). Inoltre, i MIPs hanno mostrato una buona selettività per IMA rispetto ai test eseguiti con altri farmaci, come il paracetamolo e il sunitinib.

Al fine di applicare l'approccio TDM a una nuova classe di farmaci utilizzati nella terapia del carcinoma mammario, è stato sviluppato e validato (secondo le linee guida FDA ed

EMA) un metodo LC-MS/MS per la quantificazione di ribociclib (RIBO), palbociclib (PALBO) e letrozolo (LETRO) in plasma umano. RIBO e PALBO sono farmaci appartenenti alla famiglia dei CDKIs indicati per il trattamento del carcinoma mammario localmente avanzato o metastatico HR-positivo, HER2-negativo in combinazione con un inibitore dell'aromatasi, come LETRO. La raccomandazione per il TDM di questi farmaci è attualmente solo esplorativa, sulla base di studi limitati riguardanti la correlazione tra esposizione-risposta/tossicità (PALBO e RIBO sono stati infatti approvati solo di recente). Il metodo presentato risulta adatto per essere applicato nella pratica clinica, grazie ad una semplice e rapida preparazione del campione basata sulla precipitazione proteica, la bassa quantità di plasma del paziente necessaria per l'analisi (10 µL) e il tempo limitato per l'esecuzione di una corsa cromatografica (6,5 min). È stata poi valutata la linearità (R^2 tra 0,992-0,983) nei range di concentrazione di 0,3-250 ng/mL per PALBO, 10-10000 ng/mL per RIBO e 0,5-500 ng/mL per LETRO, che coprono adeguatamente le concentrazioni plasmatiche terapeutiche. In relazione alla precisione e accuratezza *intra-day*, i valori ottenuti erano, rispettivamente, ≤ 3,6% e tra 94,5-112,3% per tutti e gli analiti. Allo stesso tempo, la precisione e l'accuratezza *inter-day* erano rispettivamente ≤ 7,3% e tra 94,5-112,9%. Una volta conclusa la validazione, è stata eseguita la quantificazione della C_{min} di PALBO, RIBO e LETRO in campioni plasmatici di pazienti affetti da carcinoma mammario. In conclusione, questo lavoro di dottorato ha permesso di sviluppare, validare e cross-validare, un metodo di quantificazione di IMA e norIMA in DBS che è stato applicato con successo per la quantificazione di campioni di pazienti affetti da GIST. Sono state inoltre indagate nuove strategie di quantificazione di questi analiti attraverso la sintesi di recettori polimerici che si sono dimostrati affini, specifici e selettivi nel riconoscimento di IMA. Infine, è stato sviluppato un nuovo metodo LC-MS/MS per la quantificazione plasmatica di PALBO, RIBO e LETRO farmaci utilizzati nella terapia del carcinoma mammario. Tale metodo è stato validato e applicato in campioni di pazienti. Con lo sviluppo di queste strategie si spera quindi di implementare l'utilizzo del TDM per i farmaci oncologici nella pratica clinica.

1. INTRODUCTION

1.1 Therapeutic drug monitoring

Therapeutic Drug Monitoring (TDM) is a branch of clinical chemistry and clinical pharmacology (Figure 1). The aim of TDM is to personalize the therapy optimizing the drug dose through the determination of drug concentration in biological fluids, such as plasma, serum, whole blood or urine [1] in defined intervals of time.

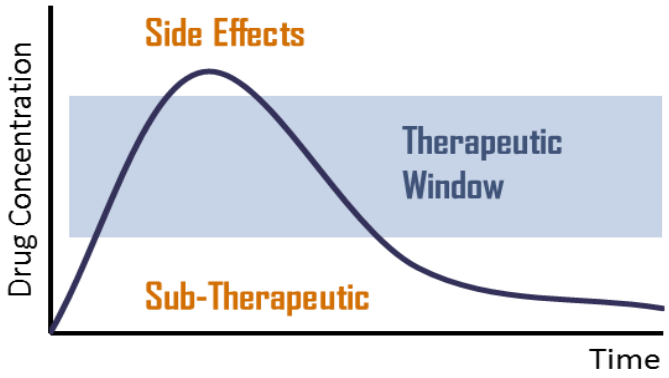

Figure 1. Schematic representation of a therapeutic window. If the drug concentration falls below the lower limit, the efficacy of the treatment might be compromised, while severe toxicity might occur if the drug concentration exceeds the upper limit.

Since the beginning of the 60s, TDM has been used in the clinical treatment of patients with the aim of simultaneously maximizing the efficacy of the therapy and minimizing the occurrence of side-effects [2]. Nowadays, this approach is widely applied in the pharmacological treatments of many pathologies, as to dose antiepileptics and cardiovascular drugs, antibiotics, anti-inflammatory agents, antidepressants, etc.

In theory, a drug should fulfil several criteria in order to be eligible for TDM:

- to show considerable inter- or intraindividual pharmacokinetic variability;
- the existence of a defined relationship between concentration and pharmacological effects;
- to have a narrow therapeutic window;
- the availability of a defined, accurate, robust and validated method for drug quantification in biological fluids [3].

In the case of metronomic therapy, that has been investigated as substitute for conventional regimens [4], an useful approach to maintain drug concentrations in the "activity range" is the monitoring of the C_{min}. The timing of the sample collection is

important as the drug concentration changes during the dose interval. In fact, the C_{min} is the least variable point in the dosing interval, namely the plasma concentration just before patient takes the next daily dose of drug [5]. Thus, samples should be taken at the steady state (4-5 half-life times after having started the therapy) [6]. Correct sample timing should also take into account absorption and distribution.

At the steady state, plasma concentration is usually at the equilibrium. For example, digoxin monitoring should be performed after six hours of a dose intake, since before this time, the drug is still undergoing distribution and plasma concentration would be erroneously high [7].

1.1.2 TDM in the context of anticancer therapy

A new era of cancer therapy has emerged over the last 10–30 years, with the treatment of several tumours moving from the use of cytotoxic drugs and nonspecific chemotherapy to chronic oral treatment with targeted molecular therapies [1].

The term “targeted therapy” refers to a new generation of anticancer drugs, with unique mechanism of action and high specificity [8], designed to interfere with a specific molecular target that has a critical role in tumour growth or progression [9]. These therapeutic agents have revolutionized cancer treatment by transforming some previously deadly malignancies into chronically manageable conditions [10].

Oral administration of these drugs is associated with a better quality of life but also have some disadvantages: generation of a complex step in the pharmacokinetics (PKs) like gastrointestinal (GI) absorption and first-pass metabolism by the liver [11], poor tolerability with consequence of therapeutic failure [12] and some cases of non-adherence to the therapy [13]. Such variability in drug response among patients is multifactorial, including pharmacogenetic background of the patient (like the activity of the cytochrome 3A4 (CYP3A4)), environmental and diet [14].

The interplay of these factors determines the plasma concentration profile over time for a drug and, therefore, its caused pharmacologic effect at the site of interaction with targets (such as receptors and enzymes) [15]. Rarely, standard dosage regimens result in similar circulating concentrations of the active drug in all patients, possibly favouring the selection of resistant cellular clones (in case of sub-therapeutic drug exposure) or the

development of undesirable toxicity (in case of overexposure) [4]. In this respect, the majority of targeted drugs are characterized by a wide spread of plasma concentrations observed following standard dosage regimens, with inter-individual variability at the end of the dosage interval up to 23-fold [8].

However, while for drugs like the aminoglycosides, phenytoin and digoxin TDM is largely applied, in the case of the anticancer drugs their quantification in plasma (or whole blood) is not a common practice to tailor the therapeutic intervention, despite the high risk of toxicity and therapeutic failure. One of the most famous exception is methotrexate, a chemotherapy and immunosuppressant agent whose concentration is commonly measured in human serum by pharmacology and clinical toxicology laboratories. This because the data obtained are useful to decide if the administration of folic acid as counter poison is a good choice in the case of too prolonged permanence of the drug in blood during a high-dose regimen[16].

Clinical usefulness of TDM in the context of anticancer drugs is actually limited by several factors:

- for most of anticancer drugs the knowledge of pharmacokinetic and pharmacodynamic aspects is not thorough. For this reason, the most evident limiting factor is the difficulty to establish a clear relationship between the concentration value obtained and the therapeutic effect; without these relationships, the TDM approach becomes a random approach. If the dose-response relationship is missing, a therapeutic window, which is the essential element for TDM, cannot be defined [17].
- due to the ample heterogeneity of cancers (identical tumours do not exist: they show different sensitivity and resistance towards anticancer drugs), every case must be analysed from scratch [18].
- The blood sampling timing is a critical factor too, in obtaining meaningful results. Samples must be taken after distribution equilibrium, when plasma concentrations better reflects tissue concentrations [19].
- cancer is often treated with more than one drug, thus making even more challenging to target the therapeutic and toxic effect at the pharmacodynamic level [20]. Drug–drug interactions are a major concern when treating patients with

oral targeted therapies [21]. Dosage adjustment in this context is therefore strongly recommended.

- several targeted anticancer drugs have active metabolites and their plasma concentrations could be impacted by variations in the enzymes responsible for metabolism. This has to be taken into account when assessing the effects of the drug [22].
- an appropriate administration of the drug, an adequate collection and processing of the biological sample, a precise and accurate measurement of the drug and/or of the metabolites and an appropriate interpretation of the results are the distinguishing factors of the correct execution of the TDM practice [23]. TDM is indeed a multidisciplinary approach embracing different professional figures such as physicians, pharmacists, nurses, pharmaceutical chemists/technicians and pharmacokinetic scientists. The entire personnel must be conscious of the limitations and difficulties of the TDM: a criticality that occurs only in one among the steps, is enough to compromise the whole process.
- the methods that can be used to quantify the analytes of interest must be accurate, precise, simple, rapid, sensitive, specific, not affected by matrix effects, and economically sustainable [24].

Despite the above mentioned problems, the high potential of TDM (if correctly applied) in the context of chemotherapy is evident, because anticancer drugs generally show both a very low therapeutic index and a large pharmacokinetic inter-individual variability [10, 25]. Moreover, anticancer therapy should be characterised by the maximum effectiveness to be useful: undertreatments, which could further compromise the low probability of recovery, are critical in the same way as the cytotoxic adverse reactions, that are typical of most anticancer drugs and could be very dangerous for patient's life. Other consequent benefits of this strategy would include the compliance increment (due to the low occurrence of toxicity), the reduction of the pharmacokinetic inter-individual variability, the possibility of correctly adjusting the dosage in patient with hepatic and/or renal impairment [18] and the accessibility of useful data to better detect the drug-drug interactions [23].

1.2 Gastro-intestinal stromal tumour

With roughly 9.5 million deaths annually, cancer is one of the leading causes of death worldwide. Cancer incidence and mortality are rapidly growing worldwide, the reasons to explain this phenomenon reflect both aging and growth of the population, as well as changes in the prevalence and distribution of the main risk factors for cancer, several of which are associated with socioeconomic development [26].

Sarcomas are a rare and heterogenous group of connective tissue tumour of mesenchymal origin. These tumours could grow everywhere in the body and are classified as either skeletal sarcomas or soft-tissue sarcomas (STS). Up to 2013, the World Health Organization (WHO) distinguished more than 50 different histological subtypes of STS, each with varying clinical phenotypes and behaviour, and new entities are continuously recognized [27].

Besides it accounts for less than 1% of all GI tumours [28], the gastrointestinal stromal tumour (GIST) is the most common STS of the GI tract and have gained considerable research and treatment interest [29]. However, the real incidence of GISTs is still unknown. Recent data suggest that the incidence may be greater than the estimated one; indeed, early (up to 1 cm large) asymptomatic GIST or micro-GIST, which are found in 20%-30% of the elderly, are very common [30]. These asymptomatic GISTs are usually found during other gastrointestinal endoscopy or imaging investigations [31]. Instead, primary GISTs are commonly symptomatic, in about the 80% of the cases, showing GI bleeding or obstructive symptoms and abdominal pain. The stomach is the most frequent onset site (60%), followed by the small intestine (30%), the colon and the rectum (5%) and the oesophagus (5%). It rarely develops outside the GI tract and in that cases the mesentery, the omentum or the retroperitoneum could be involved [32]. Estimates of 2015 show an incidence of 15 new patients out of a million of people per year with a prevalence of 1.3 cases every 10’000 people considering both the cases previously and the new one diagnosed. This means that, in Italy, between 6000 and 7000 people are affected by GIST [33].

GISTs arise at any age, even in infancy, but show proclivity toward developing in the middle-aged and elderly, with a median age of 63 years at the diagnosis [34]. Women and

men are affected almost equally [35] and there is no correlation between ethnicity and the incidence of this tumour [36].

The clinical spectrum of GISTs ranges from local lesions to highly aggressive and disseminated tumours [37]. About the 40% patients with localized GISTs at the onset will later develop metastases, while 10-20% of patients present metastases at the diagnosis time [38]. Metastases sporadically appear outside the abdomen, while they mostly involve the peritoneal cavity, the liver and the omentum [39].

Literature data regarding both the clinical behaviour and the epidemiology of GIST before the 21st century are not accurate. Before we came to know GISTs as we do today, almost all mesenchymal tumours of the GI tract were considered to be "GI smooth muscle tumours". GISTs were commonly classified in leiomyomas (if benign) and leiomyosarcomas (if malignant) [40]. Electron microscopic studies in the late 1960s and early 1970s, however, revealed evidences supporting ultrastructural differences between classical smooth muscle and GI tumours [41]. The later application of immunohistochemistry to the GIST study, which began in the 1980s, supported these electron microscopic evidences [42]. The discovery that most GISTs were positive for protein CD34 allowed to use this protein as the first clinically useful marker for distinguish GISTs from GI leiomyomas or leiomyosarcomas in clinical routine [43]. In the 1990's researchers identified similarities between GISTs and the interstitial cells of Cajal (ICCs), a population of cells in the gut. These cells were found to express cKIT/CD117 [44]. Shortly thereafter, Hirota and colleagues discovered that GISTs express cKIT as well [45]. Today, it is hypothesized that ICCs are the cells of origin for GIST. Immunohistochemistry reveals that 95% of GISTs express cKIT/CD117, whose identification is at the basis of this tumour diagnosis [46].

The histological diagnosis of GIST is primarily based on morphology, immunohistochemistry and, sometimes, on mutational analysis. Endoscopic examination, echography, computed axial tomography, magnetic resonance imaging (MRI), positron emission tomography exams with Fluorine-deoxy glucose ([^{18}F] FDG-PET) and CD117 expression evaluation represent the diagnostic tools to date [47].

The antigen CD117 is an epitope of cKIT receptor and 95% of tumour cells originated from GISTs, no matter for the origin site neither for the behaviour and histological appearance

of the tumour, are positive for this antigen. Therefore, this factor is considered one of the most reliable diagnostic markers [48].

KIT receptor is a type III tyrosine kinase (TK). Like other members of the TK family, KIT is composed by an extracellular domain, a transmembrane domain and an intracellular domain, responsible for the tyrosine kinase activity.

In its inactive form, KIT is a monomer with intrinsic factors that make its activity self-inhibited. It is able to bind stem cell factor (SCF), also known as "c-KIT ligand", a tissue and hematopoietic growth factor.

When the receptor binds to SCF it forms a dimer that activates its intrinsic tyrosine kinase activity (Figure 2); this kind of interaction is called homodimerization and leads to a phosphorylation reaction first. Then, the consequences of this interaction are a series of cascade signals with the result of the activation of cellular functions which are fundamentals for carcinogenesis like proliferation, adhesion, differentiation and apoptosis. However, SCF only represents the extrinsic mechanism of KIT activation, which can also be regulated by structural modifications of the protein itself which allow it to be activated in the absence of the ligand (intrinsic mechanism) [45].

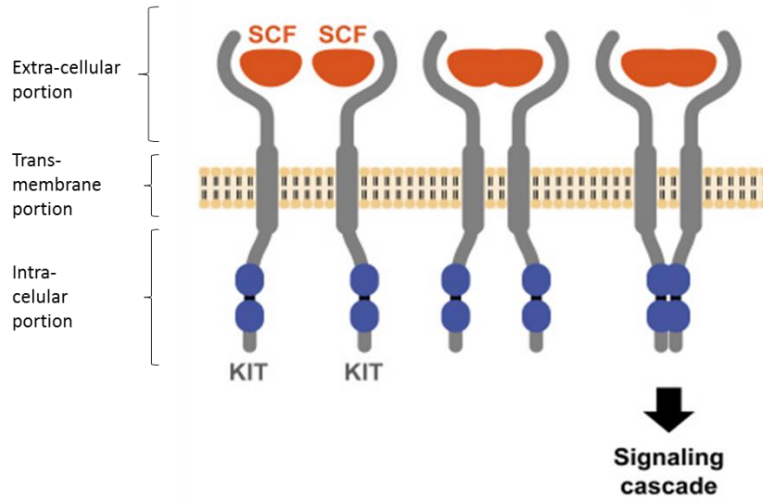

Figure 2. Representation of the KIT receptor structure and its activation. Figure adapted from [49].

The discovery of some gain-of-function mutations involving KIT or PDGFRα has significantly changed the biological comprehension and the treatment of the pathology. In about 85% of the GISTs mutations activations of the KIT oncogenes are observed, in the 5% these mutations occur in the alpha platelet-derived growth factor receptor (PDGFRα).

These alterations, that are mostly deletions, in frame insertions, missense mutations or combinations of them, could also occur in the extracellular domain or in the intracellular one with a probability of 6 and 2%, respectively. The outcome of these alterations is the constitutive activation of receptors and their pathways signal, resulting in loss of cell cycle control, proliferation and resistance apoptosis. The remaining part of GISTs (10%) is wild-type (WT), namely, tumours do not express any mutation of KIT or PDGFRα [50].
Other markers that might be positive in case of GIST are BCL-2 (80%), CD34 (70%), muscle specific actin (50%), smooth muscle actin (35%), s-100 (10%) and desmin (5%) [42]. These data are important to create targeted therapies against the genetic defect present in the tumour. One important example of the application of this strategy is the use of tyrosine kinase inhibitors (TKIs), such as imatinib (IMA).

1.2.1 GIST treatment

The treatment of GIST depends mainly on the size of the tumour, its localization, how far is spread and its mitotic rate. GIST could be divided in three different types [51].
In case of localized tumours, the standard approach consists on complete surgical excision of the lesion. Meanwhile, in case of larger and marginally resectable tumours, considering that the resection might require extensive surgery, it is advisable to start the treatment with IMA, to try to shrink the tumour and continued at least until the tumour stops shrinking. Then, surgery might be the best option if the tumour could be removed safely. In general, surgery is potentially curative for primary GISTs that have not metastasized, and the probability of recurrence will depend on the malignant potential as assessed by risk stratification criteria. When patients are at a high risk of relapse according to these criteria, 3 years of adjuvant treatment with IMA after surgery is the standard of care. The benefit of this pharmacological treatment may vary according to the type of KIT/PDGFRA mutations. In fact, patients with KIT exon 11 deletions have a better response to IMA than patients not presenting these mutations [52]. On the contrary, the presence of PDGFRA D842V mutation is associated with resistance to IMA treatment. For this reason, there is a consensus that PDGFRA D842V mutated GISTs should not be treated with any adjuvant therapy, given the lack of sensitivity to the drug demonstrated both in vitro and in vivo.

On the opposite, surgery is not the first treatment in case of unresectable or metastatic GISTs. The best option is IMA, the treatment continues as long as the tumour does not grow, and the patient can tolerate the side effects of the drug. If the cancer has spread to only 1 or 2 sites in the abdomen (such as the liver), the surgeon may advise removing the main tumour and trying to remove these other tumours as well [52].

Before the introduction of TKIs, the survival rate after 5 years from the complete resection ranged from 35 to 80% and the median survival was 10–20 months for patient with non resectable disease [53]. IMA significantly improved the treatment outcome as shown in a randomized phase II trial called B2222: after 5 years of therapy, survival was observed in 54% of patients with metastatic or inoperable GIST [54].

However, IMA does not represent the only weapon against this pathology. For patients with IMA-resistant GISTs, sunitinib is a second-line drug treatment whilst regorafenib is the third-line drug. Some drugs approved for other conditions may be prescribed off-label for GISTs at a physician's discretion. New molecular targeted drugs are being tested in many clinical trials and some are still under development.

1.2.1.1 Imatinib

Ninety-five percent of GISTs stain positively for the CD117 antigen which is, as said before, an epitope for the KIT receptor tyrosine kinase. KIT positivity is important as it is one of the targets of IMA mesylate [55]. Imatinib mesylate (Figure 3) is the active ingredient of the oral anticancer drug Glivec® and Gleevec® (the trade names given in Europe and USA, respectively). It belongs to the so-called targeted therapies, that are a class of drugs that acts specifically against a target which is only present in cancer cells, or however, which is more expressed in cancer cells than in normal ones. Generally, with this kind of approach, the target is represented by a receptor present on the surface or inside the tumour cell.

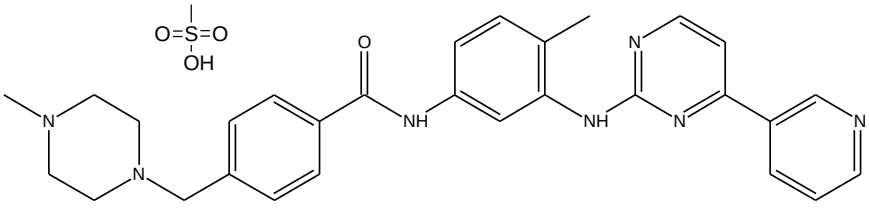

Figure 3. Structure formula of 4-[(4-Methyl-1-piperazinyl) methyl]-N-[4-methyl-3-[[4-(3-pyridinyl)-2-pyrimidinyl] amino]-phenyl] benzamide methane sulfonate, also known as imatinib mesylate.

More in detail, IMA inhibits in a selective and potent way the activity of different TKs including the intracellular ABL kinase, the transmembrane receptor KIT, the PDGFRα and PDGFRβ, the receptor for the discoidin domain (DDR1) and also the chimeric BCR-ABL fusion oncoprotein present in chronic myeloid leukaemia (CML) [42].

IMA acts as a competitive antagonist of the adenosine triphosphate (ATP) binding site. It blocks the transfer of phosphate group from ATP to tyrosine residues of the substrates. This cause the interruption of the downstream signalling process that leads to cell proliferation [56], as shown in Figure 4.

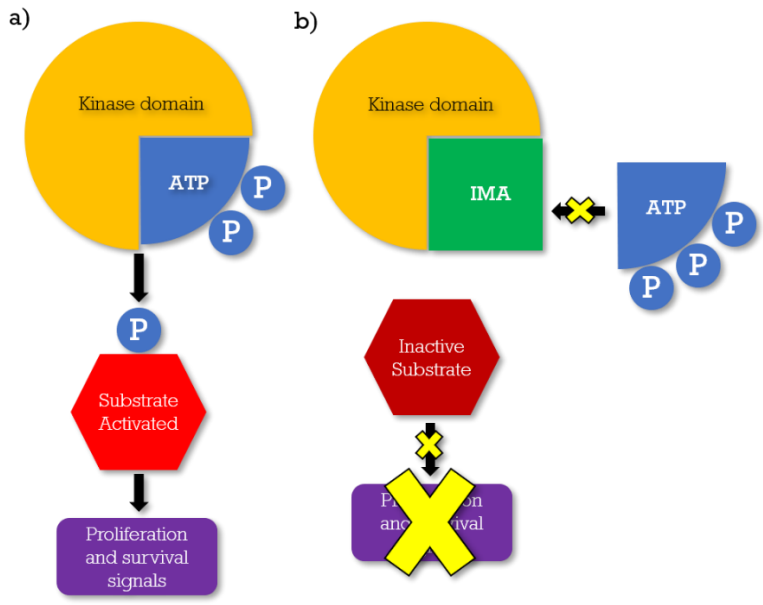

Figure 4. Comparison between the absence a) and the presence b) of IMA at the level of the kinase domain of a generic tyrosine kinase protein. In a), the phosphorilation ATP-mediated activates the substrate that leads to the diffusion of proliferation and survival signals. In b) IMA leads to the block of the substrate activation by occupying the ATP binding pocket of the kinase domain with a consequent block of proliferation and survival stimuli.

The promising results from the American-Finnish clinical trials CSTIB2222 [57] and the European organization for research and treatment of cancer [58] convinced the Food and Drug Administration (FDA) in February 2002 and the European Medicines Agency (EMA) in May 2002 to approve IMA as the first-line treatment for inoperable, metastatic or recurrent, KIT-positive GIST. Furthermore, IMA was approved by the FDA in December 2008, and by the EMA in March 2009 for adjuvant treatment following surgical resection of GIST with a high risk of recurrence, due to the increase of the overall survival (OS) observed in patients during the trials [29]. The oral intake of 400 mg/die of IMA represents the actual standard therapy. For patients affected by GIST with exon 9-mutated KIT, the

National Comprehensive Cancer Network (NCCN) [33] and the European Society of Medical Oncology (ESMO) [51] guidelines suggest a higher dose (800 mg/die) because it positively correlates with a longer progression-free survival (PFS) [59].

IMA produces a partial response in 45% of patients and a stabilization of the disease in 30% [60], while the complete response is rare. This is why it is described as an oncostatic agent rather than a cytotoxic [61]. Considering that stopping the treatment with IMA is accompanied by a disease progression [54], after a complete response or a macroscopic resection of the residual tumour, the therapy should be continued indefinitely and stopped only in the case of tumour progression or occurrence of intolerable side effects.

The pharmacokinetic profile of IMA has been evaluated in healthy volunteers, in patients affected by CML, GIST and other neoplasms [47]. These studies showed a good oral absorption and a 98% bioavailability of the preparation (solution, capsule or tablets) independently from the dosage or food intake [12, 47]. For this reason, to reduce the risk of GI irritation, patients takes IMA orally during a meal with a large glass of water and the bioavailability is not compromised [62]. After the absorption, IMA undergoes extensive and rapid tissue distribution. A minimum percentage of the drug can penetrate through the blood-brain barrier, without however reaching sufficient concentrations to determine some pharmacological activity in the central nervous system [47]. Approximately 95% of the administered drug is bound to plasma proteins, mainly to albumin and alpha 1 acid glycoprotein [12]. Peak concentrations are reached 4 hours after the administration [63]. Like most drugs, IMA is metabolized in the liver; mainly by the cytochrome P 450 enzymatic system; in particular from isoforms 3A4 and 3A5 and to a lesser extent from 1A2, 2D6, 2C9, 2C19 [47]. The main circulating metabolite of imatinib is N-desmethyl imatinib, also known as nor-imatinib (norIMA) or CGP74588. NorIMA is an N-demethylated derivative of piperazine (Figure 5), it has a biological activity similar to IMA and represents approximately 20-25% of the steady-state level of the original drug in patients with GIST [11].

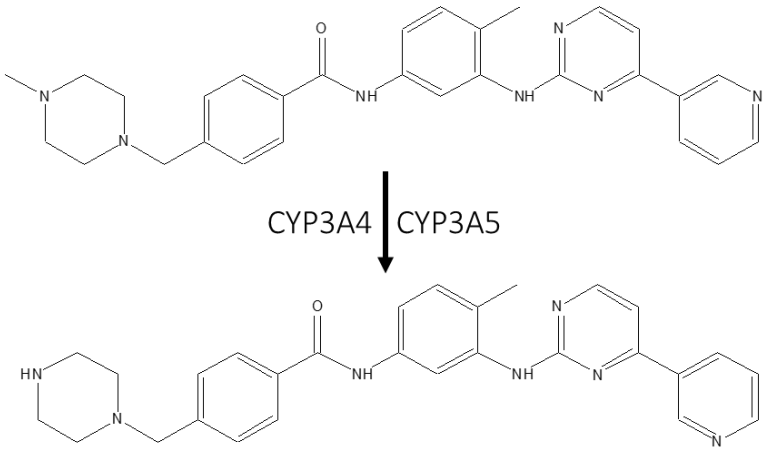

Figure 5. norIMA formation through N-demethylation reaction of IMA mediated by isoform 3A4 and 3A5 of cytochrome p450.

Being a substrate of CYP3A4, IMA may interfere with the metabolism of other drugs and natural substances co-administered as follows:

- Strong inducers of CYP3A4 such as rifampicin, carbamazepine, fluconazole and St John's Wort (*ipericum perforatum*) increase the metabolism of IMA, thus decreasing its plasma concentration [47].
- Strong inhibitors of CYP3A4 such as erythromycin, ketoconazole and grapefruit juice, decrease the metabolism of IMA, thereby increasing its plasma concentration [47, 64].

Moreover, co-administration of IMA with other drugs should be kept under control as IMA itself is a CYP3A4 and others CYPs substrate. In fact, IMA significantly increases the exposure to the statin by 2-3 times [65] and patients requiring anticoagulants during treatment with IMA should opt for standard or low molecular weight heparin, since warfarin is a substrate of both CYP3A4 and CYP2C9 and there could be a possible interaction between warfarin and IMA metabolism [66]. Other factors that could reduce IMA metabolism are hepatic and renal impairment and hepatic metastases, while age, race, gender and body weight do not significantly affect its pharmacokinetics in the treatment of GIST [55].

IMA elimination occurs primarily via the faecal route and the half-life ($T_{1/2}$) of this drug and its active metabolite norIMA is approximately 18 and 40 h respectively [67]. In patients with GIST, steady state exposure was 1.5-fold higher than that observed in CML for the same 400 mg/day dosage. This mainly seems to depend on albumin, white blood

count and bilirubin. Hepatic and renal dysfunction and liver metastases may cause variable and reduced metabolism of the drug [68].

This drug regimen is generally well tolerated and allows the patient to lead a normal life. Adverse reactions with a high incidence rate (above 10%) are gastrointestinal disorders (nausea, vomiting, diarrhoea), abdominal pain, fatigue, myalgia, muscle cramps, rash and superficial oedema, in particular periorbital and lower limb oedemas [66]. The oedemas are rarely severe and can usually be managed with diuretics, with other supportive measures or with a dose reduction. More important disorders, such as hepatic, renal or cardiac failure, haemorrhages and significant changes in haematological values, are rarely observed [66]. Haematological toxicities, such as anaemia, neutropenia and leukopenia, have an incidence rate lower than 10% [66]. Furthermore, the continuing use of the drug allows many patients to develop tolerance of these side effects [69].

Resistance to IMA therapy can be either primary, if it occurs on after initial use of drug, or secondary, if it arises after an initial response. Four drug resistance mechanisms have been identified [70]:

1. target resistance due to mutation: a new KIT or PDGFRα point mutation and protein activation, superimposed on the original mutation in that gene;
2. KIT genomic amplification with overexpression of the KIT oncoprotein, without a new point mutation;
3. target modulation: activation of an alternate receptor tyrosine kinase protein, accompanied by loss of KIT oncoprotein expression;
4. functional resistance: KIT or PDGFRα activation, outside the juxta membrane hotspot regions, in the absence of a secondary point mutation.

All these mechanisms were involved in late resistance, while only the functional resistance (point 4) was seen in primary resistance.

Approximately 10% of patients treated with IMA experience tumour progression within 3-6 months of treatment due to the onset of primary resistance. In addition, a further 40-50% of them develop drug resistance within 2 years of treatment after partial response or disease stabilization. These patients are classified as having delayed or secondary resistance [55]. In the case of drug resistance occurrence or tumour progression, the oncologist can increase the IMA dose from 400 to 800 mg/day based on two clinical trials

(EORTC 62005 [71] and SWOGS 0033 [72]), which have shown how the dose escalation at the time of disease progression provides clinical benefit in one third of patients. If dose escalation leads to disease progression or drug intolerance, it will be necessary to proceed to the second-line treatment for this pathology which consists of the administration of another TKI: sunitinib (SUNI).

1.2.1.2 Second- and third-line pharmacological treatments

Multiple novel TKIs may be potentially useful for the treatment of IMA-resistant GISTs as they interfere with KIT and PDGFRα receptors or with the downstream-signalling proteins [73].

SUNI (chemical structure reported in Figure 6), active ingredient of the drug Sutent®, is an oral, multitarget receptor TKI that has shown promise in tumour models.

Specifically, it has been shown to inhibit KIT, PDGFR, vascular endothelial growth factor receptors (VEGFR) and FMS-related tyrosine kinase 3 receptor, receptor for macrophage colony-stimulating factor and glial cell line-derived neurotrophic factor receptor, presenting both antiangiogenic and antiproliferative activities [74]. Its role was acknowledged in a randomized controlled trail against placebo or IMA resistant GIST patients [75]. SUNI was approved by the FDA as second-line TKI for the treatment of imatinib-resistant GISTs in 2006 [76] and currently it is indicated for patients whose disease progressed on IMA (even after dose escalation up to 800 mg/die). This drug is orally available, and the approved dosage is 50 mg per day for 4 weeks followed by 2 weeks rest, until disease progression or the inset of intolerable side effects.

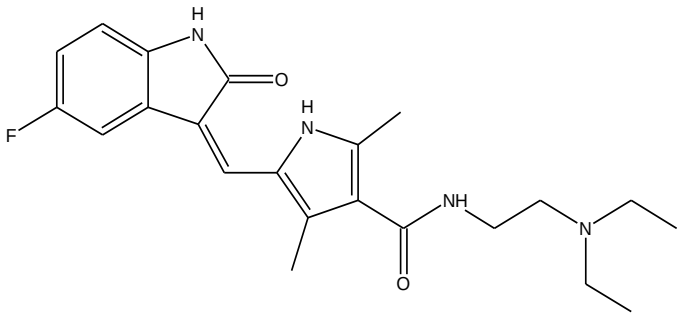

Figure 6. Chemical structure of N-[2-(diethylamino) ethyl]-5-[(Z)-(5-fluoro-2-oxo-1H-indol-3-ylidene) methyl]-2,4-dimethyl-1H-pyrrole-3-carboxamide, also known as Sunitinib.

Regorafenib (chemical structure reported in Figure 7), the active ingredient of the drug Stivarga®, is an inhibitor of several TK receptors involved in tumour angiogenesis, oncogenesis, metastasis and immunity. Regorafenib was approved by the FDA in 2013 to treat advanced GISTs that cannot be surgically removed and are resistant to other TKIs, and it is considered as third-line treatment. The long-term follow-up results of the multicentre phase II trial of regorafenib in patients with metastatic or unresectable GISTs after failure of IMA and sunitinib showed benefit in patients with primary KIT exon 11 mutations and SDH-deficient GISTs [77]. It is an oral therapy, administered at a dose of 160 mg/die following a 4 weeks schedule with a 3+1 scheme (3 weeks of treatment followed by 1 week off) until disease progression or occurrence of unacceptable toxicity.

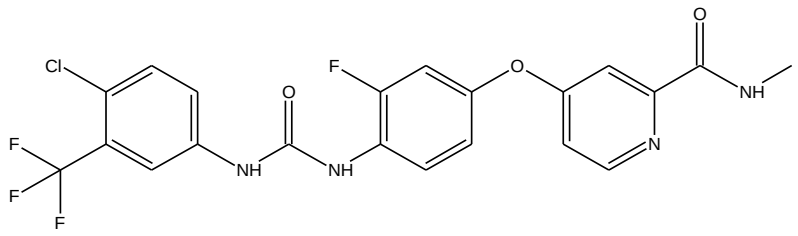

Figure 7. Chemical structure of 4-[4-[[4-chloro-3-(trifluoromethyl) phenyl] carbamoylamino]-3-fluorophenoxy]-N-methylpyridine-2-carboxamide, also known as Regorafenib.

The use of other TKIs, apart from imatinib, sunitinib and regorafenib, is still being evaluated and remains debated. About 250 clinical trials involving the use of nearly sixty drugs, including other TKIs like sorafenib, nilotinib, dasatinib and pazopanib have been approved worldwide [78]. However, at the moment, the fourth approved treatment line is still missing.

1.2.2 Why TDM is important for imatinib

As pointed out in the first chapter of this thesis, a drug has to fulfil some characteristics to be eligible to perform TDM.

For IMA most of these characteristics are respected. In fact, this drug is characterized by large inter-individual pharmacokinetic variability, which reflects the large spread of concentrations observed under standard dosage. Data from a study conducted on patients with metastatic GIST showed that IMA plasma levels ranged from 256 to 4582 ng/mL [79]. Besides the adherence to the therapy, several factors have been shown to

influence this variability, like demographic characteristics (age, sex, body weight and disease diagnosis) [47], enzyme activity (especially for the CYP3A4, that metabolises IMA to his major active metabolite), drug interactions [80], activity of efflux transporter [81] and plasma levels of alfa1-acid glycoprotein (which binds imatinib in plasma) [82]. In addition, for GIST patients, surgery further complicates the panorama: it has been described that patients undergoing partial or total gastrectomy show significant lower IMA plasma levels than patients who had not this type of surgery [83].

Therefore, due to this high variability, the dose does not predict plasma drug levels [84]. This has clear consequences on the treatment response, which, in the case of IMA treatment, has shown to be correlated with the trough level (C_{min}). The C_{min} is defined as the steady-state concentration before the subsequent administration of the drug. Increased toxicity has been associated with high plasma levels and impaired clinical efficacy with low plasma levels. Therefore, the standard dosage of IMA 400 mg/die might not represent the optimal dose intensity for every patient. While the upper concentration limit is yet not formally established, a lower limit for IMA C_{min} has been proposed for improving outcomes in GIST patients [85]. In detail, it has been reported that, a month after the beginning of the therapy, patients with a C_{min} above 1110 ng/mL (corresponding to the first quartile of concentration values) showed an improvement in time to progression (TTP) of disease compared to patients in the other quartiles [86].

Furthermore, in a recent study, Eecheoute et al. showed [87] that the IMA C_{min} decreased by about 30% in the first three months of treatment. An increase in drug clearance, which subsequently reaches a plateau, seemed to be the responsible factor for this C_{min} decrease. This hypothesis is supported by a study [88] conducted by analysing C_{min} more than three months after the beginning of the treatment. In this study, a longer PFS was associated with C_{min} values higher than 760 ng/mL, suggesting the need to repeatedly evaluate IMA plasma concentrations during the treatment period. The decrease in C_{min} also provides an explanation about the increase in drug tolerance over time, and underlines how in some patients this decrease may cause the failure to achieve effective drug concentrations [89].

However, despite no consensus has been still reached for the definition of a precise C_{min} threshold related to the treatment effectiveness, the more practical approach seems to

be the application of a C_{min} > 1100 ng/mL threshold, as it is based on PFS data from a randomized clinical trial and was confirmed in observational and retro prospective studies [90, 91].

Furthermore, for GIST patients, surgery further complicates the panorama: it has been described that patients undergoing partial or total gastrectomy show a significant decrease in IMA C_{min} [83].

TDM of IMA is thus highly recommended as a useful tool for managing and optimizing the treatment for each patient. In fact, the European Society of Medical Oncology (ESMO) guidelines suggest that measurement of IMA plasma concentrations could be important in both CML and GIST patients and is recommended especially in cases of suboptimal response, therapy failure, toxicity due to overdose or adverse events [52, 92]. It would also be essential to define unequivocally, in GIST patients, the C_{min} threshold that can be used as a reference for TDM in clinical practice.

The whole process is obviously useless if C_{min} values are unreliable. For this reason, it is necessary to adopt the most accurate and robust analytical technique for the quantitative analysis of small molecules in biological samples. Therefore, one of the aims of this thesis was the development of a robust LC-MS/MS analytical method for the quantification of IMA and its main metabolite, norIMA, in Dried Blood Spots matrices.

1.3 Breast cancer

Breast cancer is the most common cancer in women, and one of the three most common cancers worldwide, along with lung and colon cancer. In fact, one in eight to ten women will get breast cancer during her lifetime and less than one out of six women diagnosed with this disease die of it. Men account for 1% of breast cancer cases and breast cancer deaths [93].

Anyway, mortality from breast cancer in North America and European Union has decreased, and this is attributable to early detection and efficient systemic therapies [94]. At this regard, mammography provides the key qualities for the systematic screening: easy to perform and to standardize, with a minimal technical set-up [95]. Many countries with highly developed health systems have introduced systematic mammography screening for women, usually between 50 and 70 years of age, to reduce breast cancer

mortality. MRI is another widely used screening tool for breast cancer, it is more sensitive than mammography in high-risk women [96].

Based on comprehensive gene expression profiling, breast tumours are classified into at least three major subtypes: luminal, human epidermal growth factor receptor 2+ (HER2+) and basal like. Each of these subtypes has different risk factor for incidence, treatment response, risk of disease progression and preferential organ sites of metastases [97].

Luminal tumours are positive for oestrogen and progesterone receptors, and the majority respond well to hormonal interventions (anti-oestrogen receptor). Oestrogen receptor alpha (ERα) is expressed approximately in the 7% of invasive breast cancer. ERα is a steroid hormone receptor and a transcription factor that, when activated by oestrogen, activates oncogenic growth pathways in breast cancer cells. Expression of the closely related steroid hormone progesterone receptor (PR) is also a marker of ERα signalling. Tumours with expression of either ER or PR in at least 1% of tumour cells are categorized as hormone-receptor positive (HR+) [98].

HER2+ tumours have amplification and overexpression of the HER2 oncogene, a transmembrane receptor TK in the epidermal growth factor receptor family. It is amplified or overexpressed in approximately 20% of breast cancers, it is associated with poor prognosis in the absence of systemic therapy and it can be controlled with a diverse selection of anti-HER2 therapies, including antibodies like trastuzumab and pertuzumab, and small-molecule TKIs (such lapatinib and neratinib).

Basal-like tumours in general lack both hormone receptors and HER2; for this reason, the majority of these tumours are also called triple-negative breast cancer (TNBC). Currently there is no molecular-based targeted therapy for TNBC, and unfortunately only approximately 20% of these tumours respond well to standard chemotherapy. The specific molecular pathophysiology of TNBC remains poorly understood [93].

For nonmetastatic breast cancer, the main goals of therapy are eradicating tumour from the breast and regional lymph nodes and preventing metastatic recurrence. Local therapy for nonmetastatic breast cancer consists of surgical resection and sampling or removal of axillary lymph nodes, with consideration of postoperative radiation. Systemic therapy may be preoperative (neoadjuvant), postoperative (adjuvant), or both. For metastatic breast cancer, therapeutic goals are prolonging life and symptom palliation [99].

Risk factors for developing breast cancer include being female, obesity, lack of physical exercise, drinking alcohol, hormone replacement therapy during menopause, ionizing radiation, early age at first menstruation, having children late or not at all, older age, prior history of breast cancer in the family. Moreover, about 5-10% of cases are due to genes inherited, including the breast related cancer antigens: BRCA1 and BRCA2 (that are known as regulators of DNA repair, transcription and cell cycle in reply to a damage). These are abnormal genes that, when inherited, markedly increase the risk of breast cancer to a lifetime risk estimated between 40 and 80% [100].

The classic symptom for breast cancer is a lump found in the breast or armpit. The general alerting features of breast cancer are such as swelling or lump (mass) in the breast, swelling in the armpit, nipple discharge, pain in the nipple, inverted (retracted) nipple, persistent tenderness of the breast and unusual breast pain or discomfort. In advance stage od disease (metastatic) other symptoms may be presented, such as bone pain (bone metastasis), shortness of breath (lung metastases), drop in appetite (liver metastasis), headaches or weakness [101].

1.3.1 Cyclin-dependent kinase inhibitors

HR+ breast cancer represents the largest therapeutic subtype of the disease, accounting for 60 to 65% of all malignant breast neoplasms. For more than 50 years, the treatment of HR+ disease has been focused on targeting the oestrogen-receptor signalling pathway. However, both new and acquired resistance to hormonal blockade occur in a large subset of these cancers, and new approaches are needed.

In normal tissues, cell proliferation is tightly regulated by cell cycle machinery. The interaction of cyclin D with CDK4 and CDK6 facilitates the phosphorylation of the retinoblastoma (Rb) gene product, which in turn leads to the transition through the G1 checkpoint to the S phase of the cell cycle.

Alterations in the cyclin-D–CDK4/6–Rb pathway, that result in the loss of regulation of this critical Rb checkpoint, have been described in a number of malignant conditions and are associated with endocrine resistance in breast cancer. These alterations include cyclin-D amplification; loss, mutation, or both loss and mutation of Rb itself; and loss of negative regulators of the pathway [102]. For this reason, potent and selective orally bioavailable

inhibitors of CDK4/6 have become available as cancer therapeutics in the last decades. They act primarily by blocking Rb phosphorylation and thus inducing G1 cell cycle arrest and a phenotype resembling cellular senescence [103]. In human breast cancer, the subtype for which CDK4/6 inhibition has the strongest rationale is HR+ disease.

1.3.2 Ribociclib

Ribociclib (RIBO, Kisquali®) is an orally bioavailable, highly-selective small inhibitor of CDK 4/6, which in combination with letrozole (LETRO), is indicated for the treatment of postmenopausal women with HR+, HER2-negative advanced or metastatic breast cancer as initial endocrine-based therapy. The chemical name is butanedioic acid-7-cyclopentyl-N,N-dimethyl-2-{[5- (piperazin-1-yl) pyridin-2-yl] amino} -7Hpyrrolo [2,3-d] pyrimidine-6-carboxamide, the structure is reported in Figure 8.

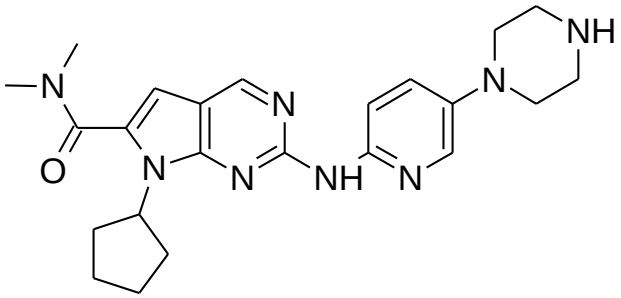

Figure 8. Chemical structure of 7-cyclopentyl-N,N-dimethyl-2-{[5- (piperazin-1-yl) pyridin-2-yl] amino} -7Hpyrrolo [2,3-d] pyrimidine-6-carboxamide, known as ribociclib.

In vitro, RIBO decreased Rb phosphorylation, leading to arrest in the G1 phase of the cell cycle, and reduced cell proliferation in breast cancer cell lines. *In vivo*, treatment with single agent RIBO led to tumour regressions which correlates with inhibition of Rb phosphorylation. RIBO was approved with the MONALEESA-2 trial [104] where its addition to LETRO demonstrated improved median PFS (25.3 (23.0-30.3) months in the RIBO + LETRO group, 16.0 (13.4 – 18.2) months in the placebo + LETRO group).

RIBO is eliminated primarily via hepatic metabolism mainly via CYP3A4 in humans. The primary metabolic pathway for this drug involves oxidation. Phase II conjugates of RIBO phase I metabolites involves N-acetylation, sulfation, cysteine conjugation, glycosylation and glucuronidation. Anyway, RIBO remains the major circulating drug-derived entity in plasma [105].

The most common toxicities observed in patients treated with RIBO were neutropenia, leukopenia, headache, back pain, QT interval prolongation, nausea, fatigue, diarrhoea, vomiting, constipation, alopecia and rash and while most common severe toxicities (G3/4) were neutropenia, leukopenia, abnormal liver function test, lymphopenia, hypophosphatemia, vomiting, nausea, fatigue and back pain.

1.3.3 Palbociclib

Palbociclib (PALBO, Ibrance®), Figure 9, is a highly selective, reversible inhibitor of CDK4 and 6. This drug is indicated for the treatment of HR+, HER2-negative locally advanced or metastatic breast cancer, in combination with an aromatase inhibitor, such as LETRO, or in combination with fulvestrant in women who have been previously treated with endocrine therapy. In pre- or perimenopausal women, the endocrine therapy should be combined with a luteinizing hormone-releasing hormone agonist.

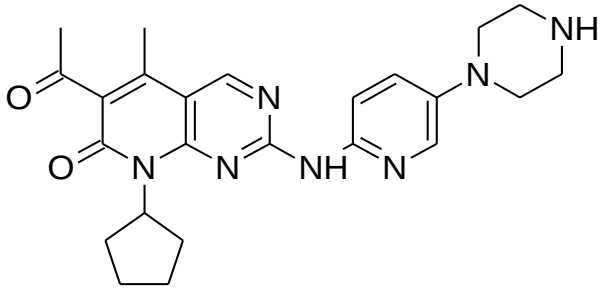

Figure 9. Chemical structure of 6-Acetyl-8-cyclopentyl-5-methyl-2-{[5-(1-piperazinyl)-2-pyridinyl]amino}pyrido[2,3-d]pyrimidin-7(8H)-one, known as palbociclib.

The efficacy of palbociclib (PALBO) in combination with LETRO *versus* LETRO plus placebo was evaluated in the PALOMA-2 study [106] conducted in women with ER-positive, HER2-negative locally advanced breast cancer not amenable to resection or radiation therapy with curative intent or metastatic breast cancer who had not received prior systemic treatment for their advanced disease. The results of this study demonstrated an improvement in PFS in favour of PALBO plus LETRO (median PFS 24.8 months (95% CI: 22.1, NE) *versus* 14.5 months (95% CI: 12.9, 17.1). Similar results have been demonstrated for the association of PALBO with fulvestrant (PALOMA-3) [107].

The primary metabolic pathways for PALBO involved oxidation and sulphonation, with acylation and glucuronidation contributing as minor pathways. CYP3A and SULT2A1 are

mainly involved in its metabolism. As for RIBO, PALBO remains the major circulating drug-derived entity in plasma.

The most common (≥20%) adverse reactions of any grade reported in patients receiving PALBO in randomized clinical studies were neutropenia, infections, leukopenia, fatigue, nausea, stomatitis, anaemia, alopecia, and diarrhoea. The most common (≥2%) Grade ≥3 adverse reactions were neutropenia, leukopenia, anaemia, fatigue, and infections.

1.3.4 TDM for CDKIs

Based on the limited exposure–response and –toxicity studies, TDM recommendation for PALBO and RIBO currently ranges from exploratory to promising. For example, a greater reduction in absolute neutrophil count appears to be associated with increased PALBO exposure, while no definitive exposure-response relationship was found in 81 patients treated at 125 mg fixed dose [108]. Thus, currently, no specific PK targets for PALBO can be formulated. However, until more complete studies come available, PALBO concentrations can be compared to the population mean C_{min} of 61 (± 42) ng/mL [109].

Regarding RIBO, some adverse events, as neutropenia or QT prolongation, have shown to be proportional to drug exposure too [110].

Thus, to deepen the knowledge about the interindividual variation in pharmacokinetics and relationship with patient outcome, large prospective clinical studies are needed, as well as more validated bioanalytical methods to support them.

1.4 LC-MS/MS as a tool for TDM

In order to obtain the drug concentration in biological matrix to perform TDM, the method and the analytical technique used are essential. In the last 40 years, there have been significant improvements in analytical technologies applied in cancer pharmacology to measure drug concentration and to study drug metabolism.

At the beginning, the concentration data from biological matrix were usually obtained by LC-UV/VIS methods. The next step was to prefer, when possible, the use of a fluorescence detector, more sensitive and reliable, but the real change in bio-analysis began with the development of bench-top mass spectrometry instrument.

Mass spectrometry (MS) is now 100 years old, in fact its basic principles were first described by Noble laureate Sir Joseph John Thomson in 1897, followed by experimental validation in 1913, when he separated a stream of ionized neon gas into two isotopic components by applying a magnetic and an electric field to it [111].

During the following decades, MS underwent rapid technical development and became a widely used analytical technique in the physical and chemical sciences. In the 1980s, John Fenn perfected soft ionization of large biomolecules by electrospray ionization (ESI) [112]. Before this discover, the use of MS for biological specimens was limited because the ionization techniques available were only suitable for low molecular weight compounds (200 Da or lower) [113]. The growth of MS use for biospecimen analysis accelerated further during the mid and late 1990s, which saw a shift from gas-chromatography (GC) as a mass spectrometry front-end technology to liquid-chromatography (LC), a technique that allowed much simpler workflows and significantly faster analytical turnaround times. This because GC requires a certain level of analyte volatility and, since most biologically active molecules are polar, thermolabile and involatile, elaborate and time-consuming extraction and derivatization protocols had to be used [114].

Nowadays, LC-MS has become a widespread technique, with applications in medical laboratories ranging from rare and highly esoteric analytes to high volume tests in drug/toxicology, new-born screening, TDM, etc.

1.4.1 Principles of liquid chromatography

Chromatography is the process that allow to separate compounds contained in a mixture based on their physico-chemical characteristics (mass, charge and polarity). The separation is founded on the different distribution of the compounds between the stationary phase (SP) and the eluent that flows through it, called mobile phase (MP).

There are several principles that allow the compounds separation, leading to the identification of different chromatographic techniques:

- normal/reverse phase chromatography: the separation of the compounds is based on the partition coefficient within a biphasic (aqueous/organic) system. In case the SP is more polar than the MP it will be called normal phase (NP), while in the opposite situation it is called reverse phase (RP);

- ion exchange chromatography: the separation of the compounds is based on their charge and the ionic bond with the SP (an ion exchange resin);
- size exclusion chromatography: also called gel permeation chromatography, the separation of the compounds is based on molecular size.

Methods reported in this thesis are based on RP chromatography. With this technique the SP is usually constituted by a matrix (silica, polymer or silica-polymer hybrid) which is derivatized with apolar chains of various length. RP chromatography is indicated for the separation of lipophilic molecules, like most of drugs, because the prevailing retention mechanism is due to hydrophobic interactions. During the process, the analytes are retained on the SP and, as the MP continues to flow through the column, there will be the detachment of the various analytes retained by the SP according to their affinity for the MP.

At the end of the chromatographic run, a chromatogram is obtained showing the detector response (Y-axis) during the chromatographic runtime (X-axis). For quantitative analysis, the peak area is used as parameter instead of peak height because it is better directly proportioned to the amount of the detected analytes. A good chromatography separation is characterized by narrow, symmetrical and well separated peaks for each analyte.

The most important thing in HPLC is to obtain optimum resolution in the minimum time. A resolution value ≥ 1.5 between two peaks will ensure that the sample components are well separated (at the baseline). The Fundamental resolution equation [1] indicates that resolution is affected by other three important parameters:

$$R_s = {}^1\!/_4 \sqrt{N} \times \frac{\alpha - 1}{\alpha} \times \frac{k}{1 + k} \qquad [1]$$

Where:

${}^1\!/_4 \sqrt{N}$: represents the efficiency;

$\frac{\alpha-1}{\alpha}$: represents the selectivity;

$\frac{k}{1+k}$: represents the retention.

- the capacity factor (k) is the measure of the analyte's retention on the chromatographic column; a high k value means that the analytes are highly retained.
- the selectivity (α), indicates the ability of the chromatographic system to distinguish between two species. A good selectivity can be achieved using the optimal SP-MP combination for the analyte of interest.
- the efficiency is a measure of the dispersion of the analyte band as it travels through the HPLC system and column. The plate number (N) is a measure of the peak dispersion on HPLC column, which reflects the column performances. Each plate represents a single equilibrium stage of analytes distribution between the MP and the SP. The higher the N, the greater the number of exchanges between the two phases, the better the quality of the separation. N value (and therefore efficiency) can be increased by using longer columns, with the collateral effect, however, of increasing the whole run time. Another approach consists in selecting columns filled with smaller sized particle, in order to decrease the plate height (H) and therefore, column length (L) being equal, to increase N.

During the development of a method in HPLC (high performance liquid chromatography), all these parameters must be considered and are crucial to obtain a robust and reliable method. Moreover, in order to obtain a more efficient chromatographic method and improve the cleaning of the sample, it is possible to change the ordinary chromatographic system, using for example a bidimensional system.

Bidimensional chromatography (2D) is a type of chromatographic technique in which the injected sample is separated by passing through two different separation stages. Two different chromatographic columns are connected in sequence, and the effluent from the first system is transferred onto the second column [1]. Typically the second column has a different separation mechanism, so that bands that are poorly resolved from the first column may be completely separated in the second column [115].

The beginning of comprehensive two-dimensional liquid chromatography can be defined in two papers: the first one of 1978 where Erni and Frei [116] described the two-dimensional separation of a Senna-glycoside extract. Then, in 1990 Bushley and Jorgenson

[117] showed a two-dimensional liquid chromatography separation of a proteins sample, the full separation took six hours.

Nowadays, two-dimensional separations are a trend in chromatography. In online 2D-LC the effluent from the first column is injected into the second column immediately after it is collected. This form of 2D-LC is the fastest and can be fully-automated. Instead, in the offline form of 2D-LC the fractions of the effluent coming from the first column are collected and stored before they are subjected to the second column separation. Naturally, this results in a longer overall analysis time compared to the online chromatography.

In this work thesis it was developed an innovative online 2D fluidic system, the mode of operation is reported in detail in the materials and method section.

1.4.2 Principles of mass spectrometry

A mass spectrometer is a device able to measure the mass-charge ratio of charged particles (*m/z*). It consists of four components (as reported in Figure 10):

- sample inlet that mediates the transition of a solid or liquid sample into gaseous phase;
- an ionization device to vaporize bio-samples;
- an ion path to transfer ions from atmospheric pressure to high vacuum of the actual mass analyser and to the detector;
- an ion detector to detect and quantify ions.

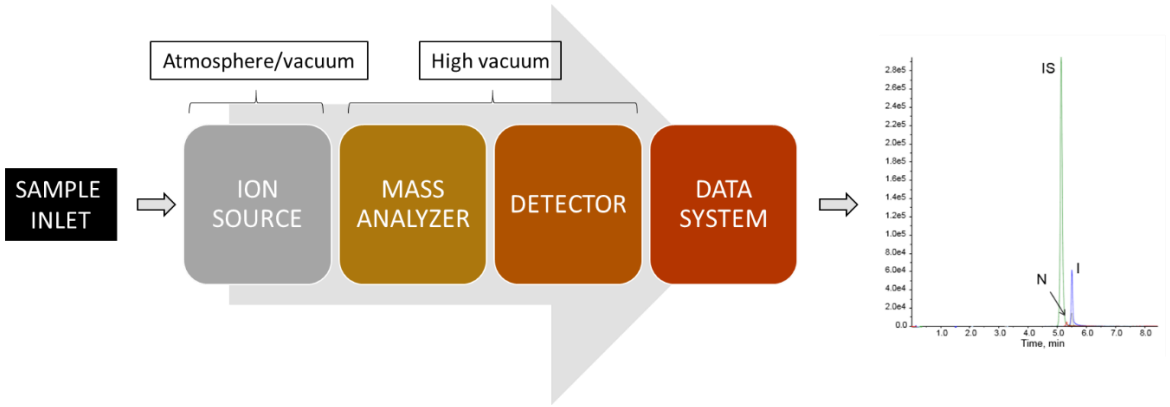

Figure 10. General scheme of a mass spectrometer.

A variety of ionization techniques are used for MS, some of them are very energetic and cause extensive fragmentation, an example of these so called “hard” sources is the electron ionization (EI). On the other hand, the so called “soft” sources only produce ions of the molecular species, such as chemical ionization (CI), and atmospheric pressure ionization sources like APCI (atmospheric-pressure chemical ionization) and ESI. Matrix-assisted laser desorption ionization (MALDI) source also belongs to the “soft” sources category and it is applied for the production of intact gas-phase ions from a broad range of large, non-volatile and thermally labile compounds such as proteins, oligonucleotides, and synthetic polymers.

MALDI and ESI are now the most common ionization sources for biomolecular mass spectrometry, offering excellent mass range and sensitivity. Since in LC-MS/MS methods reported in this thesis an ESI source was used, details of its operation mode are reported below.

ESI source produces gaseous ionized molecules directly from a liquid solution. In order to be analysed, the compound is previously dissolved in a volatile MP and then it is let to flow into a stainless-steel capillary called probe. Between the probe and its counter-electrode, a voltage (2-5 kV) is applied that allows to the formation of the Taylor’s cone (a nebulized solution) just outside the capillary. Its formation is due to the presence of charged species within the solution subjected to the electrostatic field existing between the capillary and the counter-electrode. After that, the droplets formation is observed from the cone apex and charged droplets further migrate through the atmosphere to the counter electrode. Droplets formation is strongly influenced by solvent’s chemical-physical characteristics, ionic analytes concentration, inorganic salts concentration, and the applied voltage. Either dry gas (nebulizer gas, that flows longitudinally along the capillary perimeter), heat (coming from the sides) or both are applied to the droplets at atmospheric pressure and this cause the solvent evaporation from each droplet. Thus, the droplets decrease their radius, still conserving their charge amount. As the droplet size decreases, the surface charge density rises until the droplet radius reaches the stability limits of Rayleigh, meaning that the electrostatic repulsion equals the surface tension [118]. Overcome that limit, the charged droplets are unstable and decompose through the process called "Coulombic explosion" [119] thus producing microscopic droplets

which, at the end of the process, release desolvated ions. The produced ions are then directed into an orifice through electrostatic lenses leading to the vacuum of the mass analyser.

ESI is conductive to the formation of singly charged small molecules but it is also well-known for producing multiply charged species of larger molecules. This is an important phenomenon because mass spectrometer measures the *m/z* ratio and consequently multiple charging makes the observation of large molecules possible even using an instrument with relatively small mass range (Figure 11). Many solvents can be used in ESI: they are chosen based on the solubility of the analytes, the volatility and the solvent's ability to donate a proton. Typically, solvents such as water, methanol (MeOH) or acetonitrile (AcN) are used, but other solvents, as dimethyl sulfoxide (DMSO) or isopropyl alcohol, could be employed to increase the solubility of the analytes. In some cases, the use of the 0,1% of acid (acetic or formic) is also advisable to facilitate the ionization. Buffer like Na^+, K^+ or phosphate present a problem in ESI by lowering the vapor pressure and the volatility of the droplets resulting in a reduced signal through a droplet surface tension increase. Therefore, volatile buffers such as ammonium acetate can be used more effectively.

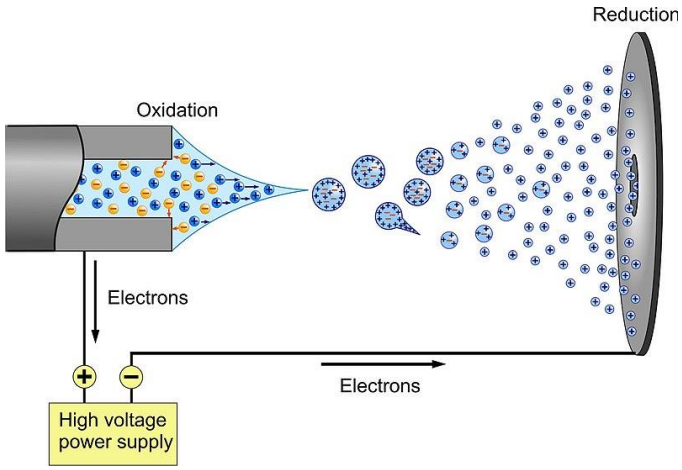

Figure 11. Diagram of electrospray ionization in positive mode. Adapted from [120].

With the advent of ionization sources that can vaporize and ionize biomolecules, it has become necessary to improve mass analyser performances with respect to speed, accuracy and resolution.

Several types of mass analysers have been developed since the separation of ions, according to their *m/z* ratio, and they can be based on different principles. While all mass

spectrometers rely on a mass analyser, not all analysers operate in the same way; some separate ions in space while others separate ions by time. In general, a mass analyser measures gas phase ion with respect to their *m/z* ratio, where the change is produced by the addition or loss of a proton, cation, anion or electron. For instance, time-of-flight (TOF) analyser discriminates ions according to their velocities when they drift in a free-field region. The quadrupole analyser consists on a device which uses the stability of the trajectories in oscillating electric fields to separate ions according to their *m/z* ratios. The ion trap analyser works by using a radiofrequency (RF) quadrupolar field that traps ions in two or three dimensions: ions of different masses are present together inside the trap and are expelled according to their masses to obtain the spectrum. Whereas, the analyser based on magnetic sectors selects the ions according to their momentum, given a specific value of magnetic field and a circular trajectory. Also, some mass spectrometers combine several types of analysers.

Among these types of analysers, coupled to an ESI-type source to perform tandem-in space MS analysis for quantitative purposes, a triple quadruple can generally be found.

This type of analyser consists in a system of three quadrupoles in series: the first and the third ones are filters able to discriminate ions with a specific *m/z* value, while the second one is a collision cell where a controlled fragmentation takes place. A quadrupole is composed by four parallel metal rods and each opposite rod pair is connected electrically (Figure 12). A two components (RF and direct-current (DC)) voltage is applied between adjacent rods: a wide range of *m/z* ions will pass through the quadrupole if only the RF component is applied, allowing to focus the ions.

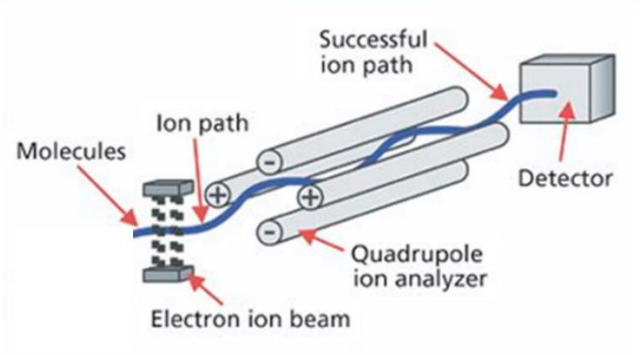

Figure 12. Graphic representation of a quadrupole ion analyser.

To select a group of ions with a specific *m/z* value, a DC voltage is added the RF voltage. In this way, the "wrong" ions (with a higher or lower *m/z* values) will be lost by colliding against the rods due to unstable trajectories, while the "correct" ones are allowed to pass the quadrupole (Figure 13). To acquire a mass spectrum, it is necessary to increase both the DC and RF voltages, while keeping their ratio constant, in a way that a certain mass range could be scanned to transmit ions of increasing *m/z.*

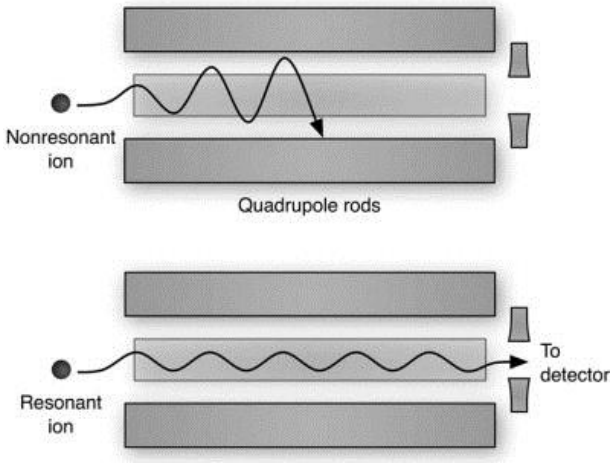

Figure 13. Representation of the functioning principle of a quadrupole mass analyser. The ion whose *m/z* does not lead to a resonance undergoes a collision against one of the four rods thus not being revealed. The resonant ion, instead, will be able to pass through the quadrupole and be recorded by the detector [121].

Depending on the analysis purpose, the first (Q1) and the third (Q3) quadrupole can be used in different modes to acquire the data. In tandem mass spectrometry (MS/MS or MS^2), the configuration of the instrument allows the controlled fragmentation (also called collision-induce dissociation or CID) of the analyte in the collision cell, represented by the second quadrupole (Q2). Before Q1 there is the Q0, which is a smaller quadrupole equipped only with RF and not with DC, characterized by an ion focusing function.

Through the MS/MS it is therefore possible to obtain information both on the mass of the analyte of interest (parent or precursor ion) and on that of the fragments (product ions) generated by its fragmentation by applying an appropriate collision energy to the cell. Generally, the *m/z* value of an analyte could be considered an information about its identity, but, especially in the case of low-resolution MS, the highest specificity is obtained by considering also the analysis of its fragmentation pattern. Indeed, for each substance, its fragmentation pattern is a sort of proper fingerprint.

Examples of the most prevalent uses of MS/MS in clinical diagnosis are: the screening of new-borns for congenital metabolic diseases such as aminoacidopathies, organic acidurias, and fatty acid oxidation disorders [122, 123]; multi-analyte TDM especially for the administration of cocktail therapies involving immunosuppressants [124], oncology drugs [125], anti-virals [126], etc.

The most obvious factor responsible for the limited throughput of LC-MS/MS is the time required for sample introduction into the LC and the subsequent time necessary for chromatography. Once a chromatographic system has been fully optimised to minimise the time needed to remove interferences and to separate analytes from solvent fronts, there is no space for further improvement in throughput from a chromatographic standpoint.

1.4.3 Validation of a LC-MS/MS method

To be used for the quantification of one or more substances in biological samples an LC-MS/MS method needs to be validated according to the FDA [127] or EMA [128] guidelines for the validation of a bioanalytical method. The main goal of method validation is to demonstrate the reliability of a particular method developed for the quantification of an analyte concentration in a specific biological matrix, like blood, serum, plasma, urine or saliva. The main characteristics that a bioanalytical method needs to ensure the acceptability of the performance and the reliability of the analytical results are: selectivity, lower limit of quantification (LLOQ), calibration curve performance, accuracy, precision, matrix effects and stability of the analytes both in biological matrix and in stock and working solutions.

There are three different types and levels of methods validation:

- full validation: for a new method, a new drug entity or a revision to an existing method that add metabolite quantification;
- partial validation: method transfers between laboratories, changing in sample processing or concentration ranges, etc;
- cross-validation: comparison of validation parameters when two or more bioanalytical method are used to generate data within the same study or across different studies.

1.5 TDM performed using dried blood spot

As reported before, TDM supported by LC-MS/MS is the strategy currently used to quantify the drug in patients. Many validated methods for performing TDM by mass spectrometry in serum or plasma have been developed [129]. Nevertheless, sample collection remains the main limitation for a routine use of TDM in clinical practice. It requires medical or nurse support, blood centrifugation and accurate sample storage before measurement. These limitations hamper most of the published TDM methodologies to be translated in a cost-effective and patient-friendly routine diagnostic tool. Dried blood spot (DBS) collection through finger prick is an attractive option in this scenario [130].

Robert Guthrie in 1963 introduced the DBS technique for screening [131]. Although the particular assay is now defunct, the term “Guthrie card” remains to colloquially describe the DBS collection technique. The first application of mass spectrometry to DBS analysis was reported 40 years ago (in 1976) for fatty acid determination by direct chemical ionisation [132].

To date, DBS have a range of applications in clinical practice, basic research, and population-based research. The most common and widely accepted clinical use of DBS is for new-born screening programs, which are primarily concerned with the detection of metabolic disorders [133]. Other clinical applications in the published literature have focused on HIV surveillance, TDM, and clinical chemistry [134]. Basic research applications for DBS include biomarker development and validation, drug discovery and development, forensic science, systems biology, and toxicology [135, 136]. Population-based research applications are variable but may be broadly categorized into human epidemiological studies and environmental population studies [137, 138].

Compared with conventional venous blood sampling, DBS is a convenient and simple sampling method with better patient comfort. In DBS sampling, capillary blood is obtained from a simple finger prick with an automatic lancet. With clear instructions and after adequate training, patients should be able to do this finger prick themselves at their home. After disinfection, the patient pricks his/her finger with the lancet. The first blood drop is discarded because it contains more tissue fluid, the next drop is collected to fill on

the filter paper. The DBS is allowed to dry at room temperature (RT) and then is packed for transportation to the laboratory. In the laboratory, the homogeneity of the blood spot is assessed, and a disc is punched out from the blood spot and is extracted. After extraction, the analyte is measured with an analytical technique, as shown in Figure 14.

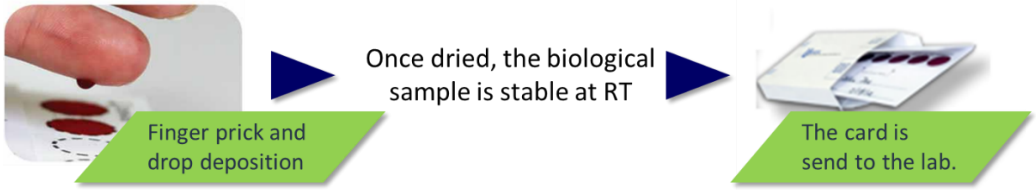

Figure 14. Graphical representation of how the DBS technique works.

The advantages of this techniques are as follows:

- easy and minimally invasive sampling: patients can perform the finger prick at home.
- only a small volume is required. In respect to that, one of the original projected advantages of using DBS technology was the easy implementation for small sample volume collection from finger and heel pricks in young children and neonates.
- most analytes are more stable in DBS than in frozen samples [139, 140].
- convenient storage and transport: DBS specimens can be shipped or transported with no reasonable expectations of exposure to blood or other infectious material by handlers [141].

On the other hand, DBS technique presents also some disadvantages:

- only small volumes are available and therefore a sensitive analysis technique is required.
- despite adequate training of the patient, the sampling is not always successful: self-sampling could be associated to contaminations and samples with unacceptable quality.
- extensive validation is required. The impact of variations of haematocrit (Hct) values on the spot size and homogeneity should be understood as well as their impact on assay performance. Any change in filter paper type and/or manufacturer requires a partial validation [142].

- capillary concentration can be different from venous concentration because the material in DBS consists of blood cells, plasma, and interstitial fluid [143].

Many assays in DBS have been reported in the literature over the previous years, only two of them including IMA [144, 145]. Both papers report the possibility to correlate the IMA concentrations found in DBS with those related to plasma, applying specific adjustments (Hct or correction factor). Anyway, neither the method proposed by Kralj et al. nor the one presented by Antunes et al. have taken in consideration the quantification of norIMA, IMA main metabolite.

1.6 TDM and biosensors

Since their discovery by Leland C. Clark, Jr. in 1962 [146], biosensors have revolutionized not only the field of health care, but also food and environmental monitoring and so, have greatly improved the quality of our life. The most popular devices are the glucose monitoring and the pregnancy test, while other devices including infectious disease, cardiac markers, lipids coagulation and haematology are mainly used by clinicians [147]. During the past 50 years, the number of developed biosensors has been considerably increased, to achieve a healthcare more focussed around the patient. The increasing interest in biosensor in the field of modern analytical chemistry is evident both from the number of published articles and from the numerous applications approaches and techniques, Figure 15.

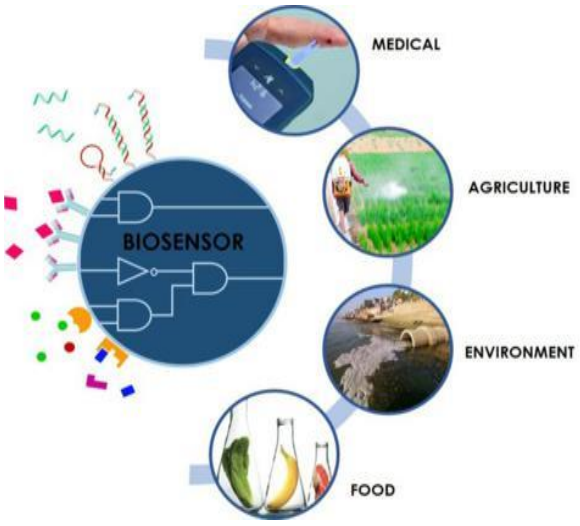

Figure 15. Application fields of biosensors. Adapted from [148].

In addition to the use of LC-MS/MS as tool for TDM analysis, other useful techniques, like the application of biosensor in the clinical routine to monitor drug concentrations in blood samples during chemotherapy, could be crucial to improve patient's life quality.

In fact, as said before, TDM applied in oncology treatments is still complex and demanding. It requires pre-analytical precautions, thorough clinical data recording, shipment to a distant laboratory, analysis using sophisticated and costly apparatus, delivery of results after a significant delay and potentially complex interpretation of the data obtained, requirement of a specialized nurses and technical scientist. Technological developments towards the miniaturisation of monitoring tests and their delivery at point-of-care based in biosensor might well represent a future approach to make TDM in cancer more feasible.

Biosensors are devices capable to detect specific biological analytes and converting their presence or concentration into signals that can be easily detected and analysed.

All biosensors can be divided into three main components, as graphically reported in Figure 16: a recognition element that binds specifically the interested analyte; a signal transducer that converts the biological signal into an electronical output; and a signal processor that relays and displays the results [149].

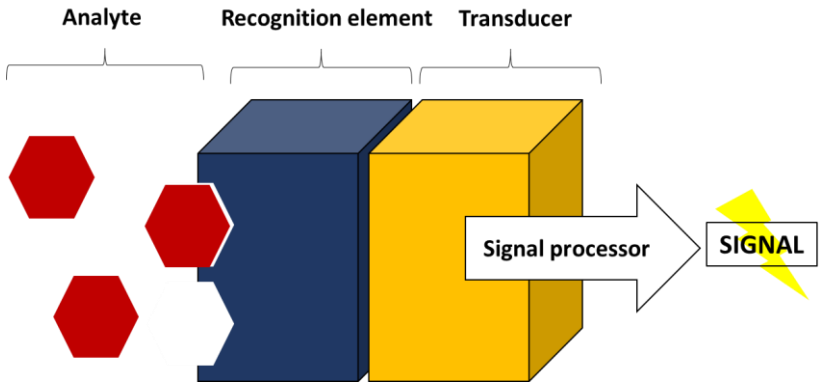

Figure 16. Graphical scheme of the components of a biosensor and how it works.

The central part of a chemical or biological sensor is the recognition element, which is at narrow contact with a suitable transducer. The recognition element is responsible for specific recognition and interaction with the target molecule, often present in a complex sample (ex: blood). In biosensors, recognition elements correspond to biological entities such as antibodies, enzymes, receptors or whole cells. In recent years there have been

numerous attempts to replace natural receptors with smaller and more stable counterparts. This has led, for example, to the development of fragments of antibodies created through bioengineering, or the development of semi-synthetic biosensor receptors such as nucleic acids and peptides [150]. However, in general, the little chemical and physical stability of biomolecules sometimes prevents their use in harsh environments, although in principle they are very favoured for the biosensors design.

An alternative approach consists in the use of biomimetic receptor systems able to bind target molecules with affinities and specificities comparable with those of natural receptors. A technique, that in recent years has been adopted more and more frequently, is the molecular imprinting in synthetic polymers. The binding sites that are generated during the imprinting process often possess affinities and selectivity that is similar to those of the antibody-antigen systems. Therefore, molecular imprinted materials have been nicknamed as "antibody imitators" or antibodies artificial [151]. These imitators show some clear advantages over real antibodies for sensory technology: due to their cross-linked polymeric nature, they are stable and robust intrinsic mode, thus facilitating their application in severe environments, such as the presence of acids and bases, organic solvents or high temperature or pressure conditions. Moreover, these materials are cheap and can be stored in solid form for long periods of time.

1.7 Molecularly imprinted polymers

Molecular imprinting is an emerging technology which enables us to synthesize the materials with highly specific receptor sites towards the target molecules.

The first scientific mention of molecularly imprinted polymers (MIPs) dates back almost 100 years, precisely in 1931 with M. V. Polyakov, a scientist who discovered that when he made polymers out of silica in the presence of another molecule, the polymers would selectively absorb that molecule. Another important goal was achieved in 1949 with Jean Dickey at *Cal Tech* who imprinted silica with organics compounds [152].

MIPs are a class of highly cross-linked polymer that can bind certain target compound with high specificity. The concept behind the formation of the selective binding sites is schematically shown in Figure 17. In brief, in a general molecular imprinted method, the template (target analyte) is added along with the functional monomer and high

proportions of cross-linker, which are polymerized under proper conditions. During the reaction, the polymeric chains self-organized around the template through functional group interactions. The template molecule can be then removed or washed from the polymeric matrix. This lead to obtain binding cavities with a complementary geometrical and chemical fitting structure of the template, and these pockets are also capable of reversibly interaction (usually hydrogen bonds, dipole-dipole and ionic interactions) with the target molecule [153].

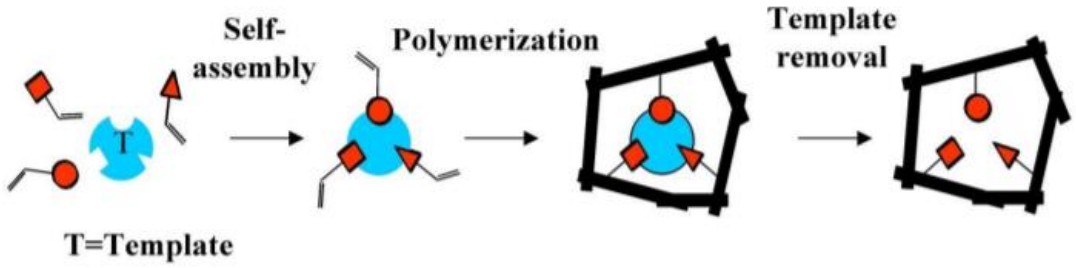

Figure 17. Schematic representation of the imprinting process.

According to the review of Vasapollo et al. [154] MIPs have higher physical strength, robustness, resistance to elevated pressure and temperature and inertness against various chemicals (organic solvents, acids, bases, and metal ions) compared to biological media such as proteins and nucleic acids. Furthermore, their production costs are low, and their lifetimes can be of several years at RT. All these advantages make them attractive for numerous applications. A wide range of chemical compounds have been successfully imprinted, ranging from small molecules, such as drugs, to large proteins and cells. The best results have been obtained for molecules with molecular weights in the range of 200–1200 Da. The resulting polymers are robust, inexpensive and, in many cases, possess affinity and specificity that is suitable for industrial applications.

For example, Lotierzo et al. reported that his MIP system, for the detection and quantification of domoic acid, was able to outperform monoclonal antibodies , with a broader detection range and better long term stability [155]. Tan Y. et al. described the fabrication of a bio-mimetic bulk acoustic wave sensor for paracetamol by using MIPs as sensing materials [156], and in Rachkov A. et al. paper it is defined a fluorescence sensing system for the determination of β-estradiol using MIPs [157].

These are just examples, but MIP technique is nowadays applied in many fields: to recognize biological and chemical molecules including proteins, pollutants, drugs and food; in the separation sciences and purification, in chemical sensors, drug delivery and so on [158–160]. Moreover, MIP receptor materials have already been demonstrated for a wide range of clinically relevant compounds and diagnostic markers [161].

The functional monomer (FM), that interacts with the template during molecular imprinting, can be selected according to two different approaches, in particular the recognition phenomena nature could be based on: weak non-covalent or covalent bonds. The so-called non-covalent or self-assembly protocol is currently the most commonly employed, since it is relatively easy to put into practice, and rather flexible since a large number of FMs, able to interact with almost any kind of target molecule, are available [162]. In this process, originally developed by Mosbach [163], FMs are positioned in a particular orientation with respect to the template prior to polymerization. The number of non-covalent interaction must be enough to allow the organization of the binding pocket during polymerization. Moreover, the use of a cross linking FM during polymerization allows to create a three-dimensional rigid structure around the template molecule and produces stable binding cavities.

In this thesis, the polymers synthesis was conducted exploiting the non-covalent approach. In this case the template-monomer complex is formed by association of non-covalent forces like hydrogen bonds dipolar interactions, van del Waals forces, ion pair and dipole-dipole interactions. The advantages of the non-covalent approach include the requirement of milder polymerization conditions and easy template removal. On the other side, one of the hitches in using this technique is that the interaction sites are not uniformly distributed over the polymeric system, which often leads to nonspecific interactions [163]. Another limit is set by the peculiar molecular recognition condition. In fact, most of the formed interactions between monomer and template are stabilized under hydrophobic environments while a polar environment can easily disrupt them. Moreover, the association between the monomer and the template is governed by an equilibrium. This gives rise to a number of different configurations of the template-FM complex, leading to a heterogeneous binding site distribution in the final MIP [164].

In imprinted polymers technique there are different methods for synthesizing the MIPs and also for tuning the functionalization of the interaction sites.

In the thesis work hereby presented was used the free radical polymerization, that involves the simplest process to prepare MIPs. This type of reaction is quite rapid, it is started by an azo-initiator, commonly azo N-N'-bis isobutyronitrile (AIBN), in Figure 18, and by thermal or photochemical initiation.

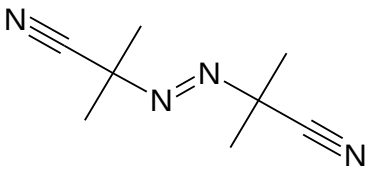

Figure 18. Chemical structure of AIBN.

The main steps that could be distinguish in the radical polymerization process are: initiation, propagation and termination. During the initiation step the production of free radicals occurs by homolytic dissociation of the initiator giving a pair of radicals. Consequently, the addition of one of these radicals to the first monomer molecule occurs, thus producing the initiating radical chain. The propagation step consists on the growth of the initiating radical chain by the consecutive addition of a large numbers of monomer molecules in sequence. These chains, as their weights increase, have an increasing probability to combine with another oligomer chain, rather than a single monomer, thus leading to the third and last step that is the termination. The polymer stops growing through the annihilation of the radical centres by a reaction between two radicals that could occurs by coupling. This random addition of various chain lengths results in a divergent reaction with thermodynamic equilibrium forces dictating ultimate polymer weight and particle size.

The rational design of MIPs is quite complicate due to a number of experimental variables, such as the template, the functional monomer, the functional monomer/template/cross-linker/solvent, etc.

The FM choice is crucial in order to create highly specific cavities designed for the template molecule. Typical FMs are carboxylic acids, sulphonic acids, heteroaromatic bases. The extensive use of methacrylic acid (MAA, structure reported in Figure 19) is due

to its capability to act both as hydrogen bond and proton donor and as hydrogen bond acceptor.

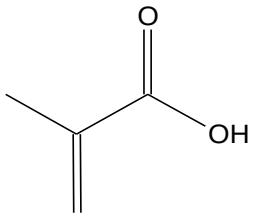

Figure 19. Structure of methacrylic acid (MAA).

Moreover, the cross-linker fulfils important functions. It is important to control the morphology of the polymer matrix, helps to stabilize the imprinted binding sites and imparts mechanical stability to the polymer in order to retain its molecular recognition capability [165]. The solvent nature and volume play an important role in molecular imprinted process: it helps to bring all components in solution and it is responsible for creating the pores in microporous polymers [154].

Besides, the solvent provides an in situ scafford, around which a pore can be formed during polymerization [166]. The presence of a non-reactive solvating medium facilitates the mixing and complexation of the template and the FM, and thus the subsequent formation of template-specific imprinted binding sites.

For their insoluble nature, MIPs are quite difficult to characterize. However, some analytical techniques can be utilized to obtain the chemical and morphological characterization. Morphological characteristics of MIPs can be properly investigated by microscopy techniques, as transmission electronic microscope (TEM) and using dynamic light scattering (DLS) technique for the size characterization. A very important level of characterization for MIPs concerns the molecular recognition behaviour, such as the binding capacity. One of the best methods for evaluating binding capacity and selectivity is performing a so-called rebinding test using HPLC coupled to an UV or MS detector.

2. AIMS OF THE PROJECT

TDM is the clinical practice of measuring a specific drug at defined intervals of time to maintain plasma concentrations within a targeted therapeutic window, to maximize efficacy and minimize toxicity. Unfortunately, this parameter is characterized by inter-individual variability in treatment outcome thus indicating the need of a personalized approach for anticancer therapy. On these bases, the PhD project presented hereby aims to develop techniques to perform the TDM of anticancer drugs exploiting different strategies.

Above all, the work done was focused on IMA, an oral potent TKI indicated as first-line treatment for patients with inoperable, metastatic or recurrent GIST. The introduction of this drug has dramatically changed GISTs treatment, transforming them, in some cases, into chronic diseases that can be treated at home.

Despite the unquestionable advantages brought by IMA in GISTs treatment, some limitations are still related to this drug. In particular, IMA shows a high interpatient variability in plasma exposure (which might affect the therapy outcome), but it is still administered following standard doses. Moreover, a relationship between IMA plasma-exposure and treatment outcome has been supposed. For these reasons, there is a strong recommendation to perform TDM, that could be useful to identify possible cases of suboptimal response, presence of severe toxicity, drug-drug interactions, cases of non-adherence to therapy, and, thus, personalize the therapy.

In this context, the first aim of my PhD project was the development, validation and cross-validation of a LC-MS/MS method for the simultaneous quantification of IMA and its active metabolite, norIMA, C_{min} in GIST patients. To reduce the sampling time and costs and to improve patient's compliance, this method was developed exploiting the DBS technique, that aims to perform the quantification of the two analytes directly on a drop of blood from a finger-prick. The method was developed optimizing both the spectrometric and chromatographic conditions but also the sample processing for an accurate and precise analysis and it was then validated according to FDA and EMA guidelines. After that a total of 67 GIST patients' samples were quantified to check the method performance and to cross-validate it with a "reference" one (i.e. a LC-MS/MS method in-house developed for the quantification of these analytes in plasma samples). Patients' were enrolled in a

clinical study ongoing at the National Cancer Institute of Aviano, (EudraCT N. 2017-002437-36, internal code: CRO-2017-19).

Despite the LC-MS/MS is considered the election technique for TDM analysis, it is quite expensive and it needs trained personnel.

Thus, the development of a point of care device usable at the bed side of patients by non-specialized personnel that can replace standard LC-MS/MS technique for the quantification of drug concentrations in biological fluids could represent a turning point for TDM of anticancer drugs, such as IMA.

Thus, the second aim of my PhD project was the development of a quantification system based on IMA recognition by polymeric receptors and its fluorometric detection. With this purpose, MIPs were synthesized, exploiting the non-covalent approach, and characterized using different techniques: ^{1}H-NMR to perform the monomer conversion studies, the DLS to evaluate the particle size, the rebinding tests to estimate the polymers affinity for the template and, finally, cross-reactivity tests, to evaluate the selectivity of MIPs for IMA versus other drugs.

This part of the thesis was carried out in the laboratory of prof. Federico Berti (Dept. Of Chemical and Pharmaceutical Sciences, University of Trieste), and in the laboratory of prof. Marina Resmini (School of Biological and Chemical Sciences, Queen Mary University of London), for an overall secondment of 6 months.

Finally, in order to apply TDM approach to a new class of drugs used in breast cancer therapy, the third aim of my project was the development and validation, according to FDA and EMA guidelines, of a LC-MS/MS method for the simultaneous quantification of RIBO, PALBO and LETRO in human plasma. RIBO and PALBO are small CDKIs indicated for the treatment of HR-positive, HER2-negative locally advanced or metastatic breast cancer in combination with an aromatase inhibitor, such as LETRO. TDM recommendation for these drugs is currently only exploratory, based on limited exposure-response and -toxicity studies. The developed method was then applied to quantify the C_{min} of the three analytes in patients' plasma samples to support a clinical study (internal code: CRO-2018-83) on-going at the National Cancer Institute of Aviano.

3. MATERIALS AND METHODS

3.1 LC-MS/MS method development for the simultaneous quantification of IMA and norIMA in DBS

The hereby method has the aim to perform a quantitative analysis of IMA and its active metabolite norIMA in DBS using an LC-MS/MS apparatus.

The development of this method followed three main steps of instrumental optimization that were necessary to achieve the best sensitivity and selectivity towards these two compounds:

1. the optimization of the mass-spectrometric conditions (see section 3.1.2) to achieve the best signal-to-noise ratio (SNR) for the analytes of interest;
2. the optimization of the chromatographic conditions (see section 3.1.3), to obtain the best selectivity and minimize the matrix effect due to other interferents present in plasma (e.g. salts, phospholipids);
3. the optimization of the sample preparation workflow (see section 3.1.4), to obtain a fast and reliable sample extraction method of interested analytes from the paper.

3.1.1 Instrumentation

The LC-MS/MS methods reported in this thesis work have been developed using a LC Nexera system (Shimadzu, Tokyo, Japan) in-house configured for the on-line clean-up. It included an autosampler, a binary pump, a column oven and an additional pump module for the trapping step. The LC system was coupled with an API 4000 QTrap (SCIEX, Massachusetts, USA), a mass spectrometer characterized by a Turbo IonSpray (TIS) source and a triple quadrupole analyser. To quantify analytes, data were processed using Analyst 1.6.3 and the chromatographic peaks were integrated with Quantitation wizard (software package SCIEX).

The plasma separation from whole blood samples was performed with a 5810R centrifuge while a 5427R benchtop centrifuge (Eppendorf, Hamburg, Germany) was adopted for the centrifugation which completes the protein precipitation procedure. Analytical standards powders were accurately weighted with a Mettler Toledo DeltaRange XPE205 analytical balance (Columbus, Ohio, USA). For the experiments involving DBS technique was used the water bath Clifton (Nickel-Electro Ltd., Weston-Super-Mare, UK) to homogenise the drug added in whole blood samples. Working solutions and biological samples were handled with a Pipetman set composed by P1000, P200, P100, P20, P10

and P2 pipettes all purchased from Gilson (Villiers-le-Bel, France). During the analysis, samples were kept in autosampler polypropylene vials with PTFE caps purchased by Agilent Technologies (Santa Clara, California, USA).

3.1.1 Standards and chemicals

Imatinib mesylate, norimatinib (des-methyl imatinib) free base and *d8*-imatinib mesylate (used as internal standard) were supplied by TRC (Toronto, Canada). Ammonium acetate, and formic acid (HCOOH) (analytical grade) were bought from Sigma-Aldrich (Milano, Italy). DMSO was supplied by Alfa Aesar (Ward Hill, MA-USA). AcN and iPrOH, (both LC-MS grade) were obtained from Merck (Rome, Italy) while LC-MS grade MeOH was purchased from Carlo-Erba (Milano, Italy). LC-MS grade water was in-house produced through a Millipore system (Merck Rome, Italy). Control human blood, used to prepare daily standard calibration curves and quality control (QC) samples, was collected in K-EDTA-Monovette of Sarstedt (Nuembrecht, Germany) and provided by the transfusion unit of the National Cancer Institute (Aviano, Italy) from healthy volunteers. Corresponding Hct values were measured at central lab with an Advia system (Siemens Medical Solutions Diagnostics Zurich, Switzerland). 31ET-CHR and 903 filter papers were supplied by GE-Whatman (Little Chalfont, UK).

3.1.2 Mass spectrometric conditions optimization

To achieve the best SNR and the greatest sensitivity for the analysed compound, two types of parameters had to be tuned:

- the compound-dependent parameters, which must be optimized individually for each compound based on its ionization efficiency and fragmentation pattern;
- the source-dependent parameters, which are dependent on the mobile phase composition and the flow rate.

3.1.2.1 Compound-dependent parameters optimization

First, to optimize all the compound-dependent parameters, three solutions, one for each analyte (IMA, norIMA and ISt) were prepared in MeOH with 0.1% HCOOH (v/v) at a concentration of 100 ng/mL. Each solution was directly infused to the TIS source at a flow rate of 20 µL/min and, for each analyte, the following procedure was performed.

With the HPLC disabled, the spectrometer configured in manual tuning mode and all source-dependent parameters set to default values, the first step consisted in the analyte presence

confirmation by the identification of its protonated molecule $[M+H]^+$. Then the spectrometer was set in Q1MS mode and other two parameters were optimized (in Figure 20 is reported a graphical representation of the mass spectrometer):

1. Declustering potential (DP), that controls the potential difference between Q0 and the orifice plate to minimize the cluster formation;
2. Entrance potential (EP), that controls the potential which guides and focused the ions through the high-pressure Q0 region. By ramping the DP from 20 to 150 V, the intensity trend of the XIC was monitored to choose the most correct DP value for the pseudo-molecular ion. This because too low DP values will result in lower ion intensity due to interferences from clusters, while too high values might cause an in-source fragmentation.
   The optimal EP value (in a range of 1-15 V) was determined in the same way, even if it is often left at 10 V (i.e. the default value) without any impact on analyte detection limit because EP has a minor effect in compound optimization. Finally, the remaining parameters were defined:
3. Collision energy (CE), that controls the potential difference between Q0 and represents the energy that the precursor ion receives once accelerated into Q2, where it collides with gas molecules and other fragments;
4. Collision cell exit potential (CXP), that controls the potential which focuses and accelerates ions existing Q2, it is the potential difference between Q2 and ST3 (a lens that separates Q2 and Q3).

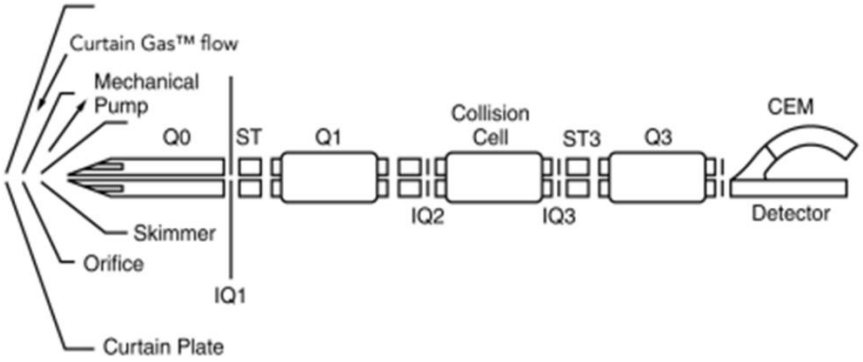

Figure 20. Graphic representation of the mass spectrometer.

To define these parameters the three quadrupoles were exploited in MS/MS configuration. First, an analysis of the fragmentation pattern was carried out for each compound with the spectrometer settled in product ion mode (MS2). In this mode the Q1 filtered only the pseudo-molecular ion, also

called precursor ions, which was fragmented in Q2 and a scan of all fragments (product ions) was performed by Q3 (Figure 21).

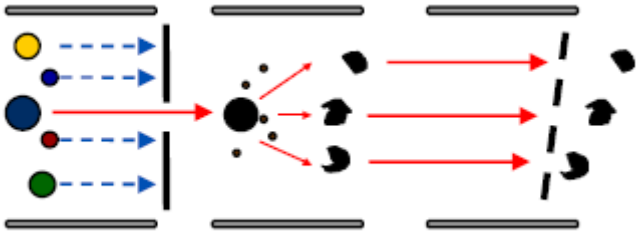

Figure 21. Schematic representation of the triple quadrupole analyser in MS2 configuration.

In this way, for each analyte, a first evaluation of the most representative fragments was carried out. Once the main fragments had been selected, the optimal CE value was simultaneously determined for each of them by setting the spectrometer in multiple reaction monitoring (MRM) mode and the spectrum was recorded by increasing the CE value during the time from 10 to 100 V. The resulting spectrum showed the XIC intensity for each transition in line with the rise of the CE values. The transition with the highest signal intensity was selected as the most suitable for the quantification, while the other one had the function of "qualifiers" to increase the specificity for the analyte of interest. The optimal CE value for each transition is the one at the apex of the XIC signal curve. A similar experiment was carried out by ramping the CXP value, while CE was set at its optimum value for each transition.

3.1.2.2 Source-dependent parameters optimization

Source-dependent parameters can be optimized based on only one analyte. For this reason, it is necessary to choose the most important compound among those that need to be quantified. In our case, a solution of IMA (100 ng/mL) was prepared in acidic MeOH (0.1% HCOOH) and was directly infused to the TIS source (flow rate of 20 µL/min) into a flowing MP coming from the HPLC pumps. The composition of the MP was 50/50 between A (MPA: 2 mM ammonium acetate aqueous solution with 0.1% HCOOH) and B (MPB: AcN-iPrOH 80:20 containing 0.1% HCOOH) and the flow rate was 400 µL/min and the mix with the IMA solution injected was achieved through a tee union. Another union was used as a substitute for the chromatographic column, which was not necessary for this workflow. The whole configuration had the function to mimic the real working conditions of the LC-MS/MS apparatus.

The parameters that were optimize in this step are the following:

- Curtain gas (CUR): controls the curtain gas pressure, which flows between the curtain plate and the orifice preventing the contaminations of the ion optics;
- CAD gas (CAD): controls the gas collision pressure in Q2;
- IonSpray Voltage (IS): controls the voltage applied to the needle that ionized the sample, to guarantee the spray stability for all the samples;
- Temperature (TEM): controls the turbo gas temperature;
- Gas 1 (GS1): controls the nebulizer gas pressure, which helps to generate small droplets of sample flow;
- Gas 2 (GS2): controls the turbo gas pressure, which has the function of helping the evaporation of the spray droplets and avoiding solvent entrance into the analyser.

To optimize these parameters, the first step consisted in launching a selected reaction monitoring (SRM) with the HPLC enabled and the spectrometer configured in manual tuning mode. The result was a XIC (selected ion current) signal, with a constant intensity. By manually varying each source-dependent parameter, a XIC intensity change was observed.

The goal of this optimization was to reach the maximum signal intensity in order to achieve the greatest sensitivity for the quantification method.

3.1.3 Chromatographic conditions optimization

The development of the chromatographic method implies the determination of the best chromatographic conditions to obtain: good separation of the two analytes (resolution), peaks with good symmetry, good control of the carryover and minimum analysis time. These conditions allow an analytical method to be selective and sensitive.

The first parameter to consider in the chromatographic method development is the column choice that depends on the physicochemical properties of analytes (type of SP), the number of compounds to be analysed (column length) and required resolution (column particle size). Once the SP had been selected, the choice of the column temperature, the flow rate and the MP composition were the next important step.

For this work of thesis an innovative fluidic system for the chromatographic separation was developed, which consists on an online bidimensional chromatography (2D-LC), graphically reported in Figure 22.

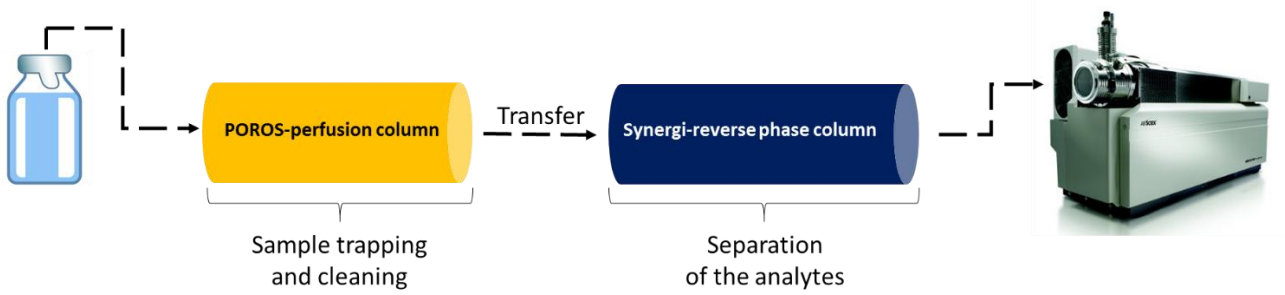

Figure 22. Graphical representation of the online bidimensional chromatography**.**

The first column was a perfusion column, POROS R1/20 (ThermoFisher), that performs a size-exclusion chromatography. In contrast with conventional chromatography media particles, which are characterized by small diffusive pores, POROS particles are characterized by the addition of large "throughpores". With this technology, flow rates can be dramatically increased without compromising capacity or resolution. POROS particles are rigid cross-linked poly(styrene-divinylbenzene) flow-through beads with a patented bimodal pore-size distribution for rapid mass transport. Thus, IMA and norIMA can be separated from the larger size denaturised proteins present in the sample.

The stability of POROS polymeric beads and surface chemistry allows for aggressive cleaning and sanitization with all the common agents used in biopharmaceutical process, including strong acids, bases and organic solvents. This column, indeed, is totally regenerable by washing it with sodium hydroxide (NaOH) [167].

The second column used was a Synergi fusion RP (4 µm, 80 Å, 50 x 2.0 mm, Phenomenex), which performed the actual chromatography. This column uses a polar embedded group and a hydrophobic ligand to achieve improved selectivity. The C18 ligand gives to the Synergi Fusion-RP column good hydrophobic retention and selectivity, while the polar embedded group provides enhanced polar retention (Figure 23). This dual-phase selectivity allows balanced polar, acidic, basic and hydrophobic compound retention and resolution [168]. Moreover, the small internal volume (less than 110 µL) allowed to decrease the run-time while the relatively large particle size of 4 µm reduced the system back pressure during the MP flow rate.

Considering that this analytical method has a triple quadrupole analyser (capable of precisely quantifying two co-eluting compounds, contrary to UV detectors), a high chromatographic resolution was not necessary. Anyway, cross-talking issues in some circumstances might occur. Moreover, the quantification of two co-eluting analytes involves the scan time to be split in two,

thus halving the number of data points describing each peak. For this reason, a minimum degree of separation between IMA and norIMA was required.

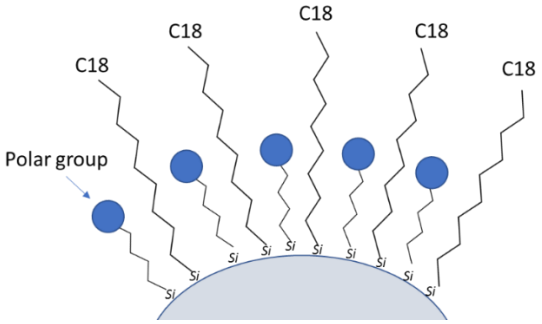

Figure 23. Graphic representation C18 Sinergy Fusion column.

In general, a chromatographic method is composed by 4 different steps:

- Conditioning phase of the column characterised by a low percentage of MPB (organic solvent) which helps the correct packing of the analytes at the head of the column.
- Elution phase of the analytes.
- Washing phase, in which a high percentage of MPB allows the elution of more lipophilic interferents in the matrix (e.g. phospholipids, peptide residuals, etc.) still bound to the SP.
- Reconditioning phase of the column, in which the eluent composition returns to the initial condition. Reconditioning failure can lead to alterations in retention times and therefore to reproducibility lack of repeated runs.

The whole 2D system is composed by the standard HPLC system with 4 pumps, two columns above described and four 10-port valves (V1-4). Pumps A (MPA: 10 mM ammonium acetate with 0.1% HCOOH) and B (MPB: MeOH-iPrOH 90:10 containing 0.1% HCOOH) performs the sample loading into the POROS column, meanwhile pumps C (MPC: 2 mM ammonium acetate aqueous solution with 0.1% HCOOH) and D (MPD: AcN-iPrOH 80:20 containing 0.1% HCOOH) performs the sample elution into the RP column. The 2D system is connected with the LC-autosampler through positions 2 (linked to AS-IN) and 7 (linked to AS-OUT) of V4 and with the MS through position 3 of V3.

As shown below (Figure 24), the 10-port valves have 2 different configurations:

- Configuration I, in which the communicating positions are: 10-1, 2-3, 4-5, 6-7, 8-9;
- Configuration II, in which the communicating positions are: 1-2, 3-4, 5-6, 7-8 and 9-10.

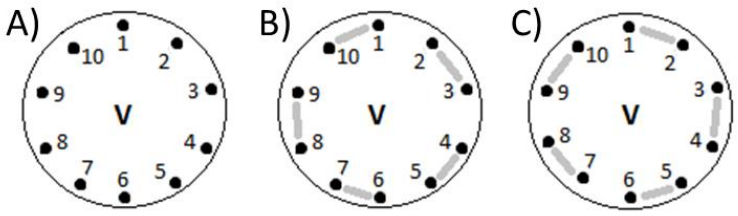

Figure 24. Graphical representation of a 10-port valve (A); 10-port valve in configuration I (B); 10-port valve in configuration II (C).

The valves were then properly linked through plastic peeks with different diameters and lengths to obtain the final model reported in Figure 25.

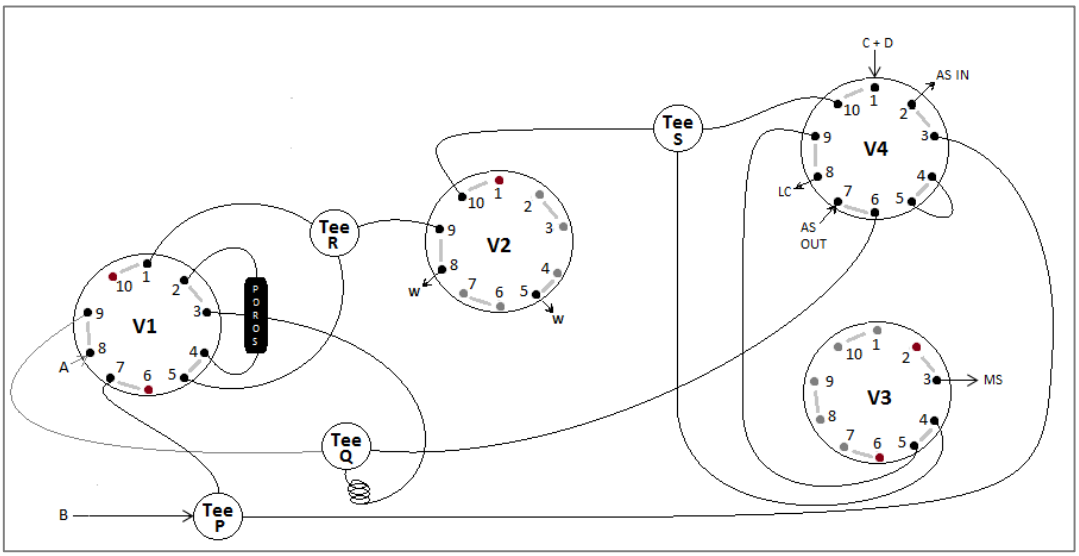

Figure 25. General scheme of the bidimensional system. A/B/C/D: pump A/B/C/D; AS IN/OUT: autosampler IN/OUT; LC: Synergi column; MS: mass spectrometer.

Each valve has a specific role:

- the first valve (V1) allows to direct the mobile phase flows from the pumps to the perfusion column;
- V2 manages the moment in which the sample had to go from the perfusion column to the RP column;
- V3 allows to exclude the analytical column in order to fine-tune the working conditions of the perfusion column, such as percentages of mobile phases and flow;
- finally, with the V4 configuration change, the system could exclude the POROS and work in mono-dimensional chromatography using only the RP column.

In respect to that, V1 and V2 are crucial to handle the sample running, in fact only these two valves change their configuration during the chromatographic run, while V3 and V4 remain in the same position from the beginning to the end of the run.

During the first step, the sample is taken by the MPB from the autosampler, it is properly mixed with MPA before being loaded in the perfusion column. In the meanwhile, the RP column is conditioned with phase C and D.

Then, the V2 configuration changes, allowing the analytes transfer from the POROS to the RP column. In this phase also the mixing of the analyte with MPs C and D occurs (Figure 26).

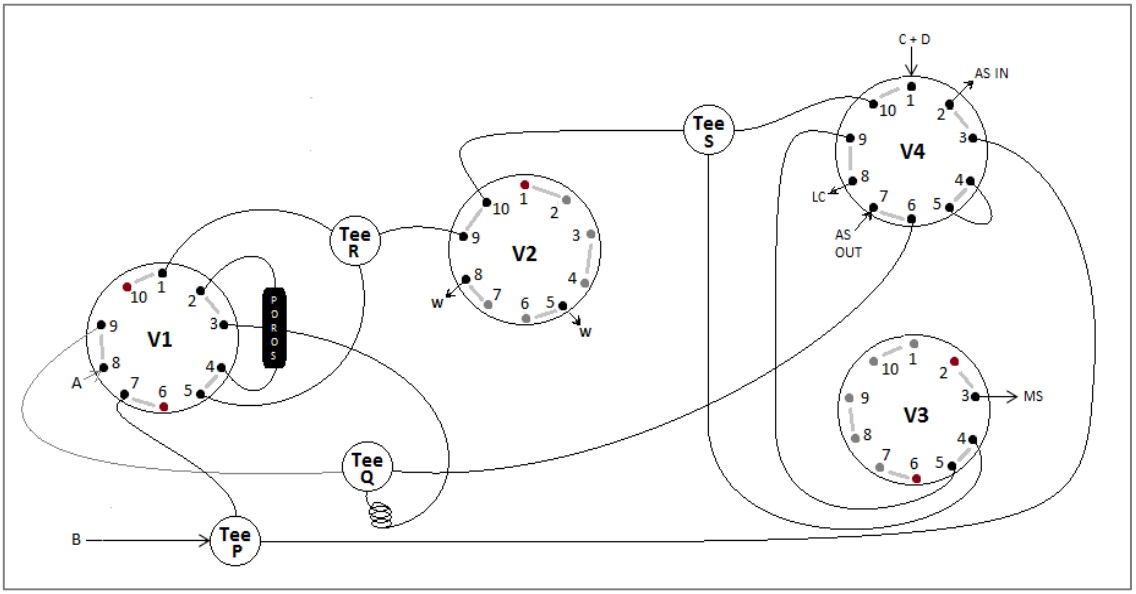

Figure 26. In this arrangement, V1 remains in the same configuration, meanwhile V2 changes it to allow analytes transfer from the POROS to the RP column.

Once the transfer is completed, the configuration change again, for both V1 and V2, as shown in Figure 27. The POROS, connected to the waste, is cleaned with MPA and MPB. In the meantime, the gradient elution (with MPC and MPD) of the analytes in the RP column starts.

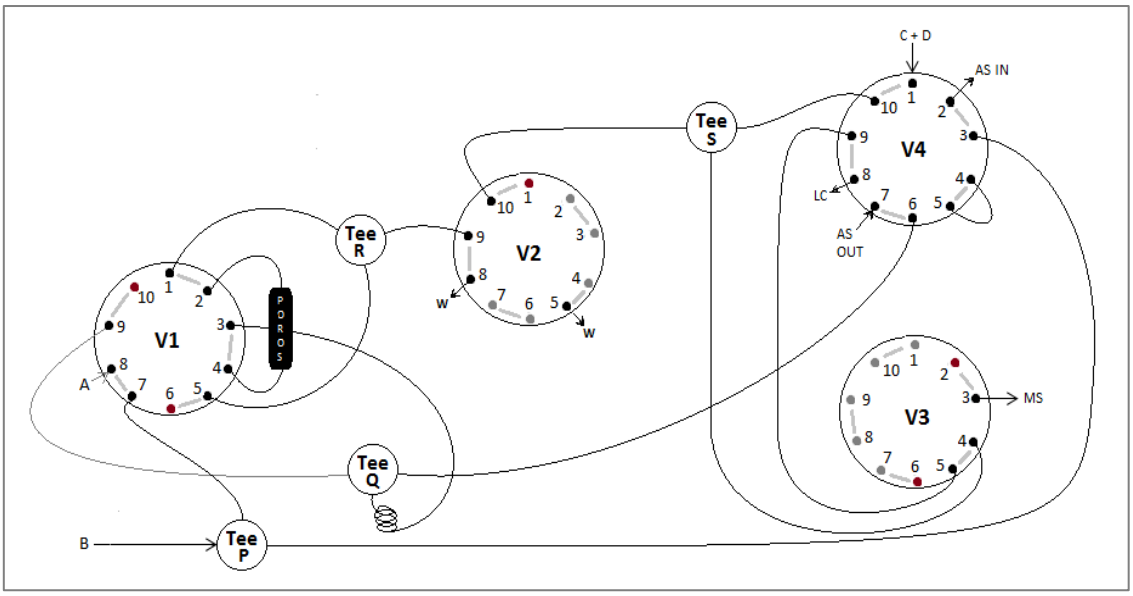

Figure 27. In this arrangement both the valves, V1 and V2, change configuration. POROS is connected with the waste again, and it is cleaned by MPA and MPB.

Finally, the configuration returns at the original conditions.

This innovative fluidic system offers two important advantages:

- allows the injection of high quantities of organic solvent without interfering with the chromatography (as reported in Figure 28) thanks to the presence of the perfusion column. Consequently, the analyte is transferred to the RP column with high percentages of weak solvent, permitting the right packing in the column, before the elution gradient begins;

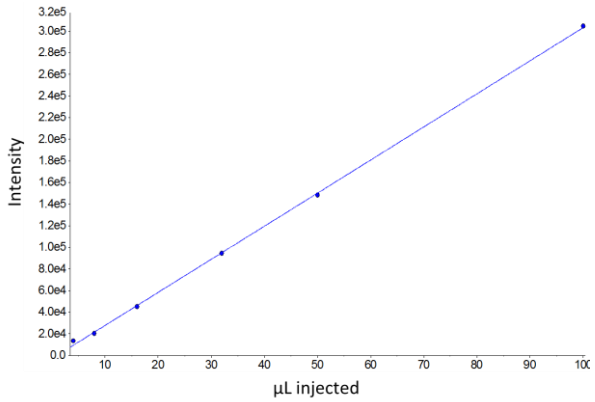

Figure 28. Linear response (intensity) obtained injecting increasing sample volumes, from 10 to 100 µL of IMA in MeOH.

- extends the duration of the RP column. The perfusion column, indeed, allows the sample purification before it is introduced into the Synergi column.

3.1.4 Sample preparation for quantitative analysis

3.1.4.1 Working solutions preparation

To perform quantitative measurements, it is necessary to calibrate the instrument (i.e. to establish a relationship between the detected signal and the analyte concentration) with a series of known samples having increasing concentrations. It is necessary to realise these calibration samples with same matrix type of the real samples. To ensure the reliability of the calibration curve, it is necessary to use during the analysis a set of samples having known concentrations: the so-called quality controls (QCs). The QCs might be purchased or, self-produced. Moreover, QCs concentration values must differ from the calibrators ones and they must be distributed within the range covered by the calibration curve in the following way: QCL, low concentration within to three times the LLOQ; QCM, average concentration which falls in the middle of the linear range and QCH, high concentration near to 75/85% of the ULOQ.

According to the FDA and EMA guidelines, a calibration curve must include at least 6 calibrators, including the LLOQ. For the method subject of this thesis, a ten point-calibration curve was selected. IMA and norIMA stock solutions were prepared in DMSO at concentrations of 3 mg/mL and 0.6 mg/mL, respectively (one was prepared to obtain the calibration curves point, another one for the QCs points). Two different stock solutions were obtained for each compound: one for the calibration curve and the other for QCs. The two stock solutions were mixed together with a 1:1 ratio (final concentrations of 1.5 mg/mL and 0.3 mg/mL for IMA and norIMA, respectively) and then further diluted in MeOH 50% for getting the working solutions to be used to build the calibration curve (from A to L) and QC samples (L-low, M-medium, and H-high). The final concentrations obtained were: 750, 625, 500, 375, 250, 100, 50, 20, 10, 5 µg/mL (from A to L) and 600, 125, 25 µg/mL (QCH, M, and L) for IMA, and 150, 125, 100, 75, 50, 20, 10, 4, 2, 1 µg/mL (from A to L) and 150, 750, 50 µg/mL (QCH, M, and L) for norIMA. IMA-D8 stock solution was prepared in DMSO at concentration of 0.5 mg/mL. Intermediate solution at 10 µg/mL was prepared by diluting the stock solution with MeOH. DBS solution was prepared diluting the intermediate IMA-D8 solution with acidified methanol (0.1% of formic acid) to obtain the final concentration of 10 ng/mL.

3.1.4.2 Standards and quality control samples in DBS preparation

Calibrators and QC samples were made by mixing the working solutions and whole blood with a 1:100 ratio. The final concentrations were: 50, 100, 200, 500, 1000, 2500, 3750, 5000, 6250, 7500

ng/ml (from L to A) and 250, 1250, 6000 ng/mL (QCL, M, H) for IMA and 10, 20, 40, 100, 200, 500, 750, 1000, 1250, 1500 ng/ml (from L to A) and 50, 250, 1200 (QCL, M, H) for norIMA.

Calibration standards and QC samples in blood were prepared by adding 3 µL of standard or QC working solutions to 297 µL of whole blood and the solution were equilibrated for 30 min (from 30 min to 4 h of incubation times were tested with no differences between them) at 37°C. Then, 20-µL aliquots of spiked blood were spotted on filter paper and allowed to air dry for 3 h at room temperature. With a pneumatically-activated device, supplied by Analytical S&S (Flanders NJ, USA), calibration standards and QC DBS were punched for getting a 3 mm-disc which was added by 150 µL of a IMA-D8 methanolic solution (10 ng/mL) containing 0.1% HCOOH. After a 30 min gentle mixing (from 30 min to 4 h of extraction times were tested with no differences between them) and a 10 min centrifugation at 16000 g and 4°C, 100 µL of supernatant were transferred to a polypropylene autosampler vial for the analysis.

3.1.5 Optimization of DBS parameters

Several pre-analytical, analytical and post-analytical variables influence the DBS analysis and must be considered during the development and validation of a new DBS assay. In the following paragraphs are addressed all the parameters that were taken into account to develop the presented method.

3.1.5.1 Type of the paper

Different types of card matrices, in combination with haematocrit (Hct) value and other parameters, may have different effects on the spreading of the blood spot and the extraction recovery of the substance. The most common matrix for DBS is cellulose-based paper and, there are two types of commercially available paper cards suitable for DBS: chemically untreated and treated papers. The untreated ones are the most commonly used, in particular the Whatman 903 card, which is composed of cotton-based filter paper within a rigid cardboard frame for handling and labelling. The paper, as reported in Figure 29 is ink-printed with five half-inch circles that direct the user to the location for depositing a specimen [169].

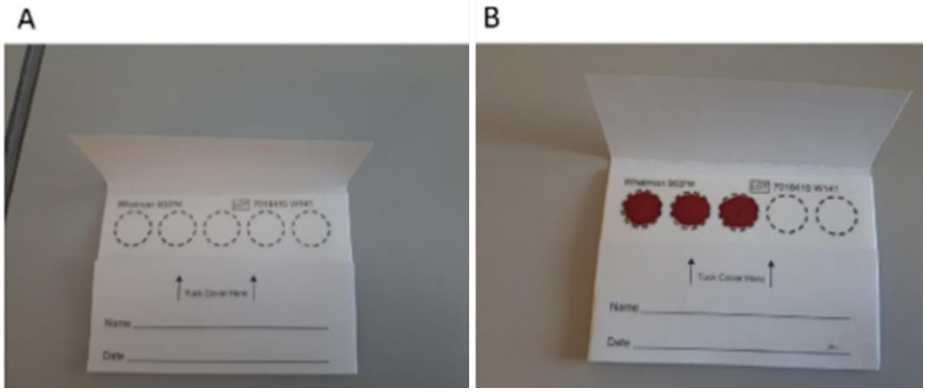

Figure 29. Example of the filter paper Whatman 903, before (A) and after (B) the deposition of the blood drops.

Moreover, Whatman 903 and Perkin Elmer 226 are the only types of DBS cards that are approved by the US FDA as clinical collection devices. These types of cards are extensively monitored for consistent performances between batches [170]. Being a validated filter paper to perform DBS sampling, the Whatman 903 is a quite expensive filter paper. Thus, to ensure that costs are kept low, in order to develop a cost-effective and reliable quantification method, another type of untreated filter paper has been tested and then chosen: Whatman 31ET-CHR. This is a pure cellulose filter paper, without any additives. This type of paper was already used by Vu et al. with moxifloxacin for the dried blood spot purpose, with good results compared to Whatman 903 [171].

To assess if these two papers have the same impact on DBS analysis, QC samples (prepared as reported in section 3.1.4.2) were prepared using both the paper Whatman 31ET-CHR and the Whatman 903. They were then quantified using a DBS calibration curve prepared with the Whatman 31ET-CHR. The difference between the two papers, on IMA and norIMA concentrations, was then determined as the accuracy percentage of the measured concentrations in QC DBS samples.

3.1.5.2 Collection procedure

DBS sample collection procedure must follow uniform procedures to minimize the pre-analytical errors that can occur, like contaminations, overlapping or messy spots. Especially contamination is the most concern for DBS sampling, which can lead to inaccurate determination of drug concentration in the sample. It can result from the use of topic anaesthetics creams, disinfectants, etc. In this regard, the European Bioanalytical Forum (EBF) proposed the concept of good blood-spotting practices [142]:

1. Prior to the collection, any contact with the target site of the matrix card must be avoided.

2. If the participant's hands are cold, massaging or warming the collection site before pricking can stimulate local blood flow and clean the puncture site with 70% isopropyl alcohol.
3. Use a sterile, single-use lancet to prick the finger just off the centre of the tip of the middle or ring finger and wipe the first blood drop away with a sterile gauze pad to remove the tissue fluid from the sample.
4. Carefully position the collection paper below the finger and allow the drop to fall. The donor's finger should never touch the DBS matrix. Furthermore, do not place blood on top of blood, what can result in sample concentration.
5. Allow the spot to dry for 3 hours in horizontal position, allowing contact with air on both sides of matrix.
6. Store/transport samples in plastic bags with desiccant, under room temperature, refrigerated or frozen, depending on analyte stability.

3.1.5.3 Drug extraction optimization

The extraction efficiency of the analytes from a complex matrix, containing hundreds of denaturated proteins, depends on several factors: the compound's chemical properties, solvents and timing of the extraction procedure, and the filter paper used. Generally, the extraction efficiency does not need to be near to 100%, but it necessarily has to be constant and reproducible over different analyte concentrations (from high to low concentration respect to the calibration curve).

Water-miscible solvents are the most commonly used to extract small molecule compounds from DBS samples [172]. MeOH, AcN or mixture of them, also with water, are the most frequent used. Based on visual observation, it appears that higher is the aqueous content, higher is the dissolution of blood cells and other endogenous components from DBS. Usually the best solvent is where the analytes are soluble in. This because the solvent needs to have the strength to extract the drug from the paper and bring it back in solution.

After the solvent addition, the DBS sample is vortexed or shacked for an amount of time that is analyte dependent, usually from 5 mins to 2 hours. The optimization of this parameter is important to develop a reproducible and no time-consuming method.

3.1.5.4 Effect of haematocrit

The interpretation of drug concentration measurements in the context of TDM is usually based on reference ranges established in plasma or serum samples. As DBS is a measurement in whole blood,

there is the need to convert the information obtained in this matrix to plasma levels. Usually, the Hct has a major influence in this process. In fact, the viscosity of the blood affects the amount of sample present in a matrix punch of fixed size and the proportion between red blood cells and plasma in the sample, thus bringing to a modifications in the relative concentration of the drug on these blood compartments [173].

To assess the Hct effect, three aliquots of whole blood were prepared at different Hct% values: EDTA whole blood was centrifuged (2450 g, at 4°C for 10 min) and then proper volumes of red blood cells and plasma were combined. To cover the entire Hct% range of GIST patients (spanning from 32 to 45%), the obtained Hct% values were 29, 38.4, and 59%. QCL, QCM, and QCH samples were prepared, in triplicate, for each of the three blood aliquots with different Hct values and quantified using a DBS calibration curve prepared at fixed Hct value (38.4%). For the DBS calibration curve and QC samples preparation see the section 3.1.4.2. The influence of Hct on IMA and norIMA concentrations was then determined as the accuracy and precision percentage of the measured concentrations in DBS samples.

3.1.5.5 Volcano effect

Due to the “volcano effect” the analyte concentration can be lower in the centre than in the peripheral area of the spot or vice versa. Thus, to assess whether there is a difference in IMA or norIMA concentrations between central and peripheral areas of the DBS, QCL, QCM, and QCH samples were prepared in triplicate, as reported in the section 3.1.4.2. Then, the punch was performed in the centre and in the edge area of the DBS for each QC sample. The homogeneity was calculated as the centre/perimeter concentration ratio (C/P) and the expecting result is C/P=1.

3.1.5.6 Influence of spot size

The influence of spot size was also investigated. QCL, M, and H samples were prepared, and the spots were performed with four different blood volumes: 10, 20, 30, 40 µL, in triplicate for each QC concentration (L, M, and H). The quantification of these QC samples was performed using a DBS calibration curve made by fixed 20 µL-volume spots. The influence of spot size on IMA and norIMA concentrations was then determined as the accuracy and precision percentage of the measured concentrations in DBS samples.

3.1.5.7 Correlation between finger-prick and venous collection

As reported by some authors, there has been a concern whether the drug concentration after a finger-prick sampling was comparable with venous collection [174]. In fact, DBS is composed from arterial capillary blood and some amount of interstitial fluid so the drug concentrations can be potentially different from venous blood.

The clinical protocol was indeed designed to collect DBS from both finger-prick and venous blood (without anticoagulant) from the same patient to compare the measurements obtained from each matrix. The comparison was performed in a subset of 10 patients' samples, estimating both the Pearson's coefficient of determination (R^2) and the percentage difference (%) between the concentrations found in finger-prick (CFP) and venous (Cv) DBS, calculated with the equation [2]:

$$\%\ diff = \frac{(CFP - Cv)}{mean} \times 100 \quad [2]$$

3.1.5.8 Internal standard application

During the sample preparation, a known quantity of a further compound, called internal standard (ISt), was added to each sample and the analytical parameter used for the quantification was the ratio between the analyte and ISt peaks areas. The ISt must have very close physical-chemical properties to the analyte of interest, then every error introduced during the sample processing or during the analysis has the same impact on both the compounds (analyte and ISt). Excellent candidate for LC-MS/MS analysis are the stable isotopic labelled analogues of the analyte (deuterium-labelled or C13-labelled compounds). For the quantification of IMA and norIMA, imatinib-D8 mesylate was selected as ISt (Figure 30).

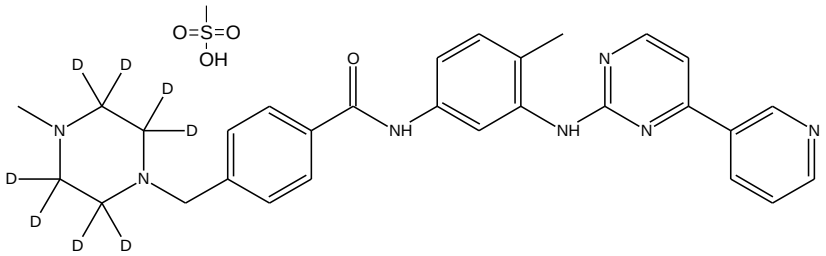

Figure 30. Structure of imatinib-d8.

The usual application of ISt in liquid samples is based on its addition of small volumes directly in the sample (for example in the plasma sample). However, since DBS is a solid matrix, this application could be not easy, appropriate and accurate.
For this reason, for the method developing the ISt was added directly in the extracting solution, as already reported in literature [175].

3.1.6 LC-MS/MS method validation study

After the method optimization, a complete validation study was carried in accordance with the EMA [128] and FDA [176] guidelines for the validation of a bioanalytical method. In particular, the validation was carried out by evaluating the following parameters: recovery of the analyte from the matrix, linearity of the calibration curve, intra- and inter-day precision and accuracy, reproducibility, lower limit of quantification (LLOQ) and selectivity, matrix effect and stability of the analyte in samples and solutions. Considering that this method was developed in DBS, the validation was also performed in accordance to the EBF recommendations [142].

3.1.6.1 Recovery

The recovery determination of an analyte from a complex matrix allows evaluating the extraction efficiency. The peak areas of IMA and norIMA, extracted from DBS QC samples, were compared to those obtained from post-extraction spiked DBS. Percentage extraction recovery was determined for each analyte (i.e. IMA and norIMA) in samples of three concentrations values (QCL, QCM and QCH) prepared in quintuplicate without adding the ISt and using the formula [3].

$$Recovery\ \% = \frac{analyte\ peak\ area\ (in\ DBS)}{analyte\ peak\ area\ (in\ extracted\ DBS)} x\ 100 \quad [3]$$

It compares the instrument response from two samples with the same concentration value but prepared with different methodologies: for the first one, blood was spiked with the proper working solution (WS), spot on the paper and extracting as usual, for the second one the sample was spiked after the extraction. The analytes recoveries do not necessarily have to be equal to 100%, however, the extent of recovery of the analyte should be consistent, precise and reproducible.

3.1.6.2 Linearity

The linearity of an analytical method is its ability (within a given concentration range) to obtain results directly proportional to the concentration of the analyte present in the sample. The linearity of the calibration curve has been assessed in five different working days. For each standard point, the ratio of the LC–MS/MS peak area for each analyte to the ISt was calculated and plotted against the nominal concentration of each analyte in the sample. A weighted quadratic regression function ($1/x^2$) was applied to generate calibration curves. The calibrators were prepared freshly every day by spiking donors' blood with the proper calibrators WSs, as reported in section 3.1.4.2. The fitting quality was calculated using the Pearson correlation coefficient (R^2).

The accuracy, which is the closeness of the measured value to the nominal concentration of the analyte (expressed in percentage) of back-calculated values of an individual point had to be within 85–115% of the theoretical concentration (80–120% at the LLOQ), and at least 75% (eight out of ten) of calibration points had to meet these criteria, including the LLOQ and highest calibrator, ULOQ. The precision, which describes the closeness of repeated individual measures of analyte expressed as the coefficient of variation (CV), should not exceed 15% for each individual calibration point.

The accuracy was determined by expressing the mean calculated concentration as a percentage of the nominal concentration, while precision was reported expressing the standard deviation (SD) as percentage of the mean calculated concentration ($\bar{X}$) (equation [4]).

$$CV\% = \frac{SD}{\bar{X}} x\ 100 \quad [4]$$

The reproducibility of each calibration curve was assessed evaluating mean values (± standard deviation (SD)) of intercept, slope and R^2.

3.1.6.3 Intra-day and inter-day precision and accuracy

The precision and accuracy of the presented method were evaluated by analysing six replicated of each QC sample (L, M and H) within a single-run analysis for intra-day assessment and three replicates of each QC sample over five different working days for inter-day assessment, using standard calibration curves freshy prepared.

For both intra- and inter-day accuracy, the measured concentration for at least 2/3 of the QC samples had to be within ± 15% of the nominal value, in each run, and only one QC sample, at each concentration level, could be excluded. The intra- and inter-day precision value should not exceed 15% for each QC sample.

3.1.6.4 Limit of quantification and selectivity

The lower limit of quantification (LLOQ) is the lowest standard concentration measured. It is defined as the smallest amount of analyte that an assay reaches to quantify (SNR≥5) in the sample with adequate precision (≤20%) and accuracy (within ±20%). In these analytical methods, the LLOQ was estimated by adding the L working solution to 6 different samples of donors' blood (50 and 10 ng/mL for IMA and norIMA, respectively), prepared as reported in the section 3.1.4.2. To be accepted, LLOQ had to show an acceptable accuracy (≤20%) and precision (between 80% and 120%).

Selectivity identifies the ability of the assay to differentiate and quantify both the analyte of interest in the presence of other interferents such as matrix components, metabolites, decomposition products, or other drugs administered concurrently. The selectivity was proved analysing blank DBS samples using blood from six different individuals, prepared according to the proposed extraction procedure and individually evaluated for interferences.

3.1.6.5 Matrix effect

As said before, matrix effect arises due to the presence of endogenous components in the biological matrix, the analyte of interest might experience variations in their ionization efficiency because of it. Although they are generally the principal cause, not only endogenous components in the biological matrix (e.g. salts, amines, triglycerides) cause matrix effect, but also some exogenous compounds (plasticizers from sample containers or anticoagulants in case of plasma) are susceptible to alter the ionization process [177]. Furthermore, other substances present in the mobile phase can alter the signal of the analyte by causing ion suppression or enhancement. Nevertheless this is not considered a matrix effect source since it is not sample specific [178].

Both ion enhancement and ion suppression phenomena might compromise precision, accuracy, sensitivity and selectivity of the developed method and, consequently, the reliability of the produced analytical data. For this reason, both FDA and EMA guidelines emphasize the importance of the matrix effect assessment.

Post-extraction spiked DBS (i.e. samples obtained by spiking analytes after the extraction of blank DBSs), prepared in quintuplicate at the three QC concentrations, were compared to the same QC samples prepared in neat solution (MeOH). The matrix effect is calculated as the ratio of the peak area in the presence of matrix to the peak area in absence of matrix. The CV should be within 15%. Effects of matrix endogenous components on the analyte's ionization was also investigated during the development of the chromatographic method by means of the post-columns infusion: a constant flow of IMA and norIMA solutions prepared in MeOH (250 ng/mL), were infused by a syringe pump, with a 20 µL/min flow, during the chromatographic run of an extracted blank DBS sample. The extracted blank DBS sample eluted from the LC column and the flow from the infusion pump were combined through a zero-dead-volume tee union and insert into the mass spectrometer source. A variation in the signal response of the infused analyte indicates ionization enhancement or suppression (Figure 31).

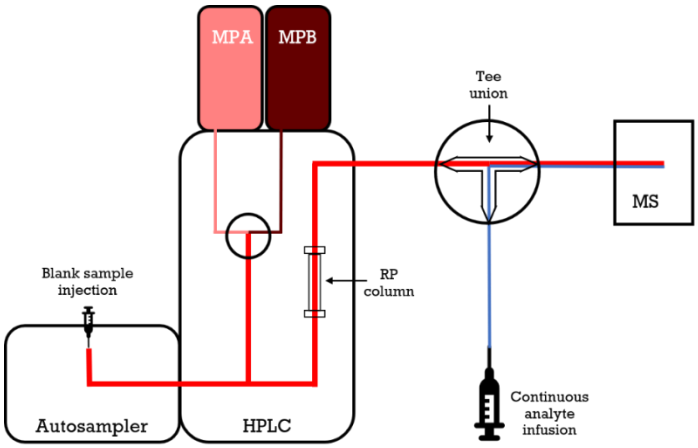

Figure 31. Instrument set up for the post column infusion.

3.1.6.6 Stability

The stability of an analyte is function of the matrix in which it is dispersed, of the conditions in which it is stored and of the chemical properties of the analyte itself. Evaluating the stability of the analyte in stock solutions and in the matrix is essential to ensure the reliability of the results obtained from the analytical method. This assessment includes all the situations that can be encountered during the whole analytical procedure such as freeze-thaw stability, short- and long-term stability, stock stability and post-processing stability.

The stability of IMA and norIMA was assessed by analysing QC DBS samples at the three concentrations L, M, and H during sample storage and handling procedures. The stability of the QC samples, processed as previously reported (section 3.1.4.2), was assessed in the autosampler by

repeatedly analysing the extracts 24 and 48 h after the first injection. Long-term stability of working solutions (MeOH matrix) was assessed stored at approximately −80°C.

During the development of this method, was also assessed the analyte stability on DBS filter paper. In fact, one of the potential benefits inherent to the DBS technique is the possibility to collect, ship and store dry samples under ambient conditions. This increase in compound stability can largely be attributed to removal of esterase activity upon drying or even enhanced photostability [179].

Analyte stability on the paper is influenced by many factors not related to the stability of the analyte itself, like filter paper type, temperature, humidity and storage time. Low humidity and temperature are essential aspects to take in consideration to preserve the DBS integrity [173]. Long-term stability of DBS samples was assessed at the storage condition applied (in plastic envelopes containing a silica-gel drying bag at room temperature) at time intervals of 1, 2, 4 weeks and then months after preparation. The two analytes were considered stable when the testing samples did not exceed 15% from the nominal concentrations at each QC concentration.

3.1.6.7 Incurred samples reanalysis

As indicated in the 2018 FDA guidance, which take into account the AAPS/FDA seminar on the reanalysis of the assayed sample [180], an additional measure of the assay reproducibility was introduced: the incurred samples reanalysis (ISR). ISR is conducted by repeating the analysis of a subset of patients' samples in separate runs on different days. Therefore, a set of 10 patients' DBS samples were re-analysed in a further analytical session. According to FDA and EMA guidelines, the two analyses can be considered equivalent if the percent difference (% diff) between the first and the second concentration measured is within ±20% for at least 67% of the samples.

To calculate the % diff, the equation [5] was used:

$$\%\, diff \;=\; \frac{R - I}{M} \times\; 100 \quad [5]$$

Where:

R = concentration value found from the repeated analysis;

I = concentration value found from the first analysis;

M = arithmetic mean between R and I.

3.2 Simultaneous quantification of IMA and norIMA in DBS samples from GIST patients

The proposed method was applied to quantify, for the first time, both IMA and norIMA in DBSs collected from GIST patients enrolled in the clinical study from February 2018 to February 2019.

3.2.1 Patients enrolment

A phase IV clinical trial entitled "Pilot study to evaluate the feasibility of an innovative approach to monitor patients with gastrointestinal stromal tumour treated with imatinib" was started at the Aviano (PN) National Cancer Institute. The aim of this study was to evaluate the feasibility of a double monitoring approach that combines the simultaneous quantification of IMA and norIMA plasma concentrations and the evaluation of circulating tumour DNA (ctDNA). The underlying hypothesis was that a merged monitoring approach could be the best solution to optimize IMA therapy. The protocol of this clinical trial (N. EudraCT 2017-002437-36, internal code: CRO-2017-19) has been revised and approved by the local Ethics Committee (CEUR) of Friuli Venezia Giulia and by the Italian Medicines Agency (AIFA). The study, which involves the collaboration of *Azienda Ospedaliera Integrata di Verona, Presidio Ospedaliero di Treviso, Azienda Ulss n. 2 Marca Trevigiana, Treviso,* and the University of Chicago Medical Centre, was approved by the ethics committees of each participating centre.

3.2.1.1 Patients' characteristics

To enter this protocol, the patients' eligibility criteria were:

- age ≥ 18 years;
- histologically or cytologically confirmed diagnosis of GIST and eligible for treatment with imatinib according to the routine clinical practice criteria both in adjuvant and first-line therapy;
- performance status, determined with the Eastern Cooperative Oncology Group (ECOG) criteria, of 0 or 1 and adequate liver, renal and bone marrow function;
- life expectancy > 3 months;
- for patients already treated with imatinib, therapy had to start more than 3 months before the first sample was collected (to reach a stable drug concentration in the blood);

- signature of the informed consent.

The exclusion criteria were:

- pregnancy status;
- non-collaborative and/or unreliable patients;
- informed consent refusal;
- the absence of possibility for the patient to undergo periodic clinical check-ups.

Fifty-five DBS samples were collected from 26 patients with a mean of two C_{min} samplings for each patient. Patient population was characterized as reported in Table 1.

Patients characteristics	N
Sex	14 females 12 males
Age (range)	66 (37-83) years
Setting	6 adjuvant therapy 20 first-line therapy
Primary tumour site	10 gastric 16 non gastric

Table 1. Demographic and clinical characteristics of enrolled patients.

Taking into account all 55 samples, the mean Hct was of 37.7% (range 26.2-44.1%) Patients were receiving IMA at the dose of: 400 mg/die in 51 samples, 200 mg/die in 1 sample, 300 mg/die in 2 samples, and 600 mg/die in 1 sample. Samplings were mostly performed 25 h after the last tablet intake (25.1 ± 6.7 h).

3.2.1.2 Treatment and sampling

Patients were treated with different doses (range 200-600 mg/die) of IMA and they were educated to take IMA tablet once a day at a fixed time (usually around 12.00 pm). Since timing is crucial for an accurate estimation of the real C_{min}, the samplings were performed immediately before the scheduled pill intake. Three different samples were collected from each patient: venous blood, control venous DBS and finger-prick DBS. Venous blood was drawn through 4.9 mL K-EDTA-Monovette tubes (Sarstedt, Nuembrecht, Germany). Before plasma separation, multiple 20 µL-aliquots of collected blood were deposited on ET31-CHR filter papers for obtaining the venous DBS. DBS collection through finger-prick was conducted after adequate training of the personnel. The

prick was performed by a sterile lancet Securlancets from Menarini Diagnostics (Firenze, Italy) following the guidelines previously reported in section 3.1.5.2.

Both the DBSs (from venous blood and from finger-prick) were let dry at room temperature (RT) for at least 3 h and cards were stored until measurement at RT in plastic envelopes containing a silica-gel drying bag. The processing method for DBS samples from patients is reported in section 3.2.1.3.

3.2.1.3 Real samples processing procedure

Once the validation had been completed, it was possible to proceed with the quantification of the patients' samples. The sample preparation method previously developed for calibrators and QCs was applied also for real samples. A punch of 3 mm was performed for each patient's DBS spot and the analytes were extracted adding 150 µL of IMA-D8 methanolic solution (10 ng/mL) containing 0,1% HCOOH. After 30 min stirring at RT and 10 min centrifugation at 16000 g at 4°C, the supernatant was transferred into polypropylene HPLC vials for the analysis, as reported in Figure 32.

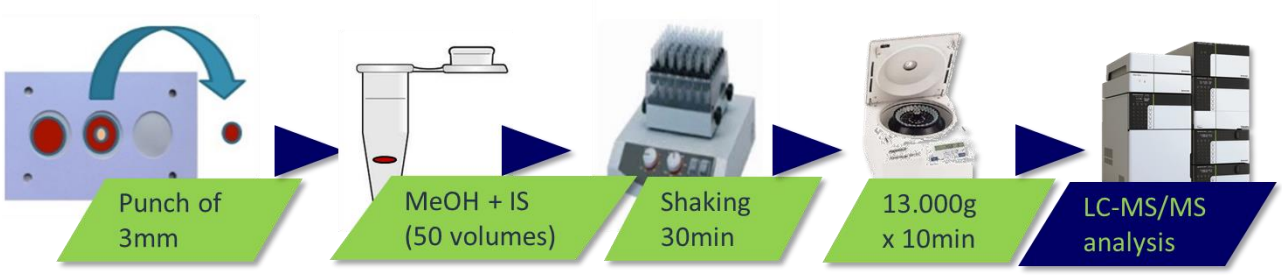

Figure 32. Graphical representation of the patients' samples processing procedure.

A set of 55 DBS samples were analysed to obtain the concentration of both IMA and norIMA.

3.2.2 Cross-validation of the DBS method

The development of a strategy for estimating plasma concentration (that is the reference value for PK studies in the literature) from the analysis of the corresponding DBS sample is a critical element for the application of DBS in therapeutic drug monitoring. Thus, cross-validation of DBS test with plasma assay is mandatory before the introduction of a DBS assay into a clinical laboratory routine [181].

All the 55 DBS samples had their corresponding plasma samples (as defined by the clinical protocol) which were analysed too in order to obtain the concentration of both IMA and norIMA in each matrix (C_{DBS} and C_{PLA}, respectively). Plasma samples were analysed with an in-house validated LC-

MS/MS method. The estimated plasma concentration (EC_{pla}) with two different methods. On one hand, it was obtained from the DBS measurement (C_{DBS}) applying the following equation [6]:

$$EC_{pla} = \frac{C_{DBS}}{\left[1 - \left(\frac{Hct}{100}\right)\right]} \quad [6]$$

On the other hand, the EC_{pla} was calculated also from C_{DBS} multiplied for a correction factor (F_c), as previously proposed by Antunes et al. [145]. The correction factor was calculated as the mean ratio of the concentrations measured in plasma to C_{DBS} ($Fc = C_{PLA}/C_{DBS}$) in all the samples analysed. This strategy allows to avoid the use of Hct correction. The F_c calculated was then applied to a set of 12 extra patients' samples for both IMA and norIMA, to further validate this method. Agreement between the two methods (plasma and DBS) was evaluated through: a) Passing-Bablok regression: intercept and slope of the regression equation are reported with relative 95% Confidence Interval (95% CI); b) Bland-Altman method: spearman correlation coefficient (r) between differences in means and mean of the measurements is reported, for the sake of simplicity the tested measure is named Y in the text, while the plasma value (reference) is indicated as X, c) Lin's concordance correlation coefficient (LCCC), and d) FDA/EMA requirements (67% of samples tested within ±20% of the mean, as reported in section 3.1.6.7). Statistical analyses were performed with Stata 14.2 (StataCorp, Texas USA).

3.3 LC-MS/MS method development for the simultaneous quantification of RIBO, PALBO and LETRO in human plasma

The hereby method has the aim to perform a quantitative analysis of RIBO, PALBO and LETRO in human plasma using an LC-MS/MS apparatus.

3.3.1 Instrumentation

The instrumentation used is the same reported in the section 3.1.1. The 2D chromatographic system was excluded for this method.

3.3.2 Standard and chemicals

Analytical standard of PALBO was provided by Toronto Research Chemicals (Toronto, Canada), RIBO and LETRO hydrochloride were supplied by Merck-Sigma Aldrich. Stable isotopically labelled internal standards D_6-RIBO, D_8-PALBO and $^{13}C_2$,$^{15}N_2$-LETRO were synthesized by Alsachim (Illkirch Graffenstaden, France). LC-MS grade isopropanol was supplied by Merck-Sigma Aldrich while LC-MS grade methanol was purchased from Carlo-Erba (Milano, Italy). "Type 1" ultrapure water was produced at our department by a Milli-Q® system (Merck). Drug-free plasma/K-EDTA from healthy volunteers to prepare daily standard calibration curves and QC samples was provided by the transfusion unit of our institution.

3.3.3 Mass spectrometric conditions optimization

To optimize source and compound dependent parameters, solutions of each analyte at the concentration of 100 ng/mL were used with a flow rate of 20 µL/min. Data were processed with Analyst 1.6.3 and the quantification of the peaks was done with MultiQuant 2.1 (software package AB SCIEX).

The quantification was done in SRM mode using the following transitions 448>380 m/z for PALBO, 435>322 *m/z* for RIBO and 286>217 *m/z* for LETRO. The transitions 448>337 m/z for PALBO, 435>367 *m/z* for RIBO and 286>190 *m/z* for LETRO were used as qualifiers. The quantification of the ISs signal was conducted using the following transitions: 456>388 *m/z* for D_8-PALBO, 441>373 *m/z* for D_6-RIBO, and 290>221 *m/z* for $^{13}C_2$,$^{15}N_2$-LETRO.

3.3.4 Chromatographic conditions

The samples separation was achieved in mono-dimensional chromatography on the Luna Omega Polar C18 column (3 µM, 100 Å, 50 x 2.1 mm) coupled with a Security Guard Cartridge (Polar, C18, 4 x 2.0 mm), both provided by Phenomenex (Castel Maggiore (BO), Italy). This column is composed by C18 ligands that provides hydrophobic interactions while a polar modified particle surface provides enhanced polar retention and aqueous stability. The MP consisted of ultrapure water with 0.1% HCOOH (MPA) and MeOH/iPrOH (9:1, v/v) with 0.1% HCOOH (MPB).

3.3.5 Working solutions preparation

Stock solutions of RIBO and LETRO were prepared in MeOH at concentration of 1 mg/mL while stock solution of PALBO was prepared in DMSO at 0.5 mg/mL. Two different stock solutions were obtained for each compound: one for the calibration curve and the other for QCs. To obtain the working solutions for the construction of the calibration curve (from A to H), the stock solutions of PALBO, RIBO and LETRO were mixed together and diluted with methanol to achieve the final concentrations of: 5, 3, 1.5, 0.5, 0.2, 0.08, 0.02, and 0.005 µg/mL for PALBO, 200, 120, 60, 20, 8, 3.2, 0.8, and 0.2 µg/mL for RIBO, and 10, 6, 3, 1, 0.4, 0.16, 0.4, 0.16, 0.04, and 0.01 µg/mL for LETRO. The stock solutions for QCs were mixed together and diluted with methanol to obtain the final concentrations of: 4, 0.4, 0.01 µg/mL for PALBO, 160, 16, 0.4 µg/mL for RIBO, and 8, 0.8, 0.02 µg/mL for LETRO. Stock solutions of IS were prepared in methanol for D_6-RIBO and $^{13}C_2$,$^{15}N_2$-LETRO at the concentrations of 1 and 0.5 mg/mL, respectively, and for D_8-PALBO in DMSO at 0.5 mg/mL. The three working solutions were mixed together and diluted with methanol to obtain the final concentrations of 12.5 ng/mL for D_8-PALBO and $^{15}N_2$-LETRO, and 45.0 ng/mL for D_6-RIBO. This solution was directly used to precipitate plasma proteins during sample treatment.

3.3.6 Standards and quality control samples preparation

Calibration curve and QCs sample preparation was conducted through the following steps:

1) 5 µL of working solutions were added to 95 µL of blank human plasma (dilution 1:20) and vortexed for 10 s;
2) A 10 µL-aliquot of this mix was added with 80 µL of cold ISt working solution (see section 3.3.5), vortexed and then centrifuged for 15 min at 16200 g and 4 °C;
3) 80 µL of the supernatant was transferred to a polypropylene tube for the following analysis.

The final concentrations thus obtained were: 0.3, 1, 4, 10, 25, 75, 150, 250 ng/mL for PALBO, 10, 40, 160, 400, 1000, 3000, 6000, 10000 ng/mL for RIBO, 0.5, 2, 8, 20, 50, 150, 300, 500 ng/mL for LETRO for the calibration curve; 0.5, 20, 200 ng/mL for PALBO, 20, 800, 8000 ng/mL for RIBO, and 1, 40, 400 ng/mL for LETRO for the QCs.

3.3.6.1 Plasma sample extraction optimization

Biological matrices are extremely complex and may contain some endogenous components, such as proteins and lipids, which might interfere with the detection and quantification of the analytes. These interferents might not only dirty and damage both the chromatographic column and the spectrometer source, but they might also cause variations in the analyte ionization efficiency. For these reasons, the main purpose in bioanalysis sample preparation is to remove the largest amount of interferents as possible and at the same time to solubilize the analytes in a suitable solvent for their quantification. The most used extraction techniques in the pharmacokinetic field are three:

- solid phase extraction (SPE);
- liquid-liquid extraction (LLE) with immiscible solvents;
- protein precipitation (PP) with organic solvents miscible with H_2O.

Regarding the analysis of drugs in human plasma samples, the simplest and less time-consuming technique to use is PP: more in detail, organic solvents miscible with H_2O, after their addition to an aqueous sample (e.g. plasma), cause the desolvation of the proteins surface by H_2O molecules displacement, thus leading to the breakage of the weak interactions responsible for their tertiary structure, to the aggregation by attractive electrostatic and dipole forces, and therefore to their precipitation. The most used PP solvents are MeOH and AcN added in volumes at least three times greater than the sample. The larger the volume of solvent added, the more efficient will be the extraction and the cleaner will be the sample injected on the LC-MS/MS apparatus. At the same time, large volumes lead also to diluted samples which might cause analytical problems if the compound of interest shows low signal intensity. Some tests using MeOH, acidic MeOH (0,1% HCOOH), AcN and acidic AcN (0,1% HCOOH) were performed. After the individuation of the best solvent to use, also the volume necessary for the deproteinization has been evaluated.

3.3.7 LC-MS/MS Method validation study

A full validation of the proposed method was conducted according to FDA and EMA guidelines on bioanalytical method validation [182, 183], as previously reported in section 1.4.3.

3.3.7.1 Recovery

Three different sets (set 1, 2, 3) of QCs were prepared in quintuplicate at each concentrations (L, M, H): set 1) normal QCs prepared as reported in section 3.3.6; set 2) post-extraction QCs (QC working solution was added to an extracted blank plasma sample); set 3) QCs in pure methanol. To evaluate PALBO, RIBO and LETRO recovery, the peak area ratio of set 1 to set 2 QCs was calculated.

3.3.7.2 Linearity

Calibration curves were built using a weighted quadratic regression method ($1/x^2$). To evaluate the linearity of the curve, five calibration curves freshly processed during different working days were used. The Pearson's determination coefficient R^2 was calculated and the comparison of the true and back-calculated concentrations (expressed as accuracy) of the calibration standards was checked. A minimum of 7 out of 8 calibration points, including the LLOQ and the ULOQ, had to be within 85–115% of the theoretical concentration (80–120% at the LLOQ).

3.3.7.3 Intra- inter-day precision and accuracy

The precision and accuracy of the method were determined during a single working day (intra-day, 6 replicates for each QC concentration) and during 5 different working days (inter-day, 3 replicates for each QC concentration). The measured concentrations had to be within 15% of the nominal value and this had to be verified for at least 2 out of 3 of QCs at each concentration level and in each run.

3.3.7.4 Limit of quantification and selectivity

The LLOQ of the present method was verified analysing the precision, accuracy and SNR obtained from 6 samples of pooled blank human plasma added with H working solution (prepared as reported in section 3.3.6).

To investigate the selectivity of the proposed bioanalytical method (i.e. the presence of interferences whose signal overlaps with the signals of the analytes of interest), 6 blank human plasma samples obtained from 6 different healthy donors were analysed. The samples analysed should be free of interference at the retention times of the analytes of interest. The absence of interference was defined as a response lower than 20% of the LLOQ for the analytes and lower than 5% for the internal standards.

3.3.7.5 Matrix effect

Effects of matrix endogenous components on the ionization of PALBO, RIBO and LETRO were evaluated with different strategies during the chromatographic method development and, successively, during the validation process.

Firstly, this phenomenon was investigated by means of the post-column infusion using standard solutions of the three analytes in 0.1% HCOOH MeOH/H_2O 1:1 at the concentration of 50 ng/mL and applying a flow rate of 20 µL/min. For more details on post-column infusion experiment see section 3.1.6.5. Then, matrix effect was investigated by calculating for each analyte the ratio of the peak area of set 2 QCs to the peak area of set 3 QCs. The CV should be within 15%.

3.3.7.6 Stability

Bench-top and long-term stability was assessed to ensure that sample preparation and sample analysis, as well as the storage conditions applied, do not affect the quantification of the analytes of interest. Stability tests were conducted using QCs prepared in triplicate at each concentration (L, M, H): bench-top stability was investigated after 4 h at room temperature; stability of the deproteinized QCs was evaluated in autosampler set at 4 °C re-analysing the samples 24, 48, and 72 h after the first injection; freeze/thaw stability was assessed by analysing three freshly prepared aliquots of each QCs concentration, and then again after one and two freeze/thaw cycles. Long term stability of PALBO, RIBO and LETRO was investigated both in plasma, to assess patients samples stability after storage at -80°C, and in solvent (MeOH) to assess working solutions stability after storage at -20°C. Stability tests were considered verified if the testing samples did not exceed 15% from the nominal concentrations at each QCs concentration.

3.3.7.7 Incurred sample reanalysis

Each of the 10 patients' samples collected till now were quantified in 2 separate runs during 2 different working days, to further assess the reproducibility of the proposed method. The two analyses can be considered equivalent if the % diff [expressed as: (repeat-original)*100/mean] between the first and the second concentration measured is within ±20% for at least 67% of the samples, as reported in section 3.1.6.7.

3.3.7.8 Carry-over

Since previously published methods [184, 185] underlined the presence of carry-over effect related to both PALBO and RIBO, during method development particular attention was paid to this phenomenon. Carry-over was evaluated as the percentage of the peak area of a blank sample injected after the ULOQ respect to the peak area of the LLOQ for each analyte. Carry-over should not exceed 20% of LLOQ.

3.3.8 Quantification of PALBO, RIBO and LETRO in breast cancer patients' plasma for TDM

3.3.8.1 Patients' enrolment

The proposed method was applied to quantify the C_{min} of PALBO, RIBO and LETRO to support a clinical study (prot. code: CRO-2018-83) on-going at the National Cancer Institute of Aviano, Italy. Patients enrolment is still at the beginning and, at the moment, method was tested on 10 plasma samples from 8 patients (from 2 patients were collected 2 sequential samples) affected by metastatic breast cancer.

The clinical study was approved by the local ethics committee of Friuli Venezia Giulia (Italy). It is conducted according to the Declaration of Helsinki principles and patients are enrolled in the clinical study only after the signature of the informed consent.

3.3.8.2 Patients' characteristics

The expected eligibility criteria were:

- patients treated with PALBO or RIBO according to the routine clinical practice criteria. The dose and the treatment cycle do not matter but patients should be at the steady state;
- age ≥18;
- life expectancy > 3 months;
- signed informed consent is required.

The exclusion criteria are:

- non-collaborative and/or unreliable patients;
- refusal of informed consent.

3.3.8.3 Treatment and sampling

The blood samplings have been performed at specific time in order to have the drug's concentration at the C_{min} level. Considering that the steady state, and thus the correct C_{min} value, is reached approximately after 5 drug half-lives, indications about the treatment days when blood sampling should be performed were decided according to its pharmacokinetics properties. Moreover, the timing of tablet intake is crucial for an accurate estimation of the real C_{min} in patient's plasma. For this reason, indication about administration time are also provided specifically for each drug.

The recommended dose for PALBO is 125 mg once daily for 21 consecutive days followed by 7 days off treatment to comprise a complete cycle of 28 days. The mean plasma elimination half-life is 29 hours *[186]*, so the steady state is reached after 6 days of treatment. Blood sampling should be performed from day 6 to 21 of every therapy cycle, moreover patients must take PALBO tablet every morning at a precise time (the last administration must be 24 h before the estimated time for the blood collection).

Meanwhile, for RIBO the recommended dose is 600 mg (three 200 mg film-coated tablets) once daily for 21 consecutive days followed by 7 days off treatment, resulting in a complete cycle of 28 days. The mean plasma elimination half-life is 32 hours *[105]*, the steady state is reached after 7 days of treatment, thus the blood sampling should be performed from day 7 to day 21 of every therapy cycle. As in the case of PALBO, patients must take RIBO pill every morning at a precise time and the last administration must be 24 h before the estimated time for the blood collection.

3.3.8.4 Patients' samples processing procedure

Once the validation had been completed, it was possible to proceed with the patient's samples quantification. The sample preparation method previously developer for calibrators and QCs was also applied for real samples. Patients' plasma was thawed at room temperature, vortexed for 10 s; 10 µL of plasma was then added with 80 µL of cold ISt solution, vortexed and centrifuged for 15 min at 16200 g and 4°C. finally, 80 µL of the supernatant were transferred to a polypropylene tube for the analysis, as shown in Figure 33.

Figure 33. Graphical representation of a patient's sample processing procedure.

3.4 Molecularly imprinted polymers

3.4.1 Instrumentation

Thin layer chromatography (TLC) were conducted on Merck plastic sheets pre-coated with 0.25 mm silica gel 60F-254. TLC plates were examined under UV light. Flash chromatography purifications were carried out with Merck silica gel 60 (230-240 Mesh).

Nuclear magnetic resonance (NMR), 500MHz ^{1}H-NMR, were obtained on a Brucker AV600 spectrometer. High performance liquid chromatography analyses were run on an Agilent 1100 series variable wavelength detector and a Kinetex C18 5 µm, 250x4.6 mm, 100 Å (Phenomenex).

Particles size was measured by Dynamic Light Scattering (DLS) on Zetasizer nano-S (Malvern). To perform DLS measurements glass cuvettes (PCS1115, Malvern) and nylon syringe filters 0,2 µm (Thermo Fisher) have been used.

3.4.2 Standards and Chemicals

Chemicals, paracetamol powder and solvents were purchased from Sigma Aldrich, deuterated solvents from Sigma Aldrich and Cambridge Isotope Laboratories (Tewksbury, Massachusetts). Imatinib free base, Imatinib mesylate and Sunitinib malate were purchased from Insight Biotechnology (Wembley, London, UK). Crimp cap Weaton vials used for polymer synthesis were purchased from Sigma Aldrich. Spectra/Por3 dialysis membrane MWCO 3500 Da was purchased from Spectrumlabs (Piraeus, Greece).

3.4.2.1 Synthesis of N,N'-(1,4-phenylene) bisacrylamide

1,4-phenylenediamine (5.6 mmol, 605 mg) was dissolved in acetone (25 mL) and cooled to 0 °C in an ice bath. Acryloyl chloride (11 mmol, 898.0 µL) was dissolved in acetone (15 mL) and added

dropwise to the solution of 1,4-phenylenediamine, while stirring, and allowed to warm and kept at room temperature overnight.

At the obtained solution was then added saturated NaHCO3 solution, the resulting precipitate was filtered and the solid was washed with 100 mL of cold H_2O. The crude product of N,N'-(1,4-phenylene) bisacrylamide (PBA) (Figure 34) was recrystallized from EtOH, to afford white crystals that were collected by filtration (1.2 g, 87%): ^{1}H-NMR (500 MHz, DMSO): δ 10.14 (s, 2H, (NH)2), 7.64 (s, 4H, (Phe-H)4), 6.42 (dd, J= 17.0, 10.0, 2H, (=CH)2), 6.26 (dd, J= 17.0, 2.0 Hz, 2H, (=CH2)2), 5.76 (dd, J= 10.0, 2.5 Hz, 2H, (=CH2)2; ESMS theoretical m/z for C12H12N2O2Na $[M + Na]^+$=239.08, found 239.1.

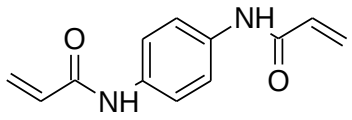

Figure 34. Chemical structure of PBA.

3.4.2.2 Recrystallization of AIBN

AIBN (2 g) was added to a two neck 50 mL round bottom flask (RBF), with condenser in top port and suba seal on side port. The RBF was put under vacuum and flushed with nitrogen for 10 times and leaved under flow of nitrogen at the end. 5mL of anhydrous methanol were added through the side port under stirring. Using a water bath, the solution was slowly heated to 52°C.

Approximately 2mL of MeOH were then added dropwise until a clear solution was obtained with the complete dissolution of AIBN. Subsequentially, heating was removed, and the solution was left to cool slowly at RT, yielding big needle crystals.

AIBN crystals were collected through suction filtration and washed with a small amount of ice-cold MeOH. Crystals were then left in desiccator for 2 hours to fully remove the solvent. Yield obtained: 65%.

3.4.3 ^{1}H-NMR titrations

^{1}H-NMR titration experiments were exploited to investigate the nature and the strength of possible interactions involved in the functional monomer-template complex during the synthesis of molecularly imprinted polymers and to identify the specific functional groups of the template that are involved [187]. The formation of the complex TM, between the template molecule (T) and the functional monomer (FM), is a dynamic process where the free molecules are in equilibrium with the bond counterpart:

$$T+FM \leftrightarrow TFM$$

Since in the hereby presented work the synthesis of MIP was performed in DMSO and chloroform (CHCl3), also the interactions were studied in deuterated DMSO (d_6-DMSO) and deuterated chloroform (CDCl3).

The interaction between the functional monomer and the template molecule was investigated by titrating the drug with the functional monomer MAA. In particular, a 4.06E-03 M solution of IMA free-base in d_6-DMSO/CDCl3 was prepared. To this solution, increasing amounts of FM solution (2.32E-01 M) were added to obtain final concentrations ranging from 2.30E-03 to 4.35E-02 M (the volume added was between 5-60 µL). A test was done adding solvent without FM and no protons chemical shift was observed.

Likewise, the interaction between PBA and IMA in d_6-DMSO was investigated. In the same way, a 4.06E-03 M IMA free-base solution was prepared and increasing amounts of PBA solution (9.25E-02 M) were added obtaining a concentration ranged from 1.81E-03 to 4.22E-02 M.

After every addition, the tubes were analysed and ^{1}H-NMR spectra were collected to monitor changed in chemical shift of protons involved in the interaction between the template and the monomer [188].

3.4.4 Synthesis of MIPs

The nanogels were synthesized exploiting the non-covalent approach, under high dilution radical polymerization (HDRP) conditions. This approach is characterized by the choice of the solvent and the overall monomer concentration.

During polymerization, could happen that unreacted double bonds on particle surface bring to the induction of inter-particles crosslinking leading to macrogelation. However, under diluted conditions and with the right solvent, each polymeric particle is stabilized avoiding intermolecular crosslinking [189]. In fact, the solvating power of the solvent prevents macrogelation via osmotic repulsion forces, for the hereby presented work DMSO was chosen as preferred solvent for polymer synthesis. The choice of the concentration of all monomers in the pre-polymerization complex is fundamental to obtain nanoparticles.

This concentration must be taken under a certain value obtained experimentally: the critical monomer concentration (C_M). It is defined as the percentage by weight of all the monomers used

for the polymerization as compared to the percentage of the overall mass of monomers and solvents used for a polymer preparation. The C_M is dependent on several factors associated with the system being studied. These include the nature and concentration of the initiator, the degree of crosslinking agent present, the temperature of which polymerization is performed and the most important factor that is the type and nature of the solvent.

The amount of solvent (m_S) necessary to obtain polymeric nanoparticles was calculated by the following equation [7]:

$$m_S = \frac{(m_{FM} + m_{CoM} + m_{CL}) \times 0.99}{0.01} \quad [7]$$

Where m_{FM}, m_{CoM} and m_{CL} are the amount in mass (mg) of functional monomer, comonomer and cross-linker as reported in the following Table 2 for each synthesis:

MIP	1	2	3	4	5	6	7	8	9
IMA	23.4	23.4	23.4	23.4	23.4	23.4	23.4	23.4	23.4
MAA	4.1	4.1	4.1	4.1	4.1	4.1	4.1	4.1	4.1
AA	3.4	1.7	0.0	10.1	6.8	3.4	10.1	23.6	10.1
MBA	22.0	25.6	29.3	43.9	51.3	58.6	29.3	-	-
PBA	-	-	-	-	-	-	20.5	20.5	61.6
AIBN	3.1	3.3	3.5	6.2	6.6	7.0	6.3	4.7	6.3

Table 2. Amount in mg of template molecule, functional monomer (MAA, methacrylic acid), comonomer (AA, acrylamide), cross-linkers (MBA, N,N'-methylenbis-acrylamide and PBA, N,N'-(1,4-phenylene) bisacrylamide) and initiator (AIBN) for each MIP prepared.

To obtain nanoparticles in DMSO, C_M was fixed at 1% w/w.

The protocol used for the preparation of the nanogels was the following: 1 equivalent of the drug was dissolved in a total amount of DMSO corresponding to the 99% in weight of total functional monomers and cross-linker (following the above-reported equation), and to this solution was added 1eq of the functional monomer, MAA. After stirring the solution for 1h in anhydrous conditions at RT, to form the pre-polymeric complex, it was transferred in a crimp cap Wheaton vial and all the other components were added. To calculate the moles number of initiator (AIBN) to add to the solution was used the following equation [8]:

$$n_I = \frac{(n_{FM} + n_{CoM} + 2n_{CL}) \times \%I}{100} \quad [8]$$

Where:

- I = initiator;
- FM = functional monomer;
- CoM = co-monomer;
- CL = cross-linker, the number of the cross-linker is doubled because it presents in its structure two double bond.

The vial was left first under vacuum and then was flushed with argon (3 times for 10 minutes). Radical polymerization was achieved heating the vial up to 70°C for 24h. Each polymer was synthesised either in presence of the template molecule, leading to MIP particles, or without the template, leading to non-imprinted polymers (NIP).

The resulting solutions were dialyzed against 1 L volume of water for one day, then against acidic MeOH (10% acetic acid (CH_3COOH) for one other day and finally for three days against H_2O, changing the solvent twice a day. Finally, the solutions were freeze-dried leading to a fluffy solid.

The preparation of nanogels in $CHCl_3$ followed the same protocol previously reported, but before dialyzing the nanogels, chloroform was evaporated, and the polymers were resuspended in MeOH. ^{1}H-NMR was used to verify that the reaction had gone to completion by monitoring the disappearance of the signals belonging to the acrylic protons. Two mg of each polymer was solubilized in DMSO-d6 and then the spectra were registered.

For all the polymer prepared, the yield percentage was also calculated with equation [9]:

$$\%\ yield = \frac{polymer\ mass}{\sum monomer\ masses} \quad [9]$$

3.4.5 Monomer conversion ^{1}H-NMR studies

To monitor and understand the percentage of reagents involved in the polymerization reaction, the monomer conversion NMR studies were performed.

Polymerization solutions used for the quantification of monomer conversion by ^{1}H-NMR were prepared on a smaller scale in Wheaton bottles following the same procedures described in section

3.4.4, using d6-DMSO as solvent. Before sealing the Wheaton bottle, the internal standard, 2-ethylnaphthalene (structure reported in Figure 35), was added to the pre-polymerization solution. A 500 µL aliquot of the mixture was transferred in an NMR tube, and a ^{1}H-NMR spectrum was recorded. The Wheaton bottle containing the remaining polymerization solution was sealed, purged with N2, and heated to 70°C in oil bath for 24h. After the polymerization, another 500 µL aliquot of the mixture was transferred to a different NMR tube. An appropriate volume of ISt was added, and ^{1}H-NMR spectra were recorded.

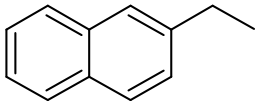

Figure 35. Chemical structure of 2-ethylnaphtalene, used as ISt in the monomer conversion NMR studies.

In both cases, the ^{1}H-NMR spectra acquired were phased and integrated identically. The concentration of monomers and crosslinker in the initial and final polymerization solutions were determined by comparing the intensities of monomer peaks at 5.75 ppm (PBA), 6.05 ppm (AAm), 6.00 ppm (MAA), 4.55 ppm (MBA), against the intensity of the IS peak at 7.85 ppm.
This test was performed for both MIPs and NIPs.

3.4.6 Dynamic light scattering

Dynamic light scattering is a well-established and non-invasive technique to measure particles size and molecules in suspensions, typically in the submicron range. This instrument uses a laser beam to illuminate the particles and measure their size by analysing the intensity fluctuations in the light scattered during their Brownian motion. The frequency of these fluctuations contains information about the diffusion coefficient of the particles, which in turn is size-dependent.
The Brownian motion consists in the movement of particles due to the random collision with the molecules of the solvent that surrounds the particle. Therefore, small particles move quickly, while large particles move slowly. The velocity of the Brownian motion is defined by the translational diffusion coefficient, that could be converted into particle size using the Stokes-Einstein equation [10]:

$$d_H = \frac{kT}{3\pi\eta D} \quad [10]$$

Where: d_h is the hydrodynamic diameter; k is the Boltzmann's constant; T is the absolute temperature, η is the viscosity and D id the diffusion coefficient.

Note that the diameter that is measured in DLS is a value that refers to how a particle diffuses within a fluid, so it is referred to a hydrodynamic diameter.

That measurement principle requires that diffusion is the only cause of motion in the sample, thus effects like sedimentation, thermal convection and fluid flow must be avoided. Therefore, the upper limit that DLS can measure as particle size is usually some micrometres. The lower size limit is determined by the time resolution of the specific measurement device and lies typically in the range of a few nanometres. The primary result that is obtained by the instrument is the intensity size distribution. The intensity distribution is naturally weighted according to the scattering intensity of each particle fraction or family. For biological materials or polymers, the particle scattering intensity is proportional to the square of the molecular weight [190]. Consequently, the intensity distribution can be somewhat misleading: a small amount of aggregating particles or the presence of a larger particle species can dominate the distribution. For this reason, size distribution by intensity could be converted, using Mie theory, to a volume or a number distribution. In these cases, distribution described the relative proportion of multiple components in the sample based on their volume or mass rather than based in their scattering (intensity).

Moreover, it could happen that the size distribution by intensity showed the presence of two particles populations, while in the size distribution by number only one peak appeared. This behaviour could be explained considering that large particles scattered the light more intensely than small particles, as reported in the Rayleigh scattering equation where the intensity of a particle is related to the 6th power of the diameter, as described in equation [11]:

$$I = I_0 \frac{1 + cos^2\theta}{2R^2} \left(\frac{2\pi}{\lambda}\right)^4 \left(\frac{n^2 - 1}{n^2 + 2}\right)^2 \left(\frac{d}{2}\right)^6 \quad [11]$$

Where λ and I_0 are respectively the wavelength and the intensity of the beam of light, ϑ is the scattering angle, R is the distance between the particle and the detector, n is the refractive index of the particle and d is the diameter of the particle.

Nanogels d_h measurements were obtained with a Zetasizer Nano ZS (Malvern Instruments Ltd., Malvern, UK) at 25°C. All measurements were performed in triplicate at a concentration of 0.2

mg/mL in 2% DMSO aqueous solution, after sonicating for 30 min and filtering through a 0.2 µm syringe filter. Particle sizes given for the nanogels represent estimates of the mean d_h by intensity and by number.

3.4.7 Rebinding tests

One of the most important aspects of imprinted polymer characterization is the rebinding study. This is an essential part that provides verification that the three-dimensional cavity formed during the imprinting process has not been greatly altered and its shape is still capable to bind the original template molecule.

The rebinding capacity of the MIPs and NIPs to capture the drug were investigated dissolving 1 mg/mL polymer suspension in different concentration of Imatinib Mesylate in water: 50, 300, 600, 1500, 3000 µM. The mixtures were incubated at RT under continues stirring for 1h. Then the solutions were centrifuged (14000 rpm for 20 min) to allow the polymer to precipitate in the bottom of the Eppendorf and the supernatant was analysed by HPLC coupled to UV-vis detector to quantify the drug concentration. The column used was a Kinetex C18 5 µm, 250x4.6 mm, 100 Å, with an isocratic gradient composed by 80% aqueous solution added with 0.1% TFA and 20% AcN; the absorption was set at 270 nm. The area of the drug peak resulted in the chromatogram of the sample treated with the polymer ($A_{treated}$) was compared with the one of a reference sample containing only the drug in water ($A_{reference}$), no treated with the polymer, to calculate the amount of drug captured by the polymer. The percentage of binding was calculated with the equation [12]:

$$\%binding = 100 - \left(\frac{A_{treated}}{A_{reference}}\right) \times 100 \quad [12]$$

The efficiency of the imprinting process was, thus, evaluated by measuring the imprinting factor (IF) obtained from the rebinding experiments of MIPs and NIPs. IF is a measure of the strength of interaction of the imprinted polymer towards the template molecule.

It is obtained from the ratio of target drug amount bound to the MIP, to the amount of the same molecule captured by the NIP (equation [13]):

$$IF = \frac{Q_{MIP}}{Q_{NIP}} \quad [13]$$

Where Q_{MIP} and Q_{NIP} are respectively the absorption capability of the MIP and the NIP having the same monomer formulation. This normalization method removes binding due to non-specific interactions.

It has been shown that there was a positive correlation of the interaction strength with the imprinting factor [191], meaning that imprinted polymers exhibiting good performance, in terms of high imprinting factor value, should interact strongly with the template molecule and therefore compared to the NIPs [192].

3.4.8 Selectivity studies

The polymer selectivity was investigated for its target molecule but also for another TKI, SUNI, used in second-line treatment in GIST patients (as reported in section 1.2.1.2), and one of the most common use drugs in case of pain in oncological patients, paracetamol (PARA).

The tests were performed as reported in the section 3.4.7. A 1 mg/mL water polymer suspension was prepared and mixed with different concentration of drugs. Then, the suspension was stirred for 1 h at RT, the polymer was precipitated by centrifugation and the supernatant was analysed by HPLC-UV/VIS. For SUNI an isocratic gradient composed by 60% AcN and 40% aqueous solution added with 0.1% TFA was used; the absorption lambda was set at 425 nm. For PARA an isocratic gradient composed by 90% aqueous solution added with 0.1% TFA and 10% can was used; the absorption lambda was set at 243 nm. Total run for all the methods was 15 min.

4. RESULTS AND DISCUSSION

4.1 LC-MS/MS method development for the simultaneous quantification of IMA and norIMA in DBS

4.1.1 Mass spectrometric conditions optimization

4.1.1.1 Compound-dependent parameters optimization

The monoisotopic mass of IMA is 493.26 Da, so working in positive ion mode with ESI source, the presence of the analyte of interest, during the first Q1 scan, was confirmed by the protonated molecule $[M+H]^+$ at 494.4 m/z (Figure 36)

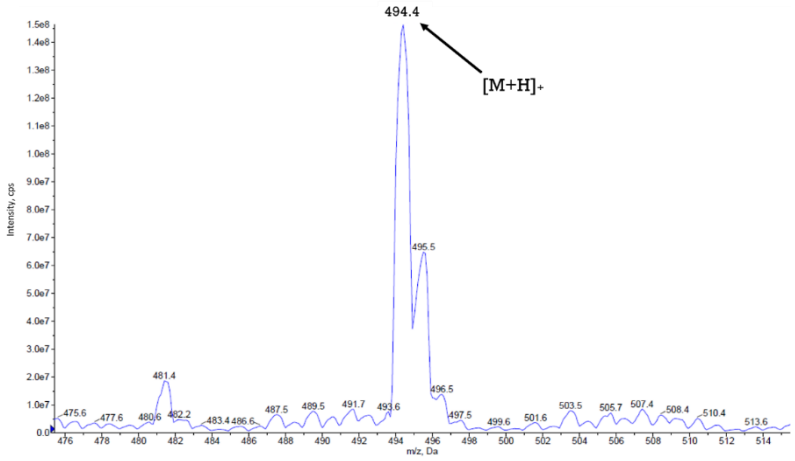

Figure 36. Spectrum obtained in positive mode with a Q1 scan from 450 to 650 Da that confirms the presence of IMA.

Through Q1MI scan mode, the XIC signal of the pseudo-molecular ion at 494.4 m/z was monitored ramping the DP value from 0 to 400 V. The XIC highest intensity was reached with DP=110 V, which represents the optimal value for a correct removal of clusters. In the same way the value of 10 V was determined as optimal for EP. In product ions (MS2) mode, the fragmentation of the IMA precursor ion was evaluated with different CE values (from 10 to 100 V) applied within the collision cell. The fragmentation patterns of IMA (Figure 37) were as follow: 494.4 > 394.3 *m/z* (quantifier, DP 110 volts, CE 40 V) and 494.4 > 217.2 *m/z* (qualifier, DP 110 volts, CE 35 V).; 502.4 > 394.2 *m/z* (DP 110 volts; CE 40 V) for IMA-D8 used as IS.

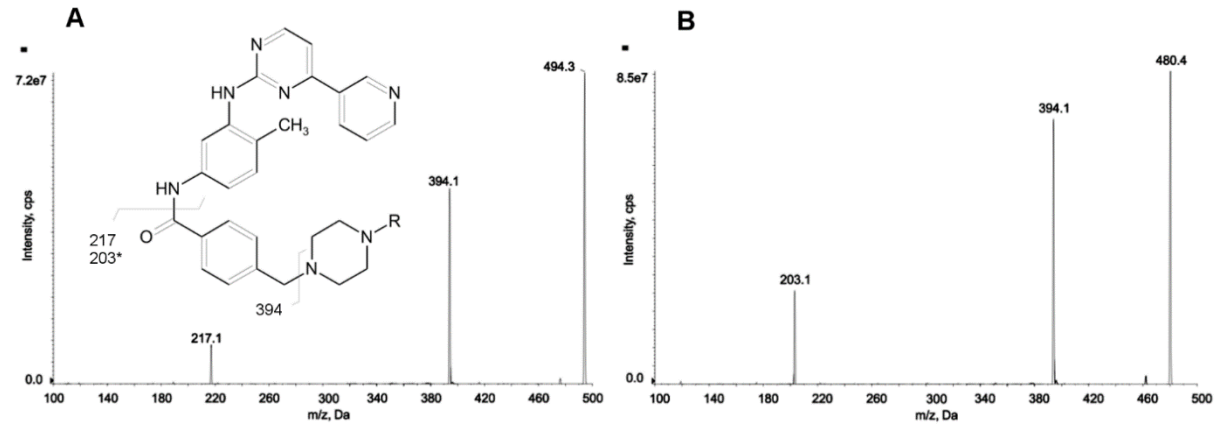

Figure 37. Spectrum recorded in product ion mode showing the fragmentation pattern of: IMA precursor ion at 494.4 m/z with a CE value of 70 V (A) and norIMA precursor ion at 480.4 m/z with a CE value of 70 V. In the figure in panel (A) is reported also the graphical representation of fragmentation for both IMA and norIMA.

An optimal CXP value of 10 V for each of these SRM transitions was obtained. Moreover, with the precursor ion scan mode it was possible to confirm the direct derivation of the three selected product ions from the precursor ion at 494.4 *m/z*.

The compound dependent parameters for norIMA and the ISt IMA-D8 were determined with the same experiments carried out for IMA and the results were summarised as follow: the presence of norIMA and IMA-D8 was confirmed by the pseudo-molecular ion $[M+H]^+$ at 480.4 and 502.4 *m/z* respectively. The optimal DP and EP values for both the analytes were 110 V and 10 V. The fragmentation patterns for norIMA was the following: 480.4 > 394.3 *m/z* (quantifier, CE 35 V) and 480.4 > 203.2 *m/z* (qualifier, CE 35 V). Meanwhile, the chosen fragmentation and the optimal CE value for IMA-D8 was: 502.4 > 394.2 *m/z,* CE 40 V. Finally, an optimal CXP value of 10 V was obtained. In Table 3 are summarized the compound-dependent parameters optimized.

Compound	Q1 (m/z)	DP (V)	EP (V)	Q3 (m/z)	CE (V)	CXP (V)
IMA	494.4	110	10	394.3	40	10
				217.2	35	10
norIMA	480.4	110	10	394.3	35	10
				203.2	35	10
D8-IMA	502.4	110	10	394.2	40	10

Table 3. Compound-dependent parameters.

4.1.1.2 Source-dependent parameters optimization

The goal of this experiment was to reach the maximum intensity in order to achieve the greatest sensitivity for the interest analytes. As reported in section 3.1.2.2 the XIC trend for IMA quantifier transition was monitored by working in SRM mode, thus tuning each source dependent parameter to obtain the highest signal intensity.

Source-dependent parameters were optimized as follow: Turbo Ion Spray source operating at 500°C, IS voltage set at 2200 V with CUR at 25 psi, and both nebulizer gas and turbo gas pressure at 40 psi.

4.1.2 Chromatographic conditions optimization

As reported in section 3.1.3, a 2D chromatographic system was applied to this LC-MS/MS method. All the system was designed to easily tuning the working parameters changing the configurations of the 4 valves.

The initial conditions to set up were those related to the perfusion column: in particular, the conditions for analytes trapping into POROS column and their transfer to the RP column. In particular, the two parameters that needed to be optimized were the organic solvent percentage and the flow rate. These parameters were set up in order to perform the analytes transfer from the POROS to the RP column within 1.7 and 3.0 min after the sample injection (V2 is in configuration II). This specific time-window was experimentally determined considering the necessary volume to completely wash the POROS from the proteins still present in the sample: 10-column volumes of solvent are necessary to this aim, in fact the POROS (with an internal volume of 0.3 mL) was washed for 1.5 min with a 2.0 mL/min flow.

The optimization of the analytes transfer was performed using the V3 that, in configuration II, allows the connection of the POROS directly to the mass spectrometer. In panels (A) and (B) of Figure 38 two examples of a high and low flow rate and/or % of MPD, respectively, are reported. Instead, panel (C) showed an example of using the optimal conditions applied to transfer the analytes. To reach this result, the following gradient was used: the MPD % was increased from the initial condition (10%) to 75% at 1.5 min and then to 98% over 0.2 min, as reported in Figure 39. The flow rate was set at 0.13 mL/min before the configuration change of V2 (1.56 min), this allows the RP to hold back IMA and norIMA.

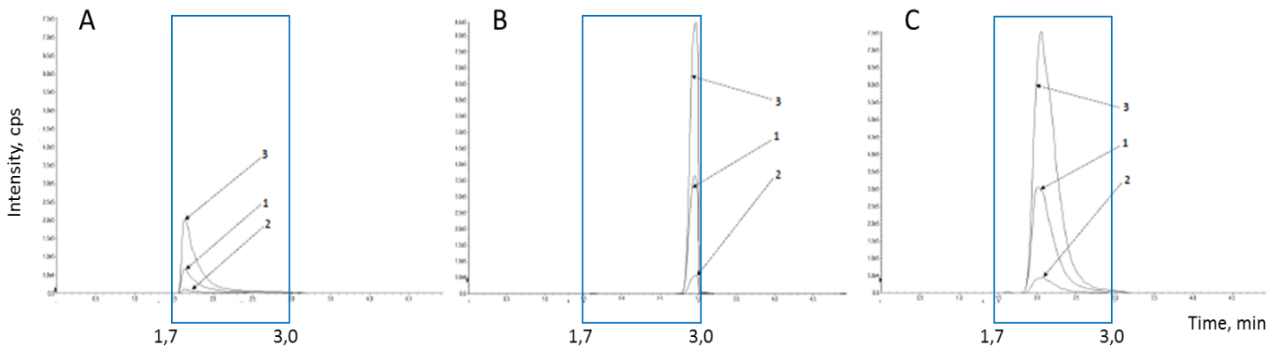

Figure 38. Tuning of the parameters to transfer of the analytes from the POROS to the RP column (from 1,7 to 3,0 min). Example of the application of: high flow rate or/and % MPB (A); low flow rate or/and % MPB (B); the right flow rate and % of MPB (C). In all the panels, (1) correspond to IMA, (2) to norIMA and (3) to D8-IMA peak.

Once the transfer was completed, the flow rate was set again at 2 mL/min allowing the cleaning and the reconditioning of the POROS.

In Figure 39 the final gradient applied to the POROS column is reported, to ensure the trapping and the transfer of the analytes, but also the cleaning and the reconditioning steps.

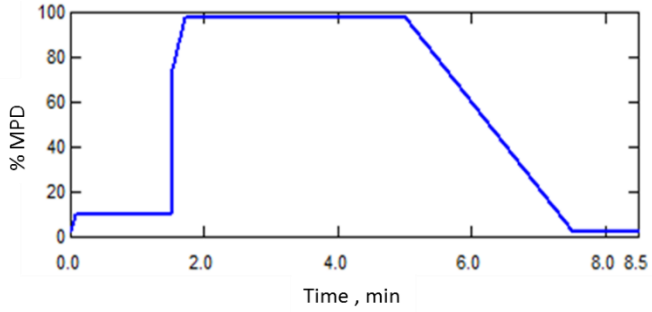

Figure 39. Graphical representation of the gradient applied to the perfusion column.

When the conditions for the perfusion column were settled, the RP column chromatographic gradient had to be defined to achieve a fast and good separation of the two analytes.

The second column, that acted the actual chromatography, was the Synergi Fusion-RP (described in section 3.3.4). To perform the analytes elution, AcN was chosen as strong solvent, with the addition of 20% of iPrOH. Meanwhile, as weak solvent, ultrapure H_2O was selected. Both the solvents were added with 0,1% HCOOH v/v to help the ionization of the analytes.

The selected flow rate was 0.45 mL/min and the column oven was set at 50°C. A high column temperature helps to lower the solvents viscosity, decreasing, therefore, the back-pressure of the pumps. This is crucial considering that in this method was used a mixture of AcN and iPrOH in the MPs, that has a very high viscosity.

In Figure 40 the gradient applied to the RP column is represented. The chromatographic separation was obtained using the following gradient: 1) initial condition with 10% of eluent B kept constant for 3 min; 2) from 10% to 60% of MPB over 3 min, to allow the analytes elution; 3) from 60 to 98% of MPB over 0.6 min and kept constant for 1 min to allow the RP column washing; 4) from 98% to the initial condition over 0.5 min and reconditioning for 1 min. This time was sufficient to perform the re-equilibration of the column, because after consecutive injections, the Rt of both IMA and norIMA were reproducible. The total run time was 8.5 min and the retention time of IMA and norIMA were 5.50 and 5.39 min, respectively.

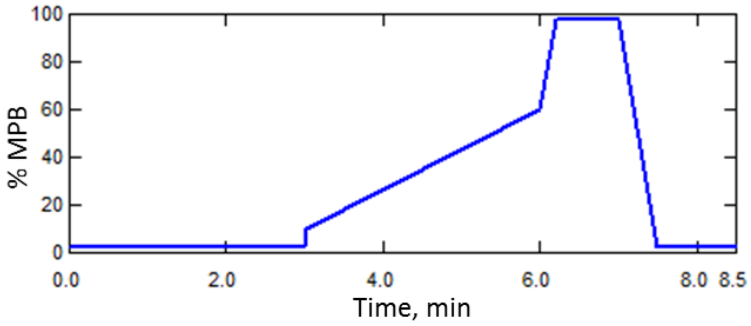

Figure 40. Multi-step optimized chromatographic method applied to the RP column.

In Figure 41 an example of MRM chromatogram was reported, produced by the analysis of a DBS calibrator (3750 ng/mL for IMA and 750 ng/mL for norIMA) with the developed LC-MS/MS method.

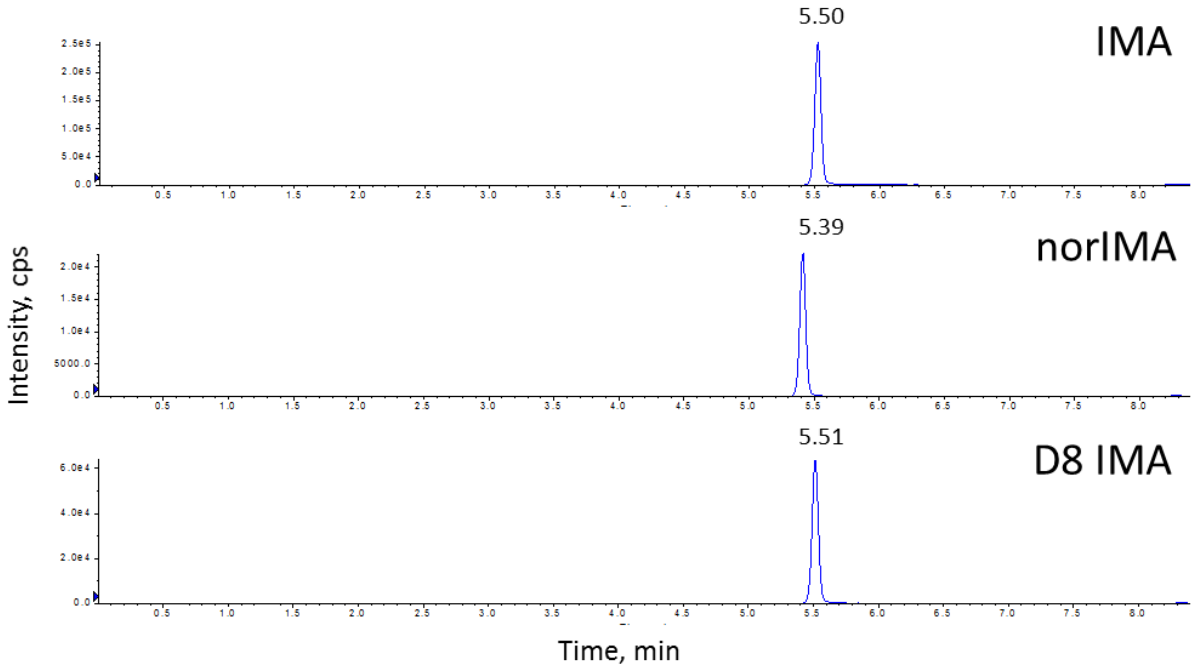

Figure 41. Example of MRM chromatogram obtained from the calibrator point D (3750 ng/mL for IMA and 750 ng/mL for norIMA).

4.1.3 Dried blood spot optimization parameters

4.1.3.1 Type of the paper

As reported in section 3.1.5.1, the matrix used to perform the DBSs is an important parameter to choose and take in consideration during the method development. No significant difference on IMA and norIMA quantification in DBS was observed using different filter papers (Whatman 31ET-CHR and Whatman 903). The QC samples spotted on Whatman 31ET-CHR and analysed using a calibration curve spotted on Whatman 903, showed an accuracy between 88.3 and 97.5 % for IMA and between 95.5 and 104.3 % for norIMA, at each concentration level (L, M, H).

4.1.3.2 Drug extraction optimization

The optimization of the analytes' extraction is one of the crucial parameters to take in considerations. Different solvents and mixtures were tested to obtain the maximum extraction of IMA and norIMA. Considering that IMA is slightly soluble in AcN, was found that the extraction yield using this solvent was just the 5%. The best solvent to ensure a good extraction of both IMA and norIMA from the DBS paper was MeOH. In this direction also mixtures of MeOH with iPrOH, basis and acids were tested. The formic acid at 0,1 % was found to help the extraction, guaranteeing a good signal for both the analytes in all the calibration curve range.

After the assessment of the extraction solvent, the time extraction optimization was performed. After the addition of the extractant, the samples were stirred for different times from 30 min to 4 h. As reported in Figure 42 the maximum extraction efficiency was already reached after 30 min of stirring.

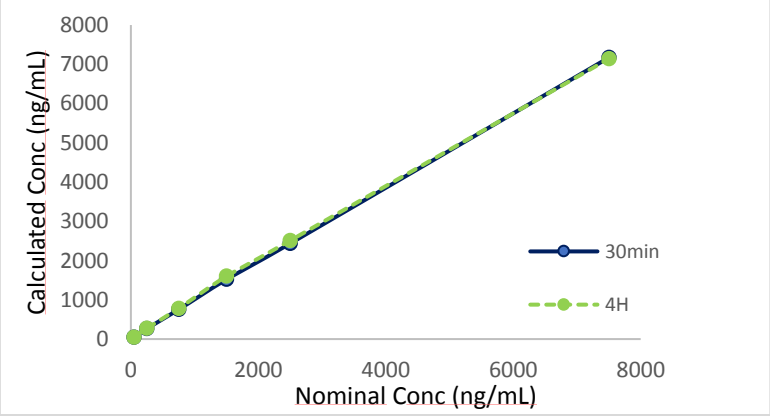

Figure 42. Extraction of IMA after 30 min and 4 h of stirring.

4.1.3.3 Effect of the haematocrit

No significant impact of Hct on IMA and norIMA quantification in DBS was observed among the Hct values range tested (29.0-59.0 %). In fact, at each Hct value tested, accuracy was between 95.3 and 104.8 % for IMA and between 95.4 and 108.9 % for norIMA at each QC level (L, M, and H), while precision was within 3.5 and 6.0 % for IMA and norIMA, respectively. Data are reported in Table 4 for IMA and in Table 5 for norIMA.

	Nominal Conc IMA	Hct%	Mean ± SD	CV%	Acc%
QCL	250	29.0	246.7 ± 8.5	3.5	98.7
		38.4	261.9 ± 1.9	0.7	104.8
		59.0	259.9 ± 6.2	2.4	104.0
QCM	1250	29.0	1278.7 ± 9.6	0.7	102.3
		38.4	1258.4 ± 16.9	1.3	100.7
		59.0	1282.7 ± 24.7	1.9	102.6
QCH	6000	29.0	5718.1 ± 202.9	3.5	95.3
		38.4	6112.9 ± 145.0	2.4	101.9
		59.0	6063.4 ± 277.2	4.6	101.1

Table 4. Effect of Hct measured for IMA DBS samples.

	Nominal Conc norIMA	Hct%	Mean ± SD	CV%	Acc%
QCL	50	29.0	50.8 ± 3.1	6,0	101.5
		38.4	51.6 ± 2.4	4,6	103.1
		59.0	48.6 ± 1.8	3,7	97.1
QCM	250	29.0	272.3 ± 2.9	1,1	108.9
		38.4	254.1 ± 4.5	1,8	101.6
		59.0	238.5 ± 7.7	3,2	95.4
QCH	1200	29.0	1293.7 ± 36.5	2,8	107.8
		38.4	1286.4 ± 48.9	3,8	107.2
		59.0	1209.5 ± 52.9	4,3	100.8

Table 5. Effect of Hct measured for norIMA DBS samples.

4.1.3.4 Effect of volcano effect

As related to the “volcano effect” assessment, no differences in IMA nor in norIMA concentrations between central and peripheral areas of the DBS were observed. As reported in Table 6, at each concentration tested (L, M, and H) the C/P was within 0.9-1.1.

Sample	Nominal conc. (ng/mL)	Mean C conc. ± SD (ng/mL)	Mean P conc. ± SD (ng/mL)	C/P
QCL (IMA)	250	258.5±2.6	253.9±2.4	1.0
QCM (IMA)	1250	1249.7±4.6	1321.6±1.8	0.9
QCH (IMA)	6000	5934.4±3.1	5844.4±1.8	1.0
QCL (norIMA)	50	48.6±4.3	44.9±1.1	1.1
QCM (norIMA)	250	225.9±3.6	243.0±2.2	0.9
QCH (norIMA)	1200	1139.1±2.3	1134.0±0.8	1.0

Table 6. Center/perimeter concentration ratio (C/P) for IMA and norIMA as evaluation of the "volcano effect".

4.1.3.5 Effect of the spot size

No influence of spot size among 10-40 µL-volume range was observed at each QC concentration. The accuracy was between 87.8-110.1 % and 88.9-104.3 % for IMA and norIMA, respectively. The precision was within 6.0 % for IMA and 6.5 % for norIMA and norIMA. All the data are reported in Table 7 for IMA and Table 8 for norIMA.

	Nominal Conc IMA	Volume (µL)	Mean ± SD	CV%	Acc%
QCL	250	10	240.9 ± 7.1	2.9	96.4
		20	271.0 ± 6.0	2.2	108.4
		30	254.0 ± 9.8	3.8	101.6
		40	275.2 ± 6.4	2.3	110.1
QCM	1250	10	1191.0 ± 71.9	6.0	95.3
		20	1274.9 ± 29.4	2.3	102.0
		30	1266.1 ± 26.0	2.1	101.3
		40	1268.6 ± 32.4	2.6	101.5
QCH	6000	10	5266.6 ± 243.0	4.6	87.8
		20	5625.2 ± 107.7	1.9	93.8
		30	6100.6 ± 28.7	0.5	101.7
		40	5918.8 ± 276.8	4.7	98.6

Table 7. Effect of spot size evaluated from 10 to 40 µL in IMA DBS samples.

	Nominal Conc norIMA	Volume (µL)	Mean ± SD	CV%	Acc%
QCL	50	10	47.2 ± 1.5	3.2	94.4
		20	52.1 ± 3.3	6.3	104.3
		30	48.6 ± 0.6	1.3	97.3
		40	52.1 ± 1.2	2.3	104.1
QCM	250	10	234.8 ± 13.3	5.7	93.9
		20	249.5 ± 4.1	1.6	99.8
		30	234.2 ± 8.2	3.5	93.7
		40	241.2 ± 8.3	3.5	96.5
QCH	1200	10	1067.1 ± 32.4	3.0	88.9
		20	1126.8 ± 39.2	3.5	93.9
		30	1182.8 ± 27.2	2.3	98.6
		40	1161.1 ± 75.8	6.5	96.8

Table 8. Effect of spot size evaluated from 10 to 40 µL in norIMA DBS samples.

4.1.3.6 Correlation between finger-prick and venous collection

The correlation between C_{min} values from finger-prick and those from venous (without anticoagulant) DBSs, collected from ten patients, demonstrated that the two samples were equivalent (R^2= 0.9967 for IMA and R^2= 0.9798 for norIMA, as reported in Figure 43). Moreover, the % diff between DBSs from venous blood and those from finger-prick were always within ±20% of the mean (from -12 to 3.8%). This agreement may be due to the fact that the C_{min} sampling, by its own definition, was performed once distribution equilibrium of the drug was reached, while differences can be expected in the early moments following drug administration [193].

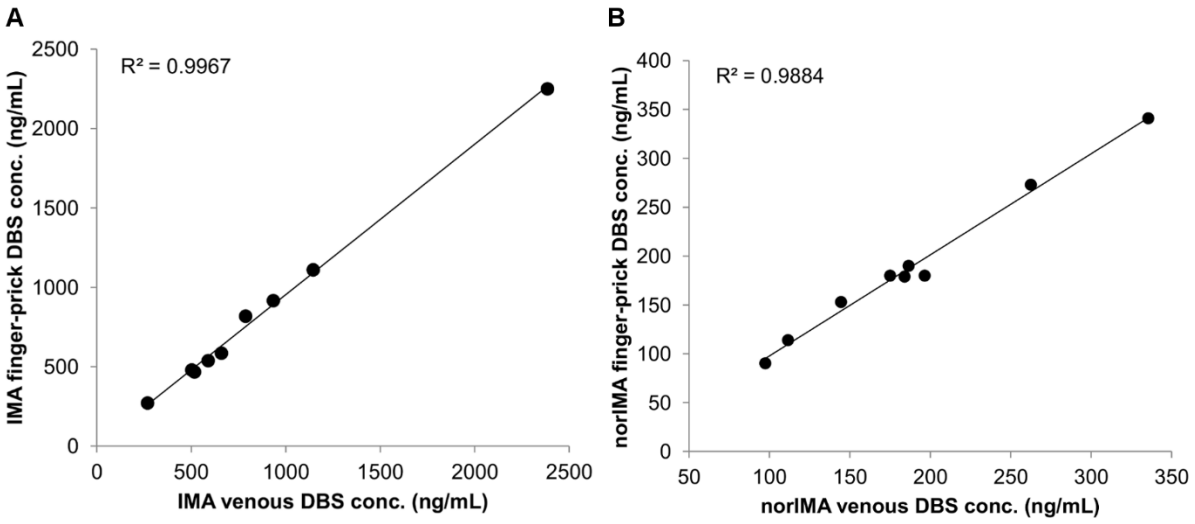

Figure 43. Correlation between finger-prick and venous collection for IMA (A) and norIMA (B) by comparing the results on DBS from venous blood (without anticoagulant, x-axes) and DBS from finger-prick (y-axes).

4.1.4 LC-MS/MS validation study

As reported above, the main parameters considered for the validation of this method, accordingly to FDA and EMA guidelines were: recovery, linearity, intra- and inter-day precision and accuracy, limit of quantification, selectivity, evaluation of the matrix effect, stability and reproducibility.

4.1.4.1 Recovery

According to the proposed method, analytes were extracted from DBS samples by simply adding to 3 mm-disc 150 µL of methanol added with 0.1 % HCOOH and IMA-D8 at the concentration of 10 ng/mL. The recovery, evaluated in five replicates at three QC concentration levels and calculated exploiting the equation [2], resulted in the range 74.8-80.5 % with a CV ≤5.4% for IMA and 66.5-68.5% with a CV ≤7.7% for norIMA, as shown in Table 9.

Analyte	Nominal conc. (ng/mL)	Recovery (%) ±SD	Recovery CV (%)
IMA	250	74.8±4.1	5.4
	1250	77.7±303	4.2
	6000	80.5±2.0	2.5
norIMA	50	66.5±5.1	7.7
	250	66.6±3.1	4.6
	1200	68.5±1.4	2.1

Table 9. Recovery of IMA and norIMA in DBS samples.

4.1.4.2 Linearity

The calibration curves were freshly prepared every day during the validation study. To generate a calibration curve, in Figure 44 an example for each compound is reported, the peak-area ratios between the analyte and the ISt compared to the nominal concentrations were plotted and a least-squares linear regression, weighted by the reciprocal of the concentrations, were plotted and a weighted ($1/x^2$) was applied. The calibration curves prepared on five different days showed good linearity.

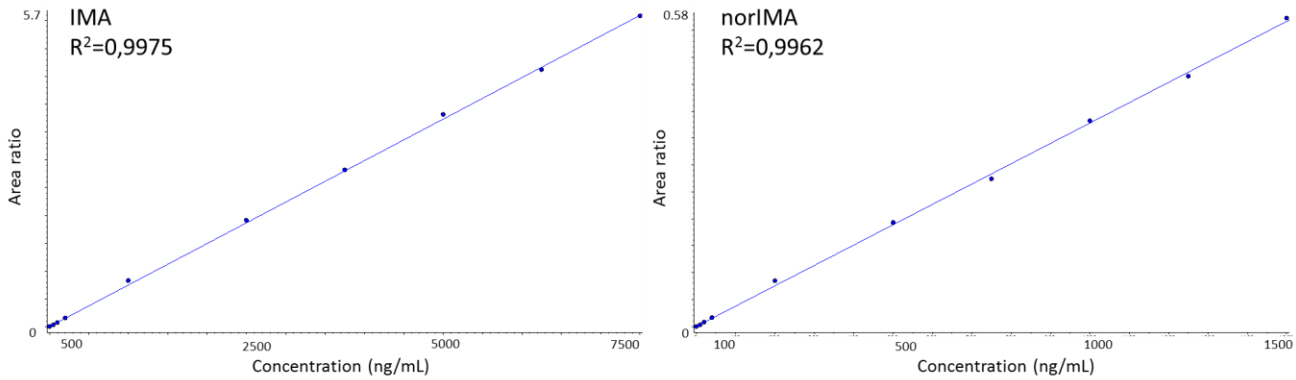

Figure 44. Example of calibration curves of IMA (left panel) and norIMA (right panel) in DBS samples.

Good linearity was obtained over the concentration range of 50-7500 ng/mL for IMA and 10-1500 ng/mL for norIMA, being the Pearson's coefficient of determination R^2 ≥0.9962 for each run. In Table 10, complete data (R^2, intercept, and slope) related to linearity of both IMA and norIMA calibration curves are reported. The accuracy resulted in the range 91.4-108.0% for IMA and 91.4-105.7% for norIMA and the precision was within 8.9% for IMA and within 8.4% for norIMA.

IMA R^2= 0.9974±0.0007 Intercept: 0.0201±0.004 Slope: 0.00087±0.00006			
nominal conc. (ng/mL)	**Mean ± SD**	**CV%**	**Acc%**
50	49.2±2.3	4.7	98.5
100	101.0±9.0	8.9	101.0
200	211.2±10.6	5.0	105.6
500	538.2±17.6	3.3	107.6
1000	1080.4±41.2	3.8	108.0
2500	2457.4±115.4	4.7	98.3
3750	3848.4±185.9	4.8	102.6
5000	4825.8±195.4	4.0	96.5
6250	5772.0±318.2	5.5	92.4
7500	6856.0±303.3	4.4	91.4

norIMA R^2= 0.9970± 0.0009 Intercept: 0.0017± 0.0007 Slope: 0.00037±0.00005			
nominal conc. (ng/mL)	**Mean ± SD**	**CV%**	**Acc%**
10	9.9±0.8	8.4	98.7
20	21.1±1.6	7.6	105.3
40	41.5±2.2	5.2	103.8
100	105.7±5.3	5.0	105.7
200	211.2±7.9	3.7	105.6
500	489.5±30.7	6.3	97.9
750	780.2±30.4	3.9	104.0
1000	980.7±54.9	5.6	98.1
1250	1170.7±76.2	6.5	93.7
1500	1370.3±76.2	5.6	91.4

Table 10. Linearity, accuracy and precision data for calibration curves of IMA and norIMA.

4.1.4.3 Intra- and inter-day precision and accuracy

The precision of the method was confirmed by the intra- and inter-day CV ≤3.1% and ≤5.6% for IMA and ≤4.3% and ≤6.6% for norIMA (Table 11). The intra- and inter-day accuracy were within the range 88.9-106.2% and 98.9-104.3% for IMA and 92.9-112.8% and 95.7-101.0% for norIMA.

Intra-day (N=6)				
Analyte	**Nominal conc. (ng/mL)**	**Mean ± SD**	**CV %**	**Accuracy %**
IMA	250	281.2 ± 6.3	2.2	88.9
	1250	1402.5 ± 43.5	3.1	89.1
	6000	5651.7±163.5	2.9	106.2
norIMA	50	52.1 ± 2.3	4.3	95.9
	250	269.2 ± 7.7	2.9	92.9
	1200	1064.0±26.08	2.5	112.8

Inter-day (N=15)				
Analyte	Nominal conc. (ng/mL)	Mean ± SD	Precision %	Accuracy %
IMA	250	260.9 ± 11.2	4.3	104.3
	1250	1282.3 ± 41.7	3.3	102.6
	6000	5932.8 ± 330.1	5.6	98.9
norIMA	50	50.5 ± 2.9	5.7	101.0
	250	248.8 ± 16.4	6.6	99.5
	1200	1196.3 ± 72.2	6.0	95.7

Table 11. Intra and inter-day precision and accuracy of the method for the quantification of IMA and norIMA.

4.1.4.4 Lower limit of quantification and selectivity

The LLOQ was defined as the lowest concentration that could be measured (SNR≥5) with a precision within 20% and accuracy between 80% and 120%. The LLOQ for the proposed method was fixed at 50 ng/mL for IMA and 10 ng/mL for norIMA. As shown in Figure 2, the SNR was 154.4 for IMA and 47.7 for nor-IMA. Through the analysis of six replicates, both the accuracy and precision were determined: the accuracy and CV% were, respectively, 97.1 and 7.6% for IMA and 91.1% and 8.7% for norIMA. The method has a good selectivity: from the analysis of six blank DBS samples no significant interferences were detected, especially at the retention times of our compounds. In Figure 45, an example of one of the six blank DBS samples analysed is reported.

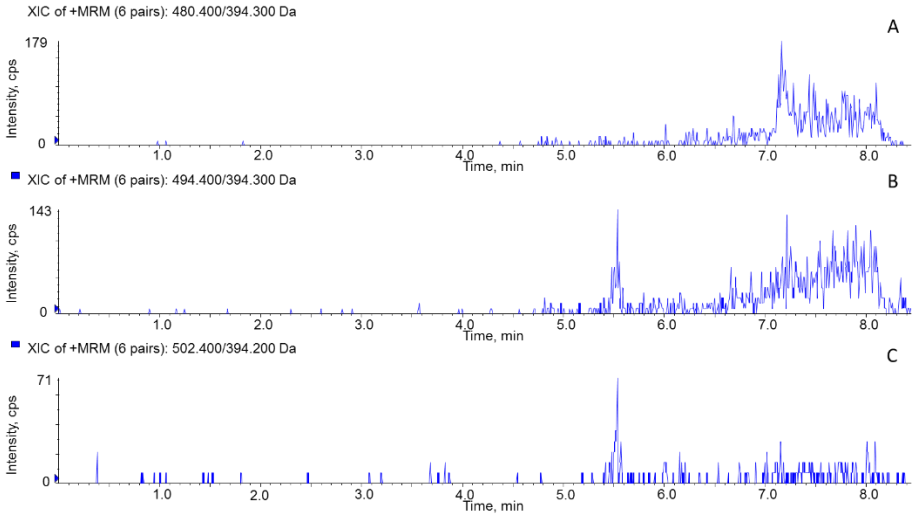

Figure 45. Example of blank DBS sample analyzed, for norIMA (A), IMA (B) and D8-IMA (C).

4.1.4.5 Matrix Effect

The method was not significantly affected by endogenous components of the matrix. The estimated matrix effect (ME%) was found between 90.0-109.7 % with a CV within 6.4 % for IMA and between 100.5-110.1 % with a CV within 7.2 % for norIMA, indicating the absence of major ion suppression or enhancement for both the analytes (Table 12).

Analyte	Nominal conc. (ng/mL)	ME (%) ±SD	ME CV (%)
IMA	250	109.7±4.4	4.0
	1250	104.8±4.9	4.7
	6000	90.0±5.7	6.4
norIMA	50	109.6±1.9	1.8
	250	110.1±1.6	1.5
	1200	100.5±7.2	7.2

Table 12. Matrix effect (ME) of IMA and norIMA in DBS samples.

This result was confirmed also by the post-column infusion test (Figure 46), with which it was observed that the intensity of the analyte signal did not undergo variations at the retention time of the analytes. Therefore, it was possible to exclude the presence of any matrix effect of ion suppression or enhancement.

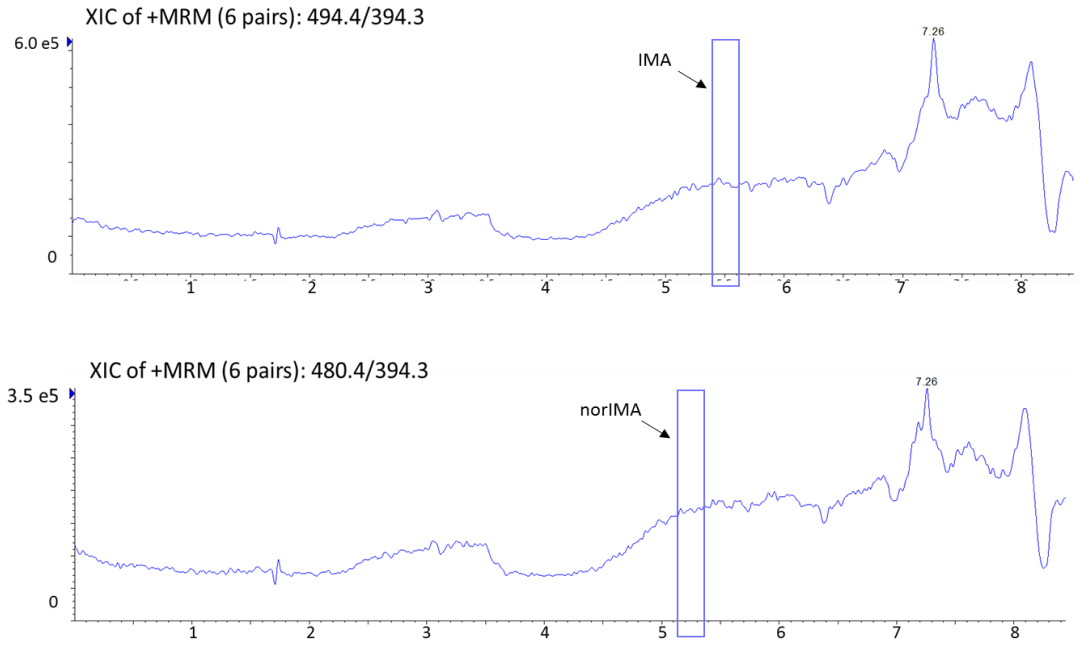

Figure 46. Matrix-effect evaluation for both IMA and norIMA with post-column infusion.

4.1.4.6 Stability

The stability of IMA and norIMA, under different conditions, was assessed by analysing QC samples in triplicate. Both the analytes resulted stable, after extraction from DBS, for 24 h at 4°C. The long-term stability in DBS, stored in plastic envelopes containing silica-gel drying bag at room temperature, was verified up to 16 months. The stability of the standard working solutions of IMA and norIMA was assessed after 24 months of storage at −80°C.

4.1.4.7 Incurred samples reanalysis

To further assessed the reproducibility of the proposed method, ten DBS patients' samples were analysed two times, with separate runs and during different working days. The concentration range of the chosen DBS samples were between 195-1700 ng/mL (quantified with the first analysis). The % diff obtained between the first and the second analysis were in all the ten samples within ±20%: from -16 to 1.9 % for IMA and from -12.2 to 12.7 % for norIMA. In Figure 47, the correlation graphs between the IMA and norIMA concentrations, calculated with the first analysis versus the second one, are reported, showing a good linearity between the two quantifications (R^2=0.9859 for IMA and R^2=0.9824 for norIMA).

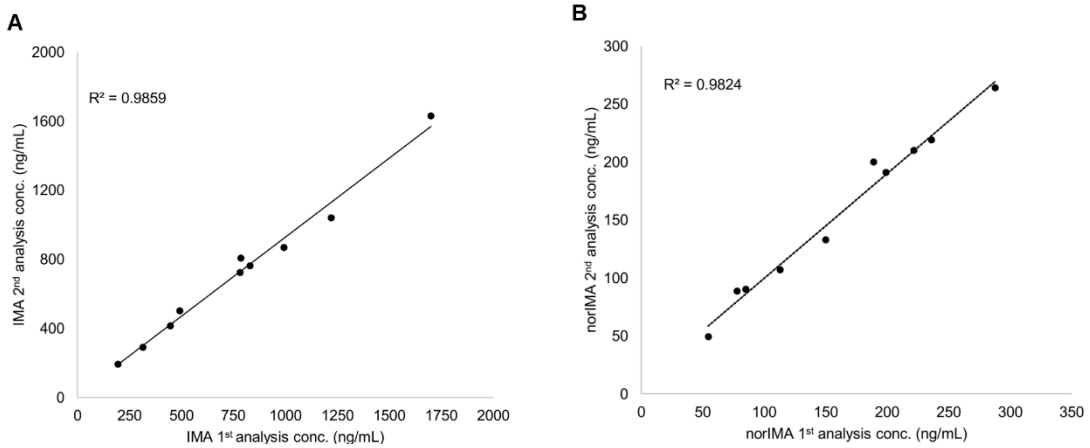

Figure 47. Correlation graphs between the first and second analysis for IMA (A) and norIMA (B).

4.1.5 Simultaneous quantification of IMA and norIMA in GIST patients' DBS for TDM

After the validation, the LC-MS/MS method was considered suitable for the quantification of both IMA and norIMA in real samples. In fact, up to 55 DBS samples of enrolled patients in the abovementioned clinical study (section 3.2.1), were analysed.

The obtained C_{min} values for both the analytes are reported in Table 13. Each sample was identified with an ID that was composed by the patient identification number followed by the sampling number.

Sample #	IMA dose during sampling (mg/die)	Hours from last intake (hh:mm)	IMA conc Plasma (ng/mL)	norIMA conc Plasma (ng/mL)	IMA conc DBS (ng/mL) normalized with Fc (1.73)	norIMA conc DBS (ng/mL) normalized with Fc (1.61)
1.5	400	26:15	896.5	269.3	840.8	251.2
2.6	400	24:15	1808.0	329.2	1799.2	322.0
2.7	400	23:00	1897.1	326.3	1937.6	349.4
7.5	400	21:45	828.8	197.6	897.7	231.6
7.6	400	24:45	976.0	314.1	937.7	294.6
7.7	400	23:45	821.9	231.1	867.1	213.9
8.4	400	22:45	708.4	139.1	743.6	129.8
8.5	400	23:00	1047.0	175.2	994.8	151.8
10.6	400	22:35	417.0	213.0	359.8	167.4
12.4	400	27:00	715.1	169.3	704.6	151.8
14.3	400	27:00	1083.7	172.9	1179.9	188.4
14.4	400	22:00	1440.7	254.2	1410.3	197.8
14.5	400	22:30	1064.2	138.0	1046.7	147.3
15.3	400	24:45	2188.8	423.0	2078.0	466.8
17.5	400	23:45	982.1	176.5	996.2	246.5
17.6	400	24:35	735.2	181.6	790.6	228.5
18.5	400	23:30	1207.0	284.3	1291.9	358.8
18.6	400	22:15	1711.0	412.2	1799.2	425.0
19.3	400	21:30	770.9	122.4	987.7	179.0
20.4	400	23:00	< LLOQ	< LLOQ	< LLOQ	< LLOQ
22.4	400	26:15	1032.1	196.4	931.0	161.7
22.5	400	01:30	5840.8	1083.6	5778.2	917.7
24.2	400	23:00	502.1	159.8	528.0	126.9
24.3	400	23:20	736.9	185.8	833.9	204.5
26.2	400	41:15	1051.8	281.5	1117.4	281.3
26.3	400	24:00	1277.6	328.4	1395.3	352.7
27.2	400	41:00	1188.3	264.7	1251.2	253.1
27.3	400	40:30	1243.1	305.8	1256.0	281.9
27.4	400	50:30	1041.1	306.0	1044.9	296.2
27.5	400	26:00	1802.7	415.0	1681.6	417.0
27.6	400	25:00	2093.0	410.3	1764.6	367.1
28.2	400	41:30	364.2	111.0	316.6	108.7
28.3	400	22:20	641.6	134.5	662.6	145.4
28.4	400	25:10	741.9	157.3	797.5	185.2
29.1	400	24:30	1330.8	195.6	1432.8	192.9
29.2	400	23:00	2336.1	383.7	1816.5	285.0
29.3	400	24:00	1800.9	240.2	1816.5	252.8

Sample #	IMA dose during sampling (mg/die)	Hours from last intake (hh:mm)	IMA conc Plasma (ng/mL)	norIMA conc Plasma (ng/mL)	IMA conc DBS (ng/mL) normalized with Fc (1.73)	norIMA conc DBS (ng/mL) normalized with Fc (1.61)
30.2	400	25:30	932.6	212.3	965.3	217.4
30.3	400	25:30	1045.8	186.9	1062.2	193.2
30.4	400	24:00	840.7	184.2	958.4	233.5
30.5	400	24:15	971.0	202.3	967.1	202.9
31.2	400	22:45	1537.9	388.5	1679.8	431.5
31.3	400	25:00	1355.2	375.0	1465.3	441.1
31.4	600	25:15	2624.1	876.8	2491.2	880.7
32.2	400	25:00	1443.2	229.0	1501.6	247.9
32.3	400	26:50	1550.7	262.7	1678.1	299.5
32.4	400	26:00	1371.9	238.8	1501.6	307.5
33.2	200	30:00	545.2	71.3	579.6	73.1
33.3	200	24:15	731.9	71.9	813.1	83.1
34.1	400	24:00	1275.4	298.6	1197.2	256.0
34.2	400	23:10	1378.3	293.1	1435.9	291.4
34.3	400	25:15	973.9	281.8	1250.8	338.1
35.1	400	23:10	1177.0	278.8	1167.8	273.7
36.1	300	22:05	1787.2	672.0	1567.4	658.5
37.1	300	23:10	1941.3	527.2	1512.0	436.3

Table 13. C_{min} values obtained from patients' samples quantification for both IMA and norIMA in plasma and in DBS samples (after normalization with F_c).

To estimate the plasma concentration of IMA and norIMA starting from the measurements of DBS samples the equation [5] ($EC_{pla}=C_{DBS}/[1-(Hct/100)]$), according to Kralj et al. was applied [144]. This EC_{pla} was compared with the actual plasma concentration of matching plasma samples. Opposite to Antunes et al. [145], it was not take into account the plasma to blood partition (f_p) since the value of f_p calculated according to Antunes et al. [194] was 0.45 and 0.48 for IMA and norIMA respectively. Moreover, EC_{pla} was also estimated with the application of a correlation factor (calculated as the mean of C_{PLA}/C_{DBS} ratio of the 55 samples analysed) in order to avoid the use of Hct. The F_c resulted 1.73±0.18 for IMA and 1.61±0.24 for norIMA. The agreement between C_{pla} and EC_{pla}, obtained from the C_{DBS} normalised with the Hct or the Fc, was evaluated through the cross-validation study reported in the section below.

4.1.6 Cross-validation study

IMA concentrations found in DBS were on average 59±6 % of those obtained from plasma, while norIMA concentrations from DBS samples were on average 63±9 % of those from plasma. Among the 55 samples analysed, IMA concentrations range from 310 to 5840 ng/mL in plasma and from

183 to 3340 ng/mL in DBS, while norIMA concentrations range from 67 to 672 ng/mL in plasma and from 45 to 409 ng/mL in DBS. In one out of 55 samples IMA and norIMA concentrations were found <LLOQ, in both plasma and DBS matrices (sample # 20.4, table 13). The intercept values for Passing-Bablok regression were 32.5 (95% CI: 2.9 – 66.0) and 1.2 (95% CI: -8.8 – 13.2) for IMA and norIMA, respectively, suggesting a small constant error for both analytes. The slope coefficients were 0.55 (95% CI: 0.52 – 0.58) and 0.61 (95% CI: 0.57 – 0.67) for IMA and norIMA respectively, indicating a proportional error (the higher concentrations were underestimated). This pattern was confirmed also by Bland-Altman analyses (Spearman correlation between (Y-X) and (X+Y)/2: R^2= -0.9449).
These values indicated that almost all these compounds were founded in plasma. A good agreement between the two methods (plasma and DBS normalized with Hct) was obtained according to EMA/FDA guidelines: 89 (49/55) and 78 (43/55) % of EC_{pla} resulted within ±20 % of the mean for IMA and norIMA, respectively. Also, with the Hct normalization, the intercept values for Passing-Bablok regression (77.1, 95% CI: 1.7 – 181.0 and 10.5, 95% CI: -5.6 – 31.4, for IMA and norIMA, respectively) indicated that the small constant error was maintained for both analytes (Figure 48).

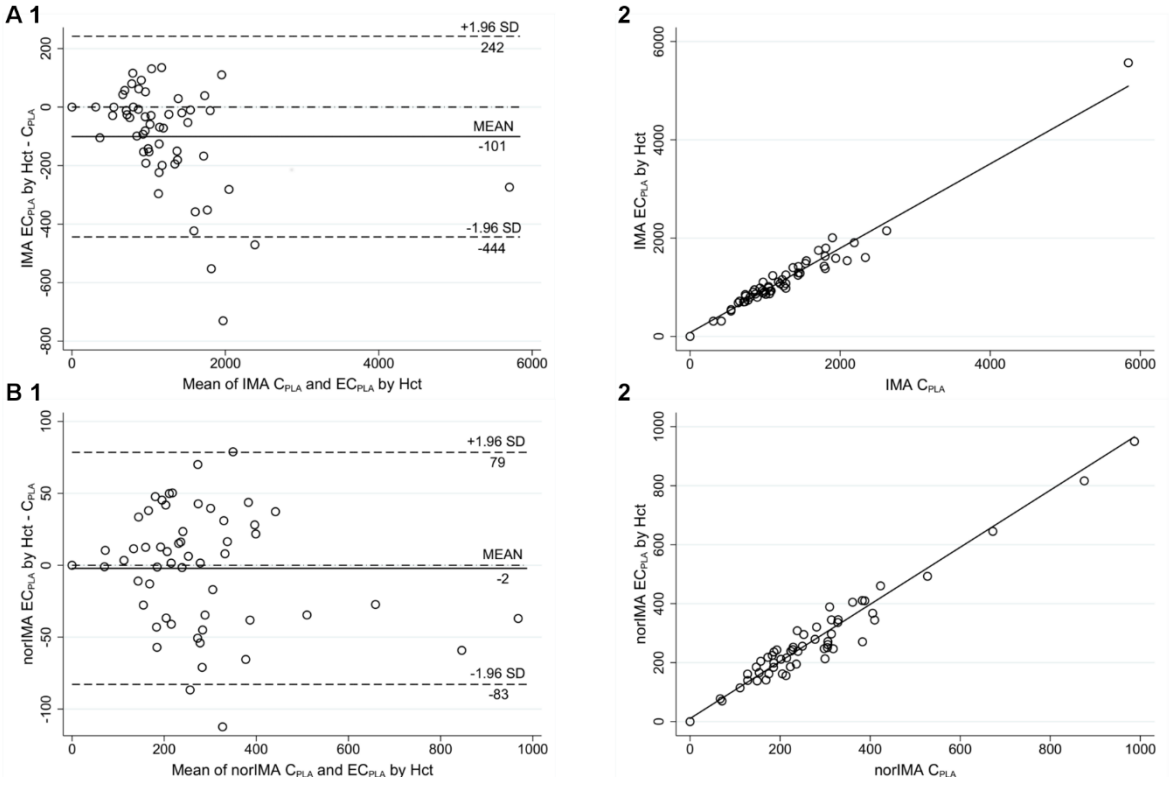

Figure 48. Correlation between IMA and norIMA concentrations in 55 DBS samples normalized by Hct. Comparison between IMA (A) and norIMA (B) EC_{PLA} by Hct with corresponding C_{PLA} through Bland-Altman plot (1) and Passing-Bablok regression (2). EC_{PLA}: estimated plasma concentration by normalization of DBS measurements; C_{PLA}: concentration found in plasma samples; Hct: hematocrit. All the concentrations are expressed as ng/mL. N=55.

Anyway, the slope coefficients were, in this case, very close to 1 (0.86, 95% CI: 0.77 – 0.94, and 0.97, 95% CI: 0.89 – 1.06 for IMA and norIMA, respectively) indicating a good agreement between the measurements and that the initial proportional error was absent or negligible. Bland-Altman analyses confirmed these results, with a Spearman correlation between (Y-X) and (X+Y)/2 of r=-0.4807 for IMA and r=-0.1132 for norIMA.

With its application the agreement between the two methods resulted better than with the Hct normalization. As related to EMA/FDA guidelines requirements, 93 (51/55) and 85 (46/55) % of EC_{pla} resulted within ±20 % of the mean for IMA and norIMA, respectively. Regarding the Passing-Bablok regression, the slope coefficients were even better than those obtained using the Hct normalization factor (0.96, 95% CI: 0.91 – 1.01, and 1.00, 95% CI: 0.92 – 1.09 for IMA and norIMA, respectively), while a considerable lower constant error resulted for both the analytes from the intercept values (53.3, 95% CI: 0.0 – 107.4 and 1.8, 95% CI: 0.9 – 1.1 for IMA and norIMA, respectively), as reported in Figure 49. The LCCC calculated were very high for both Hct and Fc normalization methods, whit a little improvement for IMA with Fc correction with respect to Hct one (IMA LCCC= 0.950 and 0.9667 after Hct and Fc normalization, respectively, norIMA LCCC= 0.9698 and 0.9742 after Hct and Fc normalization, respectively).

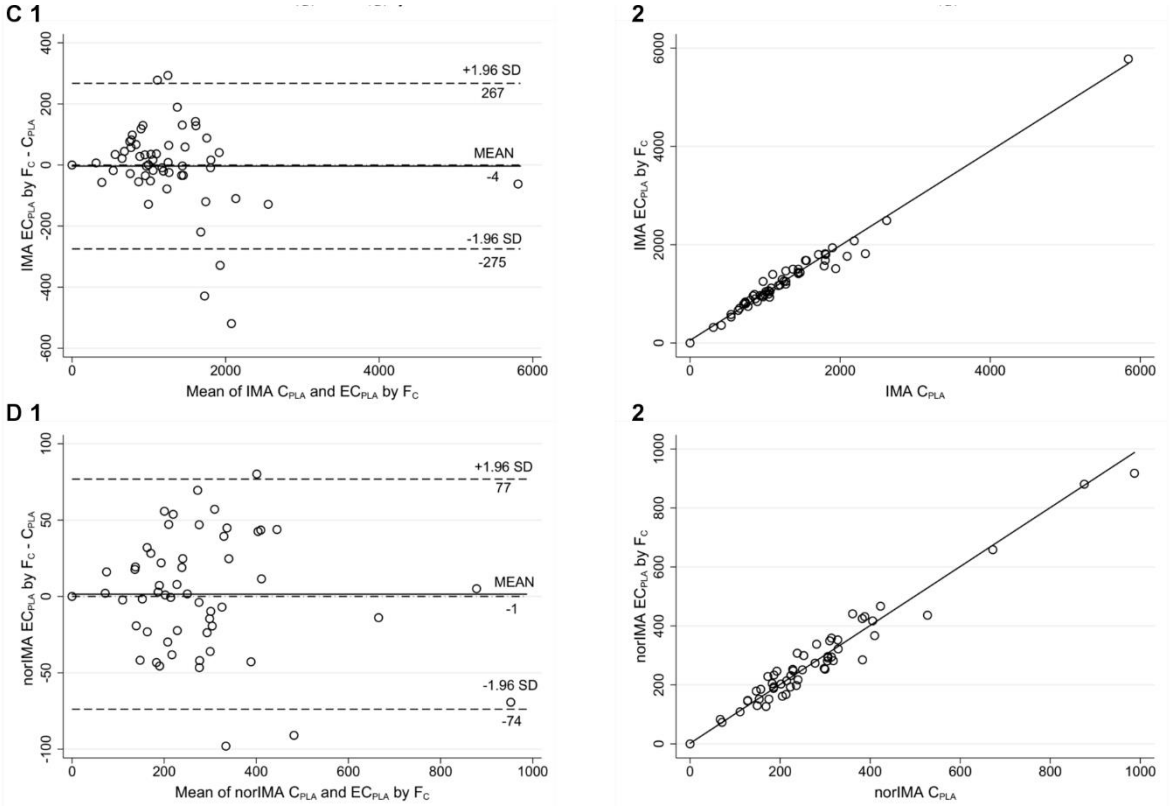

Figure 49. Correlation between IMA and norIMA concentrations in DBS samples after normalization and those obtained from plasma samples. Comparison between IMA (C) and norIMA (D) EC_{pla} by F_c with corresponding C_{PLA} through Bland-Altman plot (1) and Passing-Bablok regression (2). EC_{pla}: estimated plasma concentration by normalization of DBS measurements; C_{PLA}: concentration found in plasma samples; Hct: hematocrit; F_c: correction factor. All the concentrations are expressed as ng/mL. N=55.

A further validation of this strategy was assessed through the application of the F_c of both IMA and norIMA to 12 extra patients' samples. The agreement between concentrations in plasma and in DBS samples, after the F_c normalization, was verified. As reported in Table 14 and in Figure 50, 100 % of EC_{pla} resulted within ±20 % of the mean for both IMA (from -13.9 to 13.8 %) and norIMA (from -7.0 to 18.7 %), with a good linearity with plasma concentrations (R^2= 0.989 for IMA and R^2= 0.9474 for norIMA).

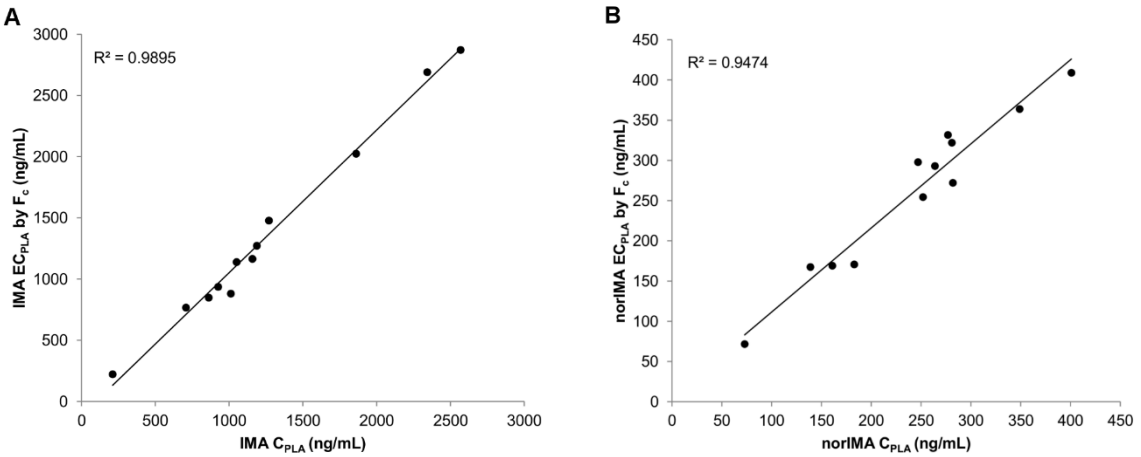

Figure 50. Fc application to 12 additional patients' DBS samples. Correlation graph between (A) IMA and (B) norIMA estimated plasma concentrations (EC_{PLA}) by Fc and their corresponding plasma measurements (C_{PLA}); N=12.

Sample #	IMA plasma conc. (ng/mL)	IMA DBS conc. F_c norm. (ng/mL)	% diff	norIMA plasma conc. (ng/mL)	norIMA DBS conc. F_c norm. (ng/mL)	% diff
4.3	2343	2690	13.8	349	364	4.2
4.4	2569	2872	11.1	401	409	2.0
14.2	1158	1164	0.5	183	171	-7.0
16.2	926	936	1.1	161	169	4.9
22.1	1861	2024	8.4	247	298	18.7
24.1	211	221	4.8	73	72	-1.9
2.3	1270	1477	15.1	277	332	18.0
26.1	862	848	-1.7	282	272	-3.6
1.4	1012	881	-13.9	252	254	0.9
26.2	1051	1138	8.0	281	322	13.6
27.2	1188	1272	6.8	264	293	10.4
8.4	708	766	7.9	139	167	18.6

Table 14. F_c application to 12 external DBS samples, all of them with a % diff < 20% for all the samples, for both IMA and norIMA.

4.1.7 Clinical observations

Excluding samples # 22.5, 26.2, 27.2, 27.3, 27.4, 28.2 and 33.2 that were not at the C_{min}, the remaining 48 samples were taken at 24 ± 3 hours (range 21.5-27 hours) from last drug administration and were considered evaluable for C_{min} estimation.

The first consideration emerging from the analysis regards the high inter-patient variability in C_{min}values: IMA concentration went from a minimum of 359.8 ng/mL to a maximum of 2491.2 ng/mL. This reflects the wide variability of IMA concentrations in GIST patients, treated with the same starting dose, in line with what was reported in the literature [86, 195]. As described in the introduction, C_{min} values higher than 1100 ng/mL were associated with a longer TTP in GIST patients treated with IMA [86]. Among these samplings different situations were highlighted. It is noteworthy that the 48% of the analysed samples revealed an under-exposure to the drug and, therefore, a risk for a reduced therapeutic effect, while in the remaining 52% of the analysed samples, the C_{min} was higher than or equal to the threshold value proposed for IMA efficacy.

In addition to that, there were some interesting cases to underline. Firstly, a suspected case of non-adherence to therapy was found (# 20.4). In fact, when repeatedly analysed, this sample gave a concentration of both IMA and norIMA below the method LLOQ suggesting that patient was not taking the drug at least in the days before the blood drawn. Secondly, sample # 10.6 showed an IMA concentration of 359.8 ng/mL that was far below the proposed threshold for efficacy. To investigate the possible reasons for this low drug plasma level, the clinical history of this patient was retraced. As reported in the clinical record, the patient was started on IMA 400 mg/die and the disease was kept under control for about 5.5 years, when disease progression occurred. Therefore, the patient was started on IMA 800 mg/die, a treatment still ongoing. The patient was also taking carbamazepine to control his epilepsy for almost 30 years. Carbamazepine is a potent CYP3A4 inducer and in IMA summary of product characteristics, a special warning reports that the concomitant use of IMA and CYP3A4 inducers (as carbamazepine) should be avoided, as the latter, increasing IMA metabolism, may significantly reduce the exposure to IMA. This would explain the low IMA concentrations found in our sample. In order to confirm the metabolism induction, the quantification of the active metabolite was investigated and a ratio of norIMA/IMA around the 50% was found in this sample, meanwhile in the other cases it was 20-25%[11]. We can speculate that, due to the absence of molecular alterations that may induce drug resistance, the low IMA concentrations due to a possible drug interaction phenomenon with carbamazepine, may have contributed to disease progression and, therefore, to the need of higher IMA dosages.

Finally, sample # 31.4 showed the highest IMA concentration within our sample set, of nearly 2500 ng/mL, a value that is closed to the 3000 ng/mL threshold associated with toxicity in CML. Interestingly, the clinical record reported that this patient was treated with IMA 400 mg/die for 7

months with no significant side effects. During this period, the samples 31.2 and 31.3 were collected and their analysis highlighted IMA and norIMA concentrations slightly higher than the mean (1295 ng/mL for IMA and 285 ng/mL for norIMA), but they were considered still adequate. Subsequently, the drug dosage was increased at 800 mg/die due to disease progression and, interestingly, the patient experienced severe drug toxicity during the treatment at higher doses, consisting in fluid retention with oedemas and gain of weight. These symptoms disappeared at IMA suspension and reappeared when the treatment was re-started at 600 mg/die. This data suggests an undoubted intolerance to high-dosage IMA, that is reflected by plasma concentrations.

4.2 LC-MS/MS method development for the simultaneous quantification of RIBO, PALBO and LETRO in human plasma

4.2.1 Chromatographic conditions

The separation of the analytes was obtained applying the following gradient (flow rate of 0.3 mL/min, column temperature fixed at 50 °C): the percentage of MPB (MeOH/iPrOH 9:1 v/v, with 0.1% HCOOH) was increased from the initial condition (10%) to 70% in 0.5 min and then kept constant for 1.75 min; MPB was further increased to 95% in 0.1 min and kept constant for 1.9 min; the initial condition was then restored in 0.25 min and the column was re-equilibrated for 2 min. The total run time was 6.5 min, as reported in Figure 51.

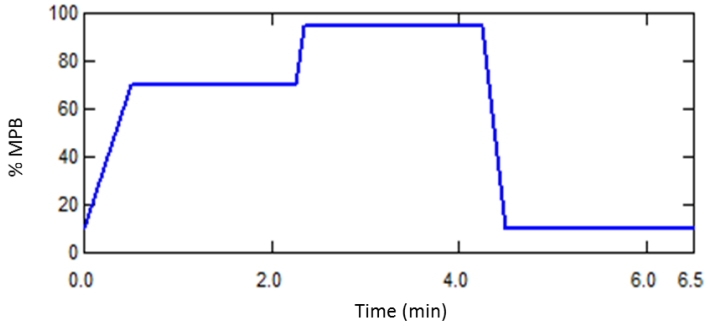

Figure 51. Multi-step optimized chromatographic method applied to the column.

As noticeable from Figure 52, the analytes were rapidly and selectively eluted achieving a good separation within 2.5 min: the retention times correspond to 1.93 min for PALBO, 1.56 min for RIBO and 2.20 min for LETRO.

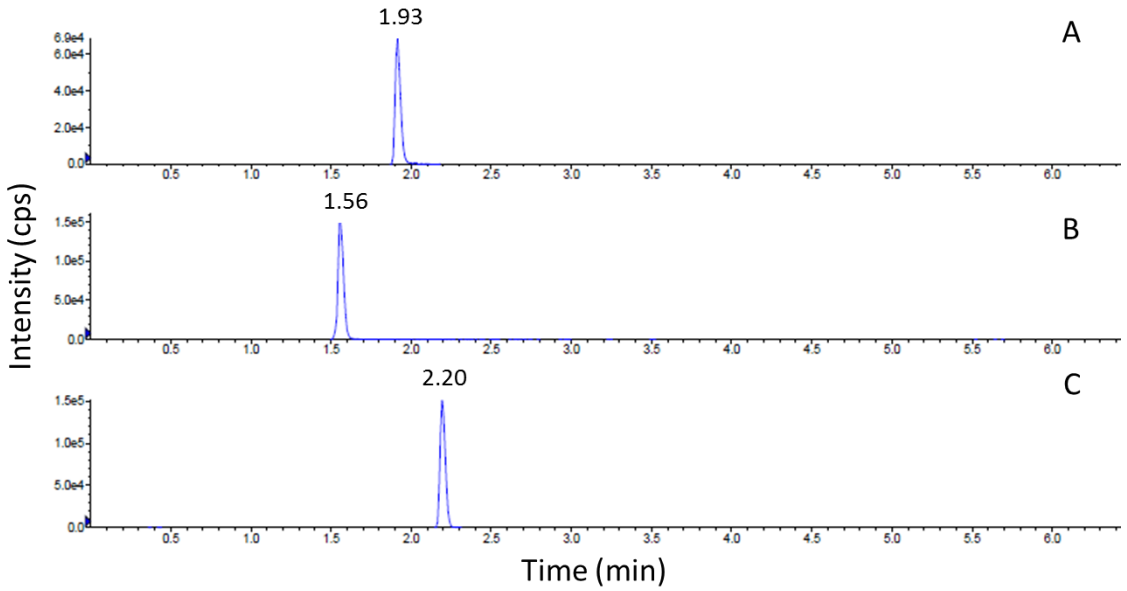

Figure 52. Example of MRM chromatogram of the calibration point C. PALBO (A) (75 ng/mL), RIBO (B) (3000 ng/mL) and LETRO (C) (150 ng/mL).

4.2.2 Mass spectrometric conditions optimization

The monoisotopic masses of PALBO, RIBO and LETRO are 448, 435 and 286 Da respectively. Working in positive ion mode with ESI source, the presence of the analyte of interest, during the first Q1 scan, was confirmed by the protonated molecule $[M+H]^+$ at 436, 449 and 287 m/z, Figure 53.

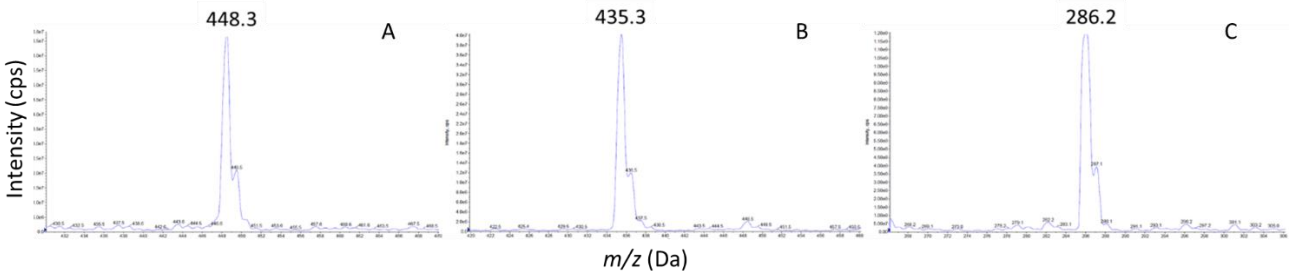

Figure 53. Spectrum obtained in positive mode with a Q1 scan that confirms the presence of PALBO (A), RIBO (B) and LETRO (C).

Compound-dependent parameters for all the analytes were determined with the same experiments carried out in the LC-MS/MS method for IMA and norIMA, section 3.1.2.

The fragmentation patterns obtained within the collision cell are represented in

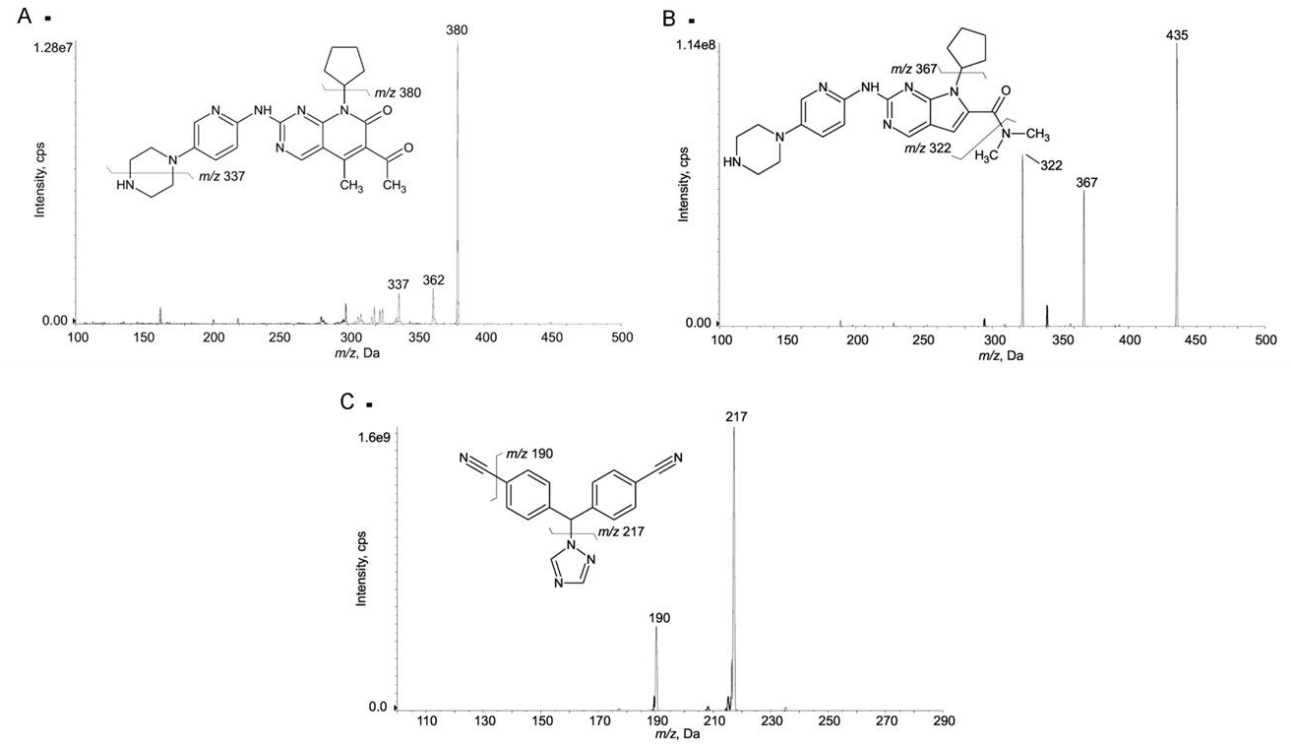

Figure 54 [184, 196, 197] and reported in Table 15 along with the optimized compound dependent parameters. The daughter ions used as quantifiers were: 448>380 m/z for PALBO, 435>367 *m/z* for RIBO and 286>217 *m/z* for LETRO. The following fragment ions were used as qualifiers: 448>337 m/z for PALBO (the *m/z* 362 peak is probably due to the loss of H_2O), 435>322 *m/z* for RIBO and 286>190 *m/z* for LETRO. The quantification of ISt signals was conducted using the following transitions: 456>388 m/z for D_8-PALBO, 441>373 m/z for D_6-RIBO, and 290>221 m/z for $^{13}C_2$,$^{15}N_2$-LETRO.

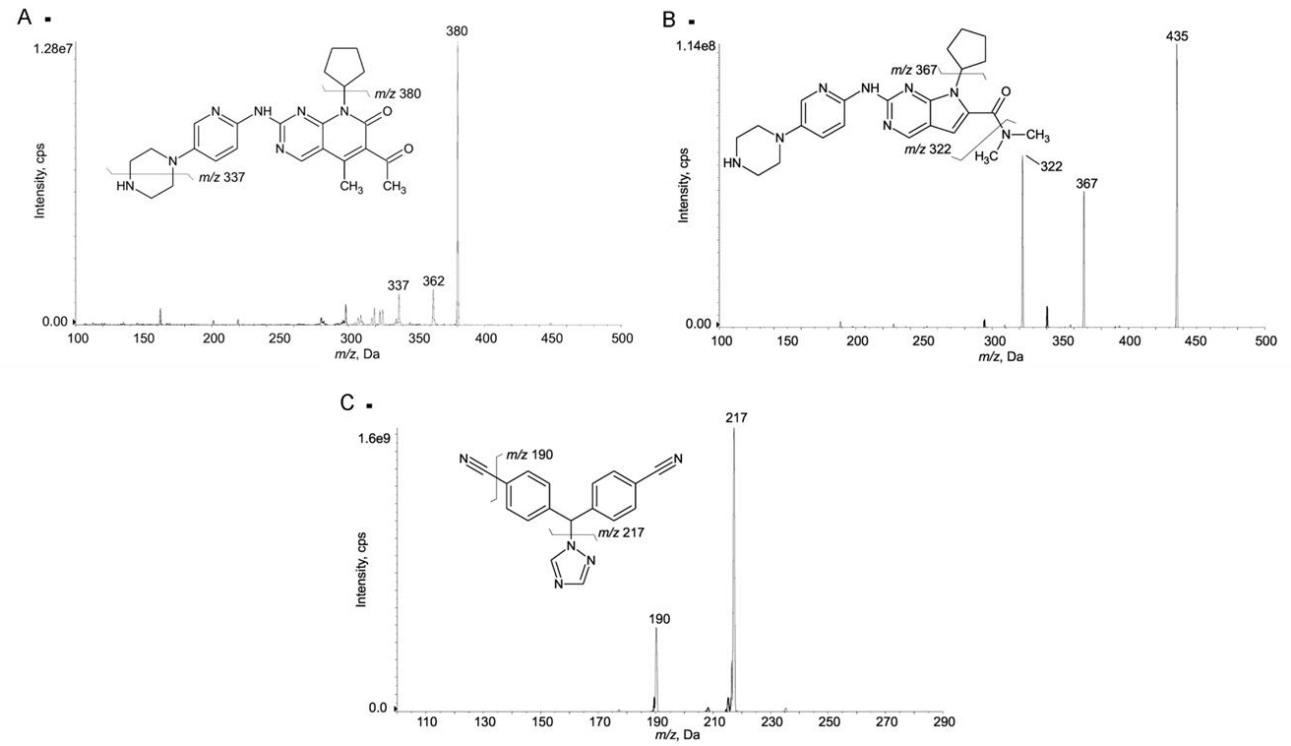

Figure 54. MS/MS mass spectra of analytes with their chemical structures and identification of the fragment ions used for the present method. (A) PALBO, recorded with CE=50 V; (B) RIBO, recorded with CE=37 V; (C) LETRO, recorded with CE=30 V.

Compound	Q1 (*m/z*)	DP (V)	EP (V)	Q3 (m/z)	CE (V)	CXP (V)
PALBO	448.3	130	10	380.2	40	10
				337.2	53	10
RIBO	435.3	110	10	367.3	55	10
				322.3	63	10
LETRO	286.2	50	10	217.2	20	10
				190.2	45	10
D_8-PALBO	456.3	130	10	388.3	40	10
D_6-RIBO	441.3	110	10	373.3	38	10
$^{13}C_2$,$^{15}N_2$-LETRO	290.2	50	10	221.2	20	10

Table 15. Compound-dependent parameters.

Source-dependent parameters were optimized as follows: temperature 500 °C, nebulizer gas 40 psi and heater gas 40 psi (zero air), CUR 35 psi and CAD 6 psi (nitrogen), IS voltage 5500 V.

4.2.3 LC-MS/MS validation study

4.2.3.1 Recovery

PALBO, RIBO and LETRO recovery, expressed as percentage and reported in Table 16, resulted high (≥ 92.3%) for all the analytes and reproducible over the concentration ranges tested.

Analyte	Nominal conc. (ng/mL)	Recovery (%) ±SD	Recovery CV (%)
PALBO	0.5	92.3±9.4	10.2
	20	97.4±3.3	3.4
	200	96.6±3.5	3.6
RIBO	20	101.1±2.6	2.6
	800	97.7±2.8	2.9
	8000	99.6±1.4	1.4
LETRO	1	98.1±4.0	4.1
	40	97.0±1.7	1.7
	400	99.2±3.1	3.1

Table 16. Recovery of PALBO, RIBO and LETRO from human plasma.

4.2.3.2 Linearity

The calibration curves were freshly prepared every day during the validation study. To generate a calibration curve (an example is reported in Figure 55 for each analyte), the peak-area ratios between the analyte and the IS compared to the nominal concentrations were plotted and a weighted ($1/x^2$) linear regression function was applied.

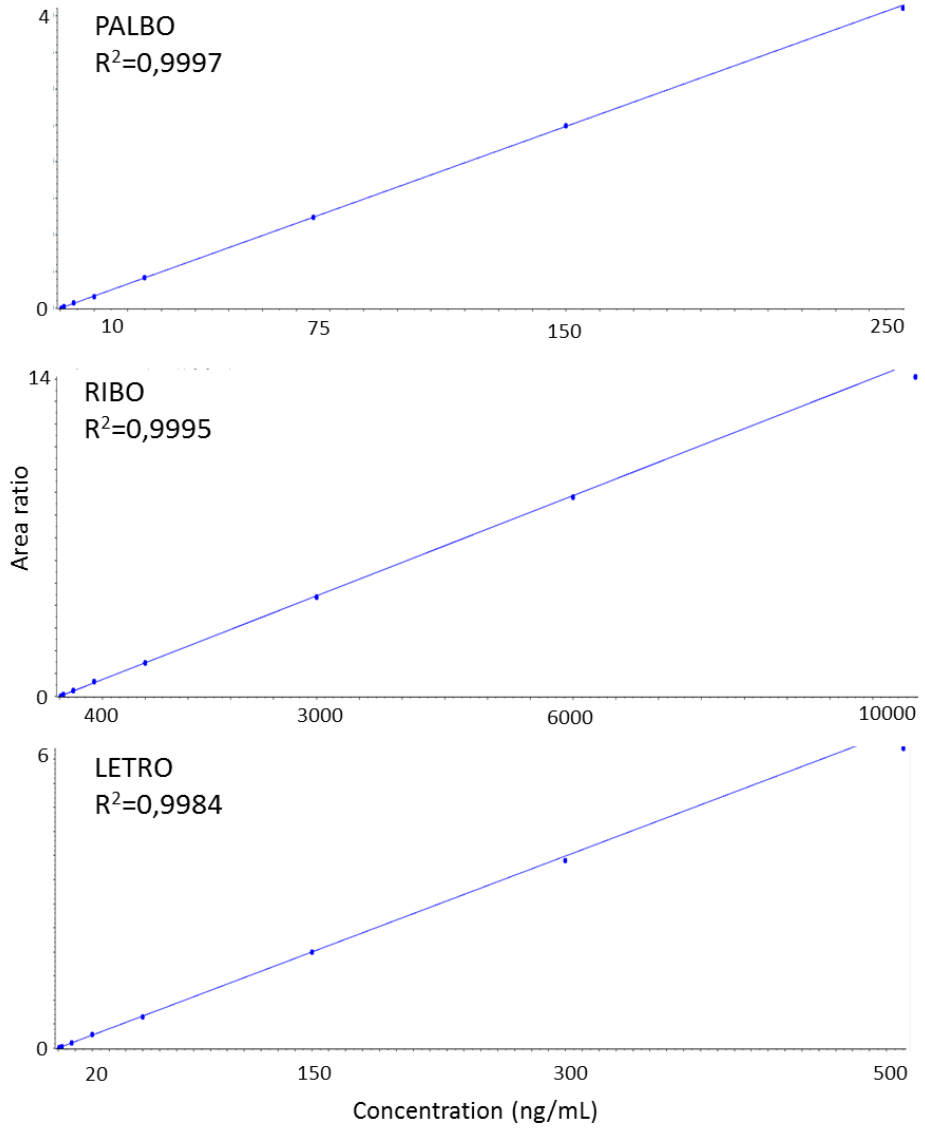

Figure 55. Example of the linearity reached with calibration curves of PALBO, RIBO and LETRO.

The linearity of the method was verified over the selected concentrations (0.3-250, 10-10000, 0.5-500 ng/mL for PALBO, RIBO and LETRO, respectively): the mean R^2 values obtained were 0.9990±0.0007 for PALBO, 0.9992±0.0002 for RIBO, and 0.9983±0.0010 for LETRO. As related to PALBO, the calculated accuracy was between 95.5 and 103.3% and precision was within 5.7%. The accuracy obtained for RIBO was between 95.1 and 102.7% while precision was ≤ 5.1%. Lastly, precision and accuracy of LETRO was between 91.8 and 104.5% and within 6.2, respectively. In Table 17 the complete list of linearity data is reported.

PALBO (N=5)			
Nominal conc. (ng/mL)	**Mean ± SD**	**CV%**	**Acc%**
0.300	0.301±0.002	0.6	100.2
1.00	1.00±0.02	2.2	100.1
4.00	3.91±0.22	5.7	97.8
10.00	9.85±0.29	2.9	98.5
25.00	25.74±0.73	2.8	103.0
75.00	76.28±1.05	1.4	101.7
150.00	154.97±5.20	3.4	103.3
250.00	238.67±12.12	5.1	95.5

RIBO (N=5)			
Nominal conc. (ng/mL)	**Mean ± SD**	**CV%**	**Acc%**
10.00	10.04±0.13	1.3	100.4
40.00	39.30±2.00	5.1	98.2
160.00	158.44±3.68	2.3	99.0
400.00	410.94±11.23	2.7	102.7
1000.00	1020.18±19.12	1.9	102.0
3000.00	3029.34±88.65	2.9	101.0
6000.00	6091.68±176.43	2.9	101.5
10000.00	9506.24±299.76	3.2	95.1

LETRO (N=5)			
Nominal conc. (ng/mL)	**Mean ± SD**	**CV%**	**Acc%**
0.50	0.49±0.01	1.6	98.6
2.00	2.09±0.12	5.7	104.5
8.00	8.25±0.20	2.4	103.2
20.00	20.74±0.45	2.1	103.7
50.00	50.05±1.30	2.6	100.1
150.00	150.70±6.02	4.0	100.5
300.00	293.00±18.07	6.2	97.7
500.00	459.19±11.19	2.4	91.8

Table 17. Accuracy and precision data of the calibration curves of PALBO, RIBO and LETRO.

4.2.3.3 Intra- and inter-day precision and accuracy

The results of intra- and inter-day precision and accuracy of the proposed method complied with FDA and EMA requirements (Table 18). As related to intra-day precision and accuracy, the obtained values were, respectively, ≤ 3.6% and between 94.5-112.3% for all three analytes. At the same time, inter-day precision and accuracy were ≤ 7.3% and between 94.5-112.9%.

Intra-day (N=6)				
Analyte	**Nominal conc. (ng/mL)**	**Mean ± SD**	**CV %**	**Acc %**
PALBO	0.50	0.56±0.02	4.0	112.3
	20.00	19.46±0.72	3.7	97.3
	200.00	195.03±7.51	3.9	97.5
RIBO	20.00	19.73±0.70	3.6	98.7
	800.00	757.56±37.94	5.0	94.7
	8000.00	7560.69±334.39	4.4	94.5
LETRO	1.00	1.00±0.06	6.3	100.2
	40.00	38.37±1.24	3.2	95.9
	400.00	382.52±13.21	3.5	95.6

Inter-day (N=15)				
Analyte	**Nominal conc. (ng/mL)**	**Mean ± SD**	**CV %**	**Acc %**
PALBO	0.50	0.56±0.04	6.2	112.9
	20.00	21.12±1.13	5.4	105.6
	200.00	206.72±8.66	4.2	103.4
RIBO	20.00	20.23±1.17	5.8	101.1
	800.00	794.70±42.33	5.3	99.3
	8000.00	7757.54±354.15	4.6	97.0
LETRO	1.00	0.95±0.07	7.3	94.5
	40.00	41.10±1.79	4.4	102.8
	400.00	394.74±20.09	5.1	98.7

Table 18. Intra- and inter-day precision and accuracy of the proposed method for PALBO, RIBO and LETRO.

4.2.3.4 Lower limit of quantification and selectivity

The LLOQ values were assessed at the concentrations of 0.3 ng/mL for PALBO, 10 ng/mL for RIBO and 0.5 ng/mL for LETRO: the accuracy and precision (CV%) obtained for the 6 LLOQ samples

prepared in pooled blank human plasma were, respectively, 98.1% and 6.5% for PALBO, 105.3% and 5.5% for RIBO and 108.2% and 4.4% for LETRO. The S/N ratios were 30.5 for PALBO, 93.5 for RIBO and 7.5 for LETRO.

The method has a good selectivity: the analysis of six blank human plasma samples, from independent sources, resulted free of interferences, especially at the retention times of the analytes, thus indicating satisfying method specificity.

4.2.3.5 Matrix effect

Both the post-column infusion test (Figure 56) and the calculation of the ratio between analytes peak area in presence of matrix (human pooled plasma) and the peak area without matrix (MeOH), evaluated at each QC concentration, demonstrated the absence of significant matrix effect. In fact, no suppression or enhancement of XIC was detected at the retention time of the analytes.

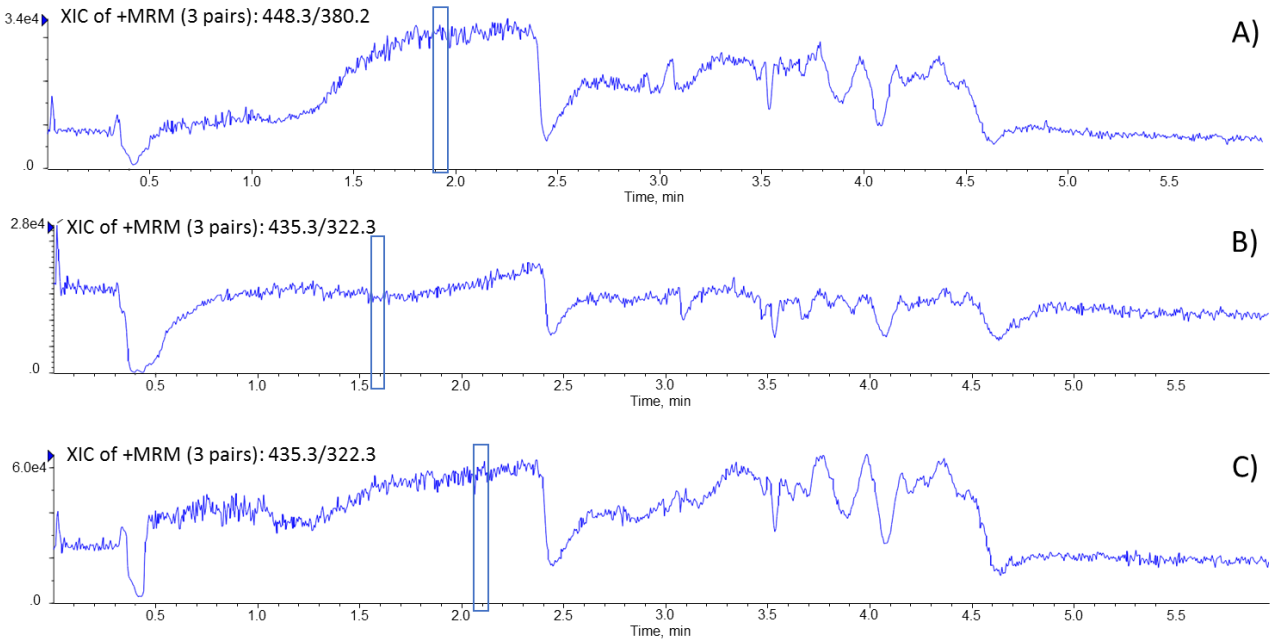

Figure 56. Post-column infusion for PALBO (A), RIBO (B) and LETRO (C).

The estimated matrix effect (ME%) is reported in Table 19 for each analyte: it was found between 91.5-98.7% with a CV% ≤10.2% for PALBO, between 85.0-113.2% with a CV% ≤4.0% for RIBO and between 86.4-91.6% with a CV% ≤9.5 for LETRO. These results confirmed that the proposed method is not affected by matrix effect.

Analyte	Nominal conc. (ng/mL)	ME (%) ±SD	ME CV (%)
PALBO	0.5	91.5±9.3	10.2
	20	98.7±1.4	1.4
	200	97.0±2.5	2.6
RIBO	20	113.2±4.5	4.0
	800	110.2±2.4	2.2
	8000	85.0±1.2	1.4
LETRO	1	86.4±8.2	9.5
	40	91.6±2.0	2.1
	400	90.5±1.9	2.1

Table 19. Estimated matrix effect (ME%) of PALBO, RIBO and LETRO in deproteinized human plasma

4.2.3.6 Stability

PALBO, RIBO, and LETRO stability in plasma matrix was verified under the following conditions: 1) after 4 h at room temperature, being precision and accuracy, respectively, within 12.2% and between 88.2% and 103.5% for the three analytes; 2) after 2 months of storage at -80 °C, being precision and accuracy, respectively, within 5.0% and between 88.3% and 105.5% for the three analytes. The deproteinized QCs were stable in autosampler set at 4 °C for 72 h as proved by precision and accuracy values obtained (≤ 7.8 % and between 93.9% and 108.2% for all the compounds). PALBO, RIBO, and LETRO resulted stable after 2 freeze/thaw cycles (taking together the 3 drugs, precision and accuracy values were ≤ 14.2% and between 102.3-11.9%, respectively). Long term stability in MeOH was verified after 2 months of storage at -20°C: for all the 3 compounds, precision and accuracy were within 4.3 and between 97.6-110.7%, respectively. In Table 20, Table 21 and Table 22 complete stability data are reported.

Analytes	Nominal conc. (ng/mL)	T = 4h (RT)			T = 72 h in AS (4°C)		
		Mean ± SD	Prec. %	Acc. %	Mean ± SD	Prec. %	Acc. %
PALBO	0.50	0.52±0.06	12.2	103.5	0.54±0.02	4.2	108.2
	20.00	20.31±0.59	2.9	101.6	21.10±1.23	5.8	105.5
	200.00	204.51±10.42	5.1	102.3	215.60±8.28	3.8	107.8
RIBO	20.00	18.86±0.74	3.9	94.3	21.24±1.45	6.8	106.2
	800.00	751.88±27.56	3.7	94.0	815.31±36.72	4.5	101.9
	8000.00	7218.92±402.94	5.6	90.2	8274.93±207.29	2.5	103.4
LETRO	1.00	0.88±0.06	7.1	88.2	0.94±0.07	7.8	93.9
	40.00	37.95±1.78	4.7	94.9	44.45±0.19	0.4	111.1
	400.00	372.54±24.58	6.6	93.1	426.23±4.43	1.0	106.6

Table 20. Short term stability of PALBO, RIBO and LETRO.

After 2 freeze-thaw cycles				
Analytes	Nominal conc. (ng/mL)	Mean ± SD	Prec. %	Acc. %
PALBO	0.50	0.56±0.08	14.2	111.9
	20.00	21.59±0.17	0.8	107.9
	200.00	207.66±9.03	4.3	103.8
RIBO	20.00	21.63±0.84	3.9	108.2
	800.00	834.99±21.64	2.6	104.4
	8000.00	8183.97±158.24	1.9	102.3
LETRO	1.00	1.06±0.08	7.5	105.8
	40.00	43.24±1.20	2.8	108.1
	400.00	411.13±5.15	1.3	102.8

Table 21.Stability data for PALBO, RIBO and LETRO after 2 freeze-thaw cycles.

Analytes	Nominal conc. (ng/mL)	Stored at -80°C over 2 months (plasma)			Stored at -20°C over 2 months (methanol)		
		Mean ± SD	Prec. %	Acc. %	Mean ± SD	Prec. %	Acc. %
PALBO	0.50	0.51±0.02	4.3	101.6	0.52±0.02	3.3	104.1
	20.00	20.46±0.74	3.6	102.3	22.43±0.63	2.8	112.1
	200.00	202.92±0.37	0.2	101.5	219.18±9.46	4.3	109.6
RIBO	20.00	21.10±1.05	5.0	105.5	19.52±0.30	1.5	97.6
	800.00	789.37±28.89	3.7	98.7	885.44±35.25	4.0	110.7
	8000.00	7699.21±117.73	1.5	96.2	8522.63±68.65	0.8	106.5
LETRO	1.00	0.88±0.01	1.4	88.3	1.05±0.03	2.7	105.1
	40.00	39.58±0.90	2.3	99.0	44.12±1.25	2.8	110.3
	400.00	386.66±6.61	1.7	96.7	413.47±6.07	1.5	103.4

Table 22. Long term stability (2 months) of PALBO, RIBO and LETRO: analytes stored in human plasma at -80°C and working solutions (methanol) stored at -20°C.

4.2.3.7 Carry-over

A marked carryover was observed after the injection of ULOQ sample, albeit the introduction of a cleaning step during the chromatographic gradient: the first blank sample after ULOQ had residual signals of PALBO and RIBO that were 2- and 1.5-fold higher than those of the LLOQ, respectively. On the contrary, no carryover post-injection was detected for LETRO, being its signal in the first blank sample after ULOQ injection lower than 10% respect to the LLOQ. The first attempt to overcome PALBO and RIBO carryover was the injection of several blank samples after the ULOQ. Unfortunately, after 7 blank samples carryover was still present (35% for PALBO and 30% for RIBO). Thus, keeping constant the mass spectrometry conditions and the MPA-B composition, we developed a washing method based on the "saw-tooth wash" gradient proposed by Williams et al. [198] to be applied to blank samples after ULOQ and unknown patients' samples: from 10% to 98% of MPB (MeOH/iPrOH 9:1, v/v, with 0.1% HCOOH) in 0.5 min and kept constant for 0.7 min; then from 98% to 5% of MPB in 0.1 min and kept constant for 0.8 min. The same profile was repeated three times overall with a final reconditioning step of 2 min at 10% of MPB. The total run time was 6.34 min (Figure 57). As a result, after the 2 blank samples run with the washing method and one blank sample run with the quantification method, no quantifiable peaks of PALBO and peaks of RIBO ≤15% respect to the LLOQ were observed in the following blank sample.

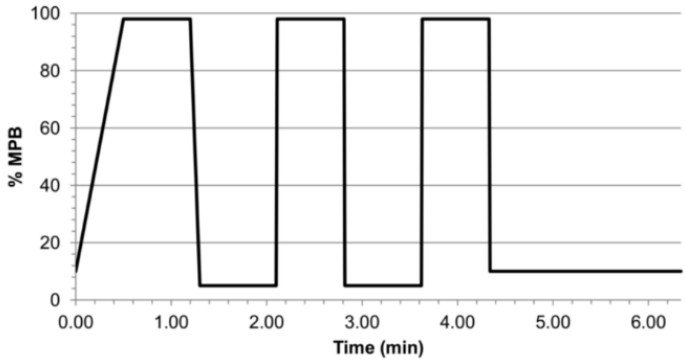

Figure 57. Chromatographic gradient used for the washing method.

4.2.4 Quantification of PALBO, RIBO and LETRO in breast cancer patients' plasma for TDM

After the validation, the LC-MS/MS method was considered suitable for the quantification of PALBO, RIBO and LETRO in real samples. Patients' recruitment into the clinical study (prot. code: CRO-2018-83) is still at the beginning and, at the moment, the method was tested on 10 plasma samples collected from 8 patients (from 2 patients we collected 2 sequential samples) affected by metastatic breast cancer. The principal demographic and clinical characteristics of the enrolled patients are reported in Table 23.

Patients characteristic	N
Sex	8 females
Age (range)	67 (50-85) years
Therapy	5 PALBO (125 mg/die) + fulvestrant 1 PALBO (100 mg/die) + fulvestrant 1 PALBO (125 mg/die) + LETRO (2.5 mg/die) 1 RIBO (600 mg/die) + LETRO (2.5 mg/die)

Table 23. Principal demographic and clinical characteristics of the enrolled patients.

Blood samples were taken between 15 and 30 h from the last pill intake. As reported in Table 24, in one case (patient 3), the last PALBO assumption was 1 week before the blood sampling. Anyway, the sensibility of the method allowed the quantification of the residual concentration of PALBO (1.6 ng/mL). Concentrations of PALBO obtained in patients 1, 2, 3, 4, and 6 were rather in line with the population mean C_{min} reported in literature (61 ng/mL) for the standard dose [199]. Patient 5

showed PALBO concentrations slightly lower in both two analysed samples (39.5 and 41.5 ng/mL) while patient 7 showed a slightly higher drug concentration (97.9 ng/mL). This latter result was probably because the last pill intake was 15 h before the sampling. In sample 6.2 (patient 6), although the patient was treated with PALBO in combination with fulvestrant, a residual amount of LETRO (2.8 ng/mL) was detected: the patient completed her adjuvant therapy with LETRO 2 weeks before the sampling.

The concentrations of RIBO and LETRO obtained from the patient 8 (samples 8.1 and 8.2), resulted quite lower than the mean C_{min} reported in literature for both drugs: RIBO concentration was 396.0 ng/mL while the population mean is 711 ng/mL [200], LETRO was measured at the concentration of 46.8 ng/mL while the reported mean is 107.0 ng/mL [201].

Patient N	Sample N	PALBO (mg/die)	RIBO (mg/die)	LETRO (mg/die)	I quantif. (ng/mL)	II quantif. (ng/mL)	% diff.
1	1.1	125	-	-	53.0	55.9	5.3
2	2.1	125	-	-	76.9	84.2	9.1
2	2.2	125	-	-	77.5	82.4	6.1
3	3.1	125	-	-	1.6	1.5	-6.5
4	4.1	100	-	-	70.7	74.3	5.0
5	5.1	125	-	-	39.5	43.0	8.5
5	5.2	125	-	-	41.5	46.1	10.5
6	6.1	125	-	-	69.7	74.0	6.0
6	6.2	-	-	2.5	63.3	67.8	6.9
7	7.1	125	-	-	97.9	96.2	-1.8
7	7.2	-	-	2.5	2.8	2.9	3.5
8	8.1	-	600	-	396.0	419.3	5.7
8	8.2	-	-	2.5	46.8	46.9	0.2

Table 24. Incurred samples reanalysis. Measured drugs' concentrations (ng/mL) with the % difference (% diff.) calculated between the two analyses (I and II quantification).

4.2.4.1 Incurred samples reanalysis

To further assessed the reproducibility of the proposed method, the 10 patients' plasma samples (reported in the previous section) were analysed two times, with separate runs and during different working days. In Table 24 ISR data are reported: the concentrations of PALBO, RIBO and LETRO obtained with the first and the second quantification along with the percentage differences

calculated. Despite this test is limited by the low number of available samples, preliminary results seemed to indicate a good reproducibility of the method: the percentage differences were always within ±10% for all the analytes (between -6.5% and 10.5%) and the R^2 of the correlation graph between the two quantifications was 0.9994 (Figure 58).

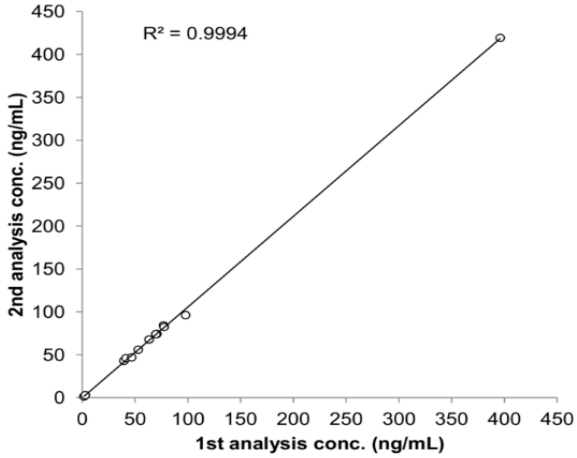

Figure 58. Correlation graph between the first and the second analysis of PALBO, RIBO and LETRO in patients' samples (N=6).

4.3 Molecularly imprinted polymers

The experiments described in this chapter are part of a large project granted by the Italian Association for Cancer Research (AIRC) on "*Application of Advanced Nanotechnology in the development of innovative cancer diagnostic tools*". In this context, the aim was to synthesize imprinted polymers as receptors for IMA. The work hereby presented was carried out in the laboratory of prof. Federico Berti (Dept. Of Chemical and Pharmaceutical Sciences, University of Trieste), and in the laboratory of prof. Marina Resmini (School of Biological and Chemical Sciences, Queen Mary University of London), for an overall secondment of 6 months.

4.3.1 MIPs synthesis and characterization

In order to obtain specific polymers for IMA, the first step consisted on the selection of a FM able to interact with the target molecule, exploiting the non-covalent imprinting process (as reported in section 3.4.4). This process was the only evaluated, because it is an easy method that requires only a low number of synthetic steps.

Other PhD students worked on this project too, synthesizing MIPs/NIPs for IMA with different types of FMs (like AMPS and 4-vinylpyridine). Thus, the FM took in consideration for the interaction with

IMA, in this thesis, was MAA. A preliminary evaluation of its ability to bind the target was carried out by NMR titration (protocol reported in section 3.4.3). The experiment was performed in deuterated DMSO, as it was the solvent chosen to perform the MIP synthesis. In particular, to a 4 mM solution of IMA free-base in d_6-DMSO, increasing amounts of FM solution were added to obtain final concentrations ranging from 2.3 to 44 mM. The type of exchange observed in all titrations is mainly fast, suggesting that weak interactions are established between the drug and the FM.

Analysing the obtained data, in particular looking at the chemical shift of each proton, it was possible to notice that MAA interacts with IMA through weak interactions (there is not a clear saturation trend that could suggest the occurrence of tight interactions) in correspondence of H1 and H4, as reported in panel (B) of Figure 59. In panel (A) of the same Figure also the variation of the proton chemical shift of the target drug after the addition of 10.7 equivalents of FM is shown.

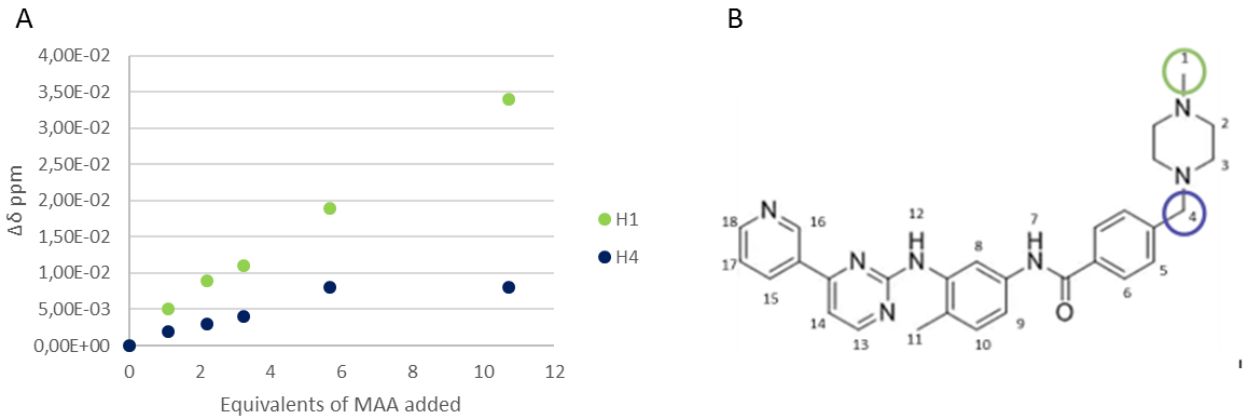

Figure 59. Variation of IMA proton chemical shift, in d6-DMSO, upon the addition of MAA, from 0 to 10.71 equivalents (A), graphical representation of IMA protons involved in the interaction with MAA (B).

Both protons at position 1 and at position 4 are close to sp^3 piperazine nitrogens. The pKa of all IMA nitrogens have been evaluated [202] and those of piperazine groups are most likely to be protonated since they are the most basic groups in the molecule. The change in chemical shift at such protons may be due to the protonation (either direct or water-mediated) of one of the nitrogen atoms and to the subsequent formation of an ionic pair between IMA^+ and MAA^-. Depending on the polarity of the environment, as well as on water amount, the formation of a strong hydrogen bond without proton transfer can also be an explanation. These two pictures represent the extremes of the actual behaviour occurring inside a MIP binding site, depending on its polarity, when the rebinding is performed in water. However, the interaction will take place both in DMSO during the synthesis of MIPs, and in water when exploiting the material in the real sample matrix. DMSO was

therefore chosen as the solvent to perform the synthesis since it allows a good dissolving of all the reagents involved in the polymerization.

MAA was used in all polymers' synthesis. The synthesis of several MIPs was carried out, testing whether using different percentages of FM has effect in MIP binding capacity, and also whether exploiting different percentages of co-monomer (acrylamide, AA) and different type of cross-linkers (MBA and PBA) has effect in MIP size and performances.

The performances evaluation was carried out according to two main criteria: the polymers' rebinding capacity for the template and the IF as measure of specificity (given by comparison with the NIP, as reported in section 3.4.7).

The synthesis of MIPs, and the corresponding NIPs, was performed following the protocol described in section 3.4.4. The initiator (AIBN) concentration was fixed at 5%, the C_M at 1% (to avoid macrogelation phenomena) and the porogenic solvent (DMSO) was the 99% (in weight). The ratio between FM and IMA was fixed at 1:1. The relevant data for all the MIPs and NIPs synthesised are reported in Table 25 and Table 26, respectively. In particular, the mol% composition of the reacting mixtures leading to MIPs/NIPs, the yield (%) calculated from the total mass of reagents and the mass of the resulting MIPs/NIPs; the IMA amount (nmol) bound measured by HPLC/UVvis, with a IMA concentration of 3000 μM; the specificity (IF value, reported only in the MIPs table); the triplicate of DLS size measurement both by intensity and by number (mean (±SD) in nm) were reported.

Considering that during all the rebinding tests performed, the plateaux was never reached increasing the concentrations of the template, IMA rebinding was evaluated at the maximum concentration exploited: 3000 μM. It was not possible to increase further IMA concentration due to problems with detector saturation, neither to decrease the polymers' concentration for their solubility in water and the consequent problems to achieve the polymers precipitation (necessary to perform the rebinding tests).

MIP	MAA (%)	AA (%)	Cross-linker (%)	Yield (%)	IMA rebinding (nmol/mg)	Specificity IF	DLS size by intensity Mean (±SD) (nm)	DLS size by number Mean (±SD) (nm)
1	20	20	MBA (60)	84.2	480	0.89	70.3 (±7.1)	14.7 (±2.1)
2	20	10	MBA (70)	82.5	543	1.09	122 (±13.2)	46.9 (±18.5)
3	20	-	MBA (80)	71.5	504	1.06	90.3 (±2.6)	53.9 (±3.0)
4	10	30	MBA (60)	98.6	599	2.35	114 (±5.8)	28.1 (±25.7)
5	10	20	MBA (70)	99.0	530	1.31	95.4 (±4.3)	45.8 (±10.5)
6	10	10	MBA (80)	79.7	465	0.98	101 (±22.4)	84 (±9.8)
7	10	30	MBA:PBA (40:20)	71.3	446	0.72	84.3 (±3.3)	51.9 (±44.0)
8	10	70	PBA (20)	91.4	559	1.71	94.2 (±3.2)	7.47 (±2.3)
9	10	30	PBA (60)	89.3	385	0.83	131 (±15.4)	27.2 (±4.2)

Table 25. Summary table with the data obtained for the MIPs synthesized in DMSO.

NIP	MAA (%)	AA (%)	Cross-linker (%)	Yield (%)	IMA rebinding (nmol/mg)	DLS size by intensity Mean (±SD) (nm)	DLS size by number Mean (±SD) (nm)
1	20	20	MBA (60)	84.5	540	73.3 (±1.9)	41.2 (±5.2)
2	20	10	MBA (70)	90.6	495	78.2 (±1.9)	14.8 (±4.5)
3	20	-	MBA (80)	75.1	473	52.7 (±4.0)	22.5 (±12.6)
4	10	30	MBA (60)	83.1	255	65.9 (±2.5)	20.6 (±6.9)
5	10	20	MBA (70)	85.2	405	79.1 (±10.1)	18.0 (±3.5)
6	10	10	MBA (80)	75.3	474	129 (±35.5)	123 (±29.1)
7	10	30	MBA:PBA (40:20)	95.5	623	71 (±11.0)	16.6 (±15.6)
8	10	70	PBA (20)	89.3	327	86.4 (±2.6)	9.4 (±1.2)
9	10	30	PBA (60)	67.5	465	76.7 (±3.2)	53.1 (±4.5)

Table 26. Summary table with data obtained for the NIPs synthesized in DMSO.

A first set of polymers was designed using MBA as cross-linker (MIPs/NIPs 1-6) and changing the reagents' percentages. From the obtained data, it was possible to exclude a relationship between the MAA percentage presented in the composition and the polymer binding capability: MIPs/NIPs 1-3 (with 20% MAA) showed a IMA rebinding comparable to MIPs/NIPs 4-6 (with 10% MAA). Meanwhile, a more detailed discussion has to be made considering a correlation between the size and the cross-linker quantity: analysing the size by intensity data, no relationship can be highlighted. However, as reported in section 3.4.6, the intensity distribution can be misleading, for example the presence of a small number of aggregating particles or larger particle species could dominate the distribution, hiding the presence of smaller particles. In fact, examining the size by number data for the MIPs, it was possible to notice that the increment of MBA %, corresponded to an increase in particle size. This behaviour could be due to the higher MIP rigidity, that could therefore favor the

formation of specific and structured sites. Thus, when the nanoparticles were produced, they contained more template and they remained larger even after having released it, just because of their rigidity. In fact, this behavior in NIPs was not noticed.

An example of the DLS graphs obtained by intensity (panel A) and by number (panel B) is reported in Figure 60.

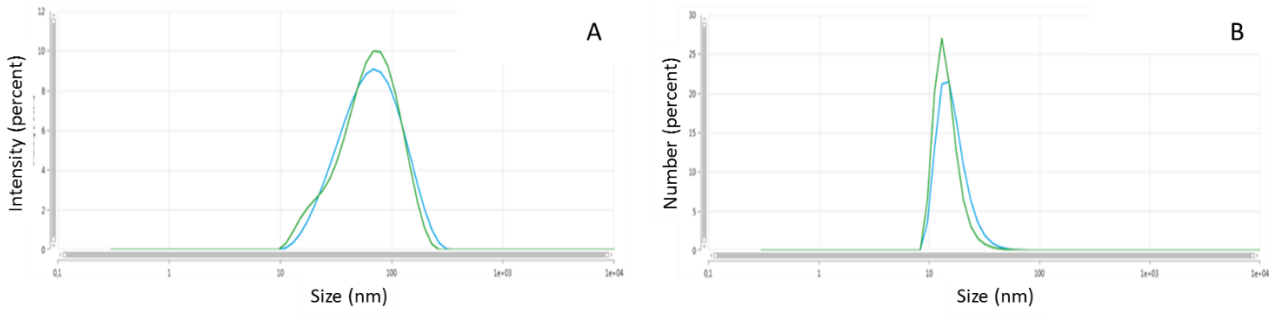

Figure 60. Size distribution by intensity (A) and by number (B) of NIP5 in triplicate.

To monitor and understand the percentage of reagents involved in the polymerization reaction, the monomer conversion ^{1}H-NMR studies were performed, as reported in section 3.4.5. These studies were useful also to verify that the reaction had gone to completion, by monitoring the disappearance of the signals belonging to the acroyl protons.

The monomers and crosslinker concentrations, in the initial and final polymerization solutions, were determined by comparing the intensities of monomer peaks at 5.75 ppm (PBA), 6.05 ppm (AAm), 6.00 ppm (MAA), 4.55 ppm (MBA), against the intensity of the ISt peak at 7.85 ppm.

In Figure 61 an example of ^{1}H-NMR spectra is reported before and after the polymerization.

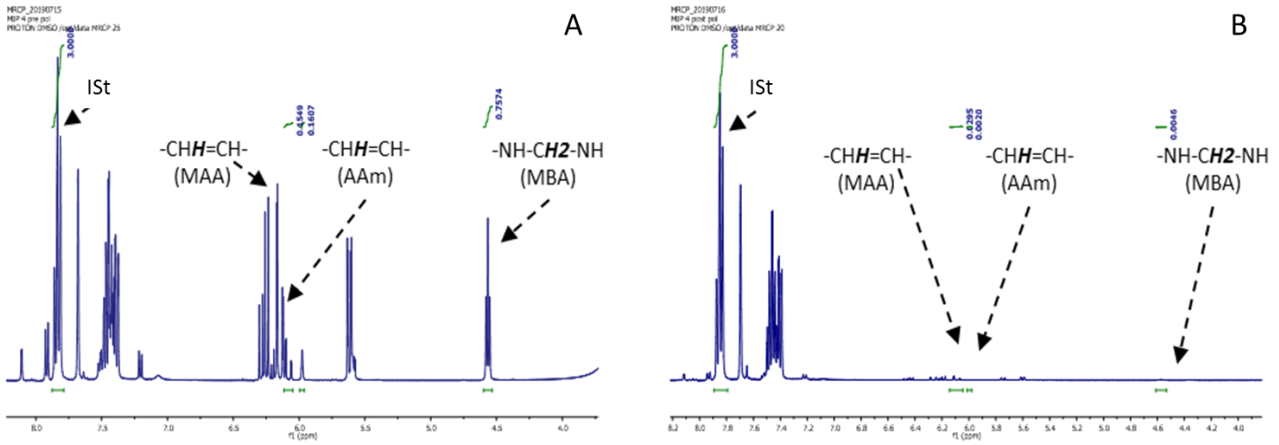

Figure 61. Example of ^{1}H-NMR spectra before (A) and after (B) the polymerization.

In the Table 27, the percentages of reagent that polymerized are reported. Data were comparable between MIPs and NIPs. Moreover, the percentages varied from 70.9.0 to 99.3 % for all the reagents, meaning that almost all components underwent the polymerization process.

	MIP4	NIP4
MAA	98.6%	98.7%
MBA	98.0%	99.3%
AAm	93.0%	97.4%

	MIP8	NIP8
MAA	99.5%	85.4%
PBA	70.9%	73.1%
AAm	83.05%	85.4%

	MIP9	NIP9
MAA	96.4%	93.5%
PBA	95.6%	96.7%
AAm	96.8%	92.5%

Table 27. Percentages (%) of reagents (MAA, MBA, PBA and AAm) that polymerized for MIP/NIP4, MIP/NIP8 and MIP/NIP9.

Polymers binding capacity was investigated through rebinding tests (that consisted in the quantification, after 1 h, of the amount of free drug in 1 mg/mL polymer water solution containing different concentrations of IMA, as reported in section 3.4.7).

Before to perform these tests, the binding kinetic of MIPs and NIPs was evaluated, from 30 min to 6 h (30, 60, 180, 360 min), using a fixed IMA concentration of 500 µM. An example is reported in Figure 62, where the maximum binding capacity was reached after 1 h and it remained stable within the tested time window, going from 237.5 to 240.7 (SD: ± 1.31) nmol/mg for MIP and from 233.6 to 234.6 (SD: ± 0.46%) nmol/mg for NIP. Data are reported in Figure 62 where time (expressed in minutes) is plotted versus the bound IMA concentration, expressed as the quantity of bounded IMA (nmol) over the quantity of MIP/NIP added (mg) ratio.

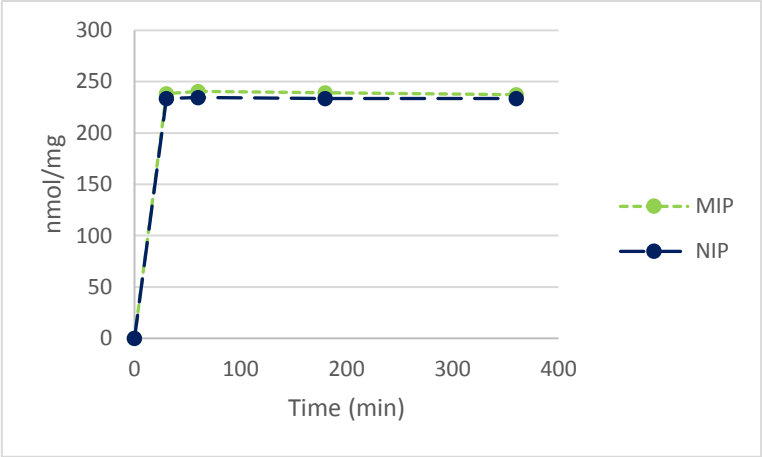

Figure 62. Example of kinetic test to evaluate the MIP/NIP binding capability during time, from 30 to 360 min.

In the first set of polymers prepared, all the MIPs (and their corresponding NIPs) showed a good rebinding of IMA in water. Regarding the specificity (evaluated through the IF), only MIP4 showed specificity for the template (IF=2.35), while all the others gave almost the same rebinding of their corresponding NIPs (IF ranging from 0.89 to 1.31). The rebinding affinity data of MIP/NIP4, obtained increasing IMA concentrations from 100 to 3000 µM, are reported in Figure 63, where the IMA initial concentration (µM) versus the bound IMA amount (nmol)/ polymer quantity (mg) ratio is plotted.

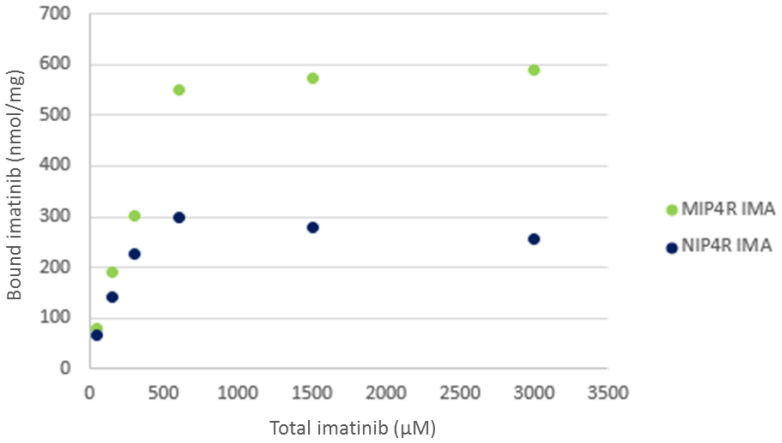

Figure 63. Binding isotherms of MIP/NIP4 increasing IMA from 100 to 3000 µM.

Although the result obtained with the MIP4 was considered good, a second set of polymers, always using DMSO as porogenic solvent, was prepared (MIPs/NIPs 7-9) with the aim to implement the selectivity.

These polymers were designed employing a different cross-linker. In particular, PBA (chemical structure reported in Figure 64) was chosen to increase the polymer affinity for the target analyte:

considering the aromatic ring present in its structure, it should interact with the lipophilic part of IMA, the aromatic one.

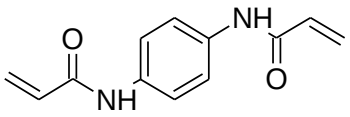

Figure 64. Chemical structure of PBA.

Nanoparticles with size comparable to that of the first set were obtained.

Anyway, the incorporation of PBA as cross-linker, in combination with MBA (MIP/NIP7) or alone at different percentages (MIPs/NIPs 8-9), did not improve nor MIPs specificity neither the rebinding capacity (which remained consistent with the previous set of polymers). Anyway, a good result was obtained with MIP8, obtaining an IF of 1.71 (Figure 65). This could be explained considering that, in the case of MIP8 very small particles were obtained (7.47 ± 2.34 nm by number, as reported in Table 25), the volume to surface ratio should be larger, with more active sites that could capture and bind IMA.

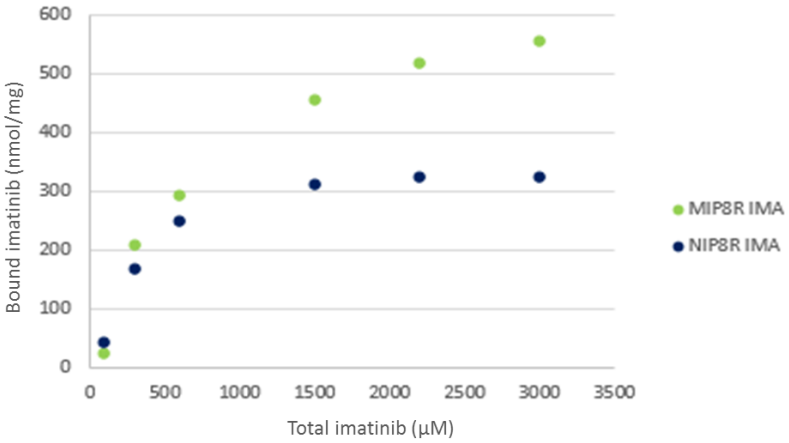

Figure 65. Binding isotherms of MIP/NIP8 increasing IMA from 100 to 3000 µM.

Another strategy to increase the specificity was attempted: to perform the synthesis of MIP/NIP4 in $CHCl_3$. In fact, $CHCl_3$ should be less able to disrupt hydrogen bonds and solvate charged species since it is a less polar solvent compared to DMSO. Therefore, the expectation was to see stronger hydrogen bonding and/or electrostatic interactions. To confirm this theoretical supposition, an ^{1}H-NMR titration between MAA and IMA free-base in $CDCL_3$ was carried out under the same conditions described above. Analysing the data obtained, it was possible to confirm all the theoretical supposition done. In fact, more protons, compared to the results observed performing the titration

in d_6-DMSO, are involved in the interaction with the MAA, as reported in Figure 66. Moreover, the chemical shift is much higher, even ten times higher in the case of protons 2 and 3.

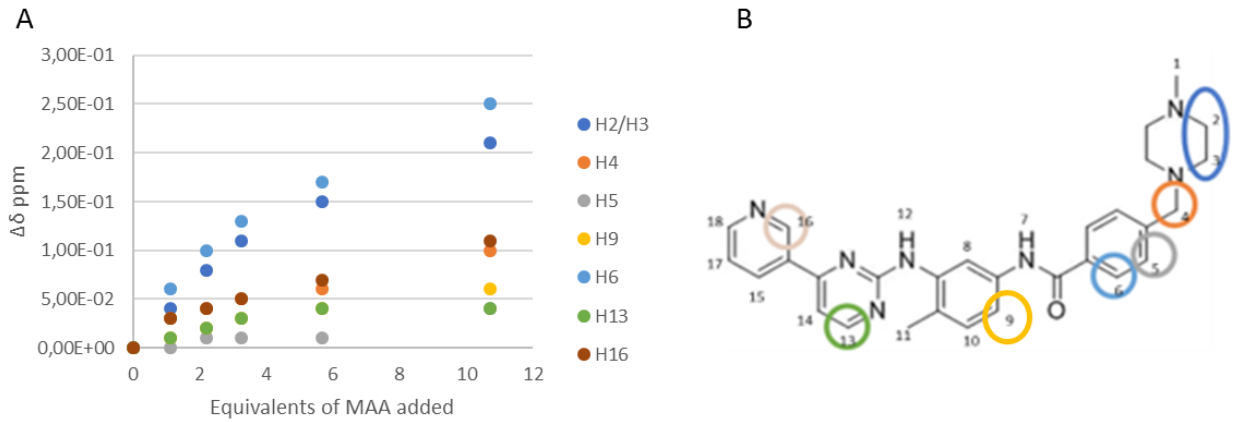

Figure 66. Variation of IMA proton chemical shift, in $CDCL_3$, upon the addition of MAA, from 0 to 10.71 equivalents (A), graphical representation of IMA protons involved in the interaction with MAA (B).

The relevant data for all the MIP4_CHCl3 are reported in Table 28.

MIP	MAA (%)	AA (%)	Cross-linker (%)	Yield (%)	IMA rebinding (nmol/mg)	Specificity IF	DLS size intensity Mean (±SD) (nm)	DLS size number Mean (±SD) (nm)
4_CHCl3	10	30	MBA (60)	59.1	233.46	1.44	672 (±6.4)	532 (±23.5)

Table 28. Summary table with data obtained for the MIP4_CHCl3 synthesized in DMSO.

In this case, particles with a bigger dimension were obtained, almost in the µm range. This is probably because $CHCl_3$ is not a good solvent as DMSO for the synthesis of MIPs/NIPs, it has a lower solvating power to prevent macrogelation phenomena.

Despite expectations, the MIP/NIP4_$CHCl_3$ did not show a better IF, rather it became worse with a maximum value of 1.4; moreover, also the capacity to bind IMA became worse, almost halved compared to the corresponding MIP4. These data could be explained considering the solvent used. DMSO, indeed, is able to create more cavities and porosity during the polymerization compared to $CHCl_3$. This means that the sites available for the binding within the polymer are fewer. Furthermore, as mentioned above, with $CHCl_3$ larger particles have been obtained compared to that in DMSO (almost 6 times bigger by intensity and 8 times by number). This led to obtain particles with a smaller surface area ratio, with fewer cavities on the outside able to bind the target analyte.

Subsequentially, to evaluate the importance of having MAA as FM in the polymer composition, a NIP (with the same composition of MIP/NIP8, but without the MAA) has been prepared, with a polymerization yield of 80%.

To assess the binding difference, a rebinding test has been performed (with the same modalities reported in section 3.4.7). From the results reported in Figure 67, it was possible to notice that without the presence of MAA in the polymer composition, the affinity for the analyte is lost.

Thus, it is possible to affirm that the presence of MAA in the polymer is fundamental to obtain a good binding and to have a good affinity for IMA.

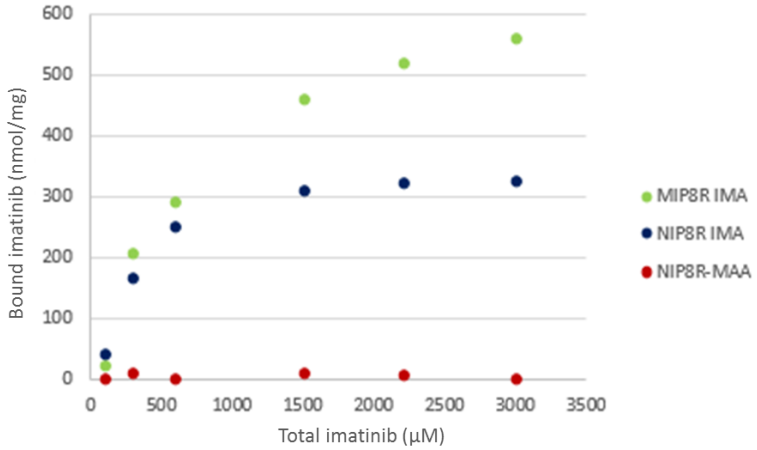

Figure 67. Binding isotherms of MIP/NIP8 increasing IMA concentrations from 100 to 3000 μM versus the NIP8R prepared without adding the functional monomer, MAA.

4.3.2 Selectivity tests

After the results of the rebinding experiments, reported in section 3.4.8, a first evaluation of selectivity was carried out for both MIP4 and 8.

In fact, the obtained IF values should be considered along with selectivity results since a better or less retention of a certain compound over another one may just be due to their particular physicochemical properties rather than to specific imprinted sites.

Likewise the rebinding tests, the cross-reactivity ones were performed in H_2O. The drugs that have been chosen are: SUNI and PARA.

SUNI was chosen because it belongs to the same class of drugs of IMA, the TKIs. Moreover, it is used in unresectable or metastatic cases of imatinib-resistant GIST as second-line chemotherapy (as described in section 1.2.1.2). PARA, instead, is the mainstay of the first two steps of the WHO analgesic ladder in many countries. In particular, in the treatment of mild pain, WHO ladder involves

the use of a non-opioid (non-steroidal anti-inflammatory drug or paracetamol). The subsequent step requires the addition of an opioid [203].

From data reported in figures presented below, there is the evidence that SUNI was equally bound to IMA in the case of the NIPs (Figure 69 and Figure 71), especially for the NIP8 (Figure 71). While, studying the MIPs behavior, in both MIP4 (Figure 68) and MIP8 (Figure 70) a decrease in affinity for SUNI compared to the one for IMA could be noticed.

This difference between MIPs and NIPs could represent an evidence that, in the case of MIPs, specific imprinted sites have been formed during the polymerization for the template.

A completely different behavior could be observed for the binding experiment performed with PARA: the binding of all MIPs/NIPs 4R and 8R was almost negligible. In fact, besides having a different chemical structure, PARA presented also different chemical-physical properties compared to IMA and SUNI. Even if PARA and IMA are both slightly acidic compound (pKa ranging from 8.3 to 9.4), for the imprinting and consequentially the binding, also the size of the molecule has an impact. PARA (MW = 151.15 g/mol), indeed, is smaller compared to IMA (MW = 493.4).

Furthermore, PARA is much more hydrophilic (logP=0.6) than IMA (logP=4.4) and there could be secondary hydrophobic interactions that stabilize the complex of IMA and the polymer.

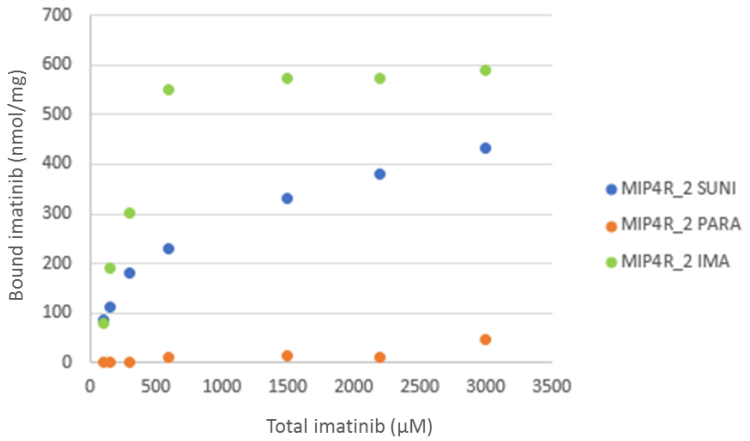

Figure 68. Binding isotherms of MIP4 increasing the concentrations of IMA, SUNI and PARA from 100 to 3000 µM.

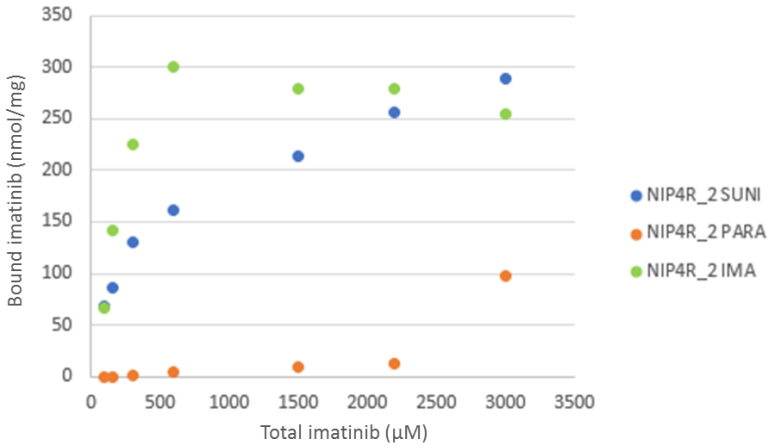

Figure 69. Binding isotherms of NIP4 increasing the concentrations of IMA, SUNI and PARA from 100 to 3000 µM.

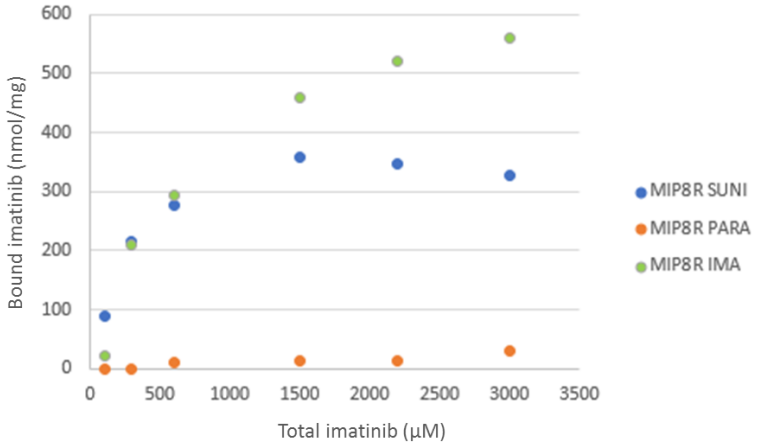

Figure 70. Binding isotherms of MIP8 increasing the concentrations of IMA, SUNI and PARA from 100 to 3000 µM

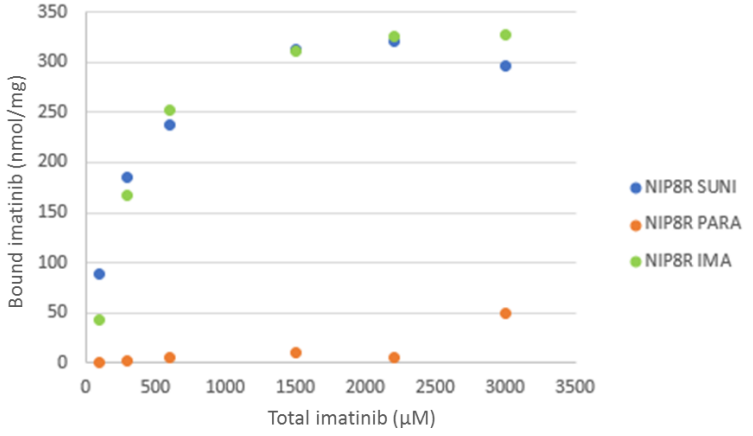

Figure 71. Binding isotherms of NIP8 increasing the concentrations of IMA, SUNI and PARA from 100 to 3000 µM

To conclude, these two polymers, considering the good binding affinity towards IMA and their specificity and selectivity, could be tested in complex matrices, like plasma samples. The most

promising could be then applied in a future prototype of point of care device. The idea is to apply them as receptors in a system based on IMA indirect fluorimetric quantification, exploiting a fluorescent-derivative of this drug, shown in Figure 72 (its synthesis is in progress).

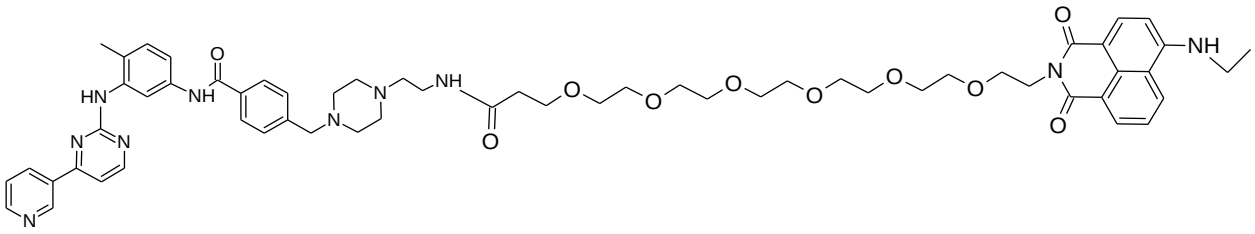

Figure 72. Chemical structure of IMA fluorescent-derivative.

.

5. CONCLUSIONS

5.1 LC-MS/MS method for the simultaneous quantification of IMA and norIMA in DBS

The introduction of IMA, an oral TKI, as first-line standard therapy in patients with unresectable, metastatic, or recurrent GISTs, strongly improved their treatment outcomes. However, TDM is recommended for this drug due to the large inter-individual variability in plasma concentration when standard dose is administered. A C_{min} higher than 1100 ng/mL was associated with a longer TTP.

Thus, a LC-MS/MS method has been developed, fully validated and cross-validated to quantify IMA and its active metabolite, norIMA, in finger-prick DBS. This sampling technique should be useful to reduce the sampling time and costs and to improve patient's compliance.

The validation, performed according to FDA and EMA guidelines, was carried out by evaluating the following parameters: recovery of the analytes from the matrix, calibration curve linearity, intra- and inter-day precision and accuracy, reproducibility, LLOQ and selectivity, matrix effect and stability of the analytes in samples and solutions.

Moreover, other variables that could affect specifically the DBS analysis were considered during the method development. Thus, the analytes' extraction conditions from the filter paper, the influence of Hct, the sample homogeneity (volcano effect), the spot size and the correlation between finger-prick and venous DBS measurements were assessed and optimized.

The method showed a good linearity (R^2 > 0,996) between 50-7500 ng/mL for IMA and 10-1500 ng/mL for norIMA. Analytes were extracted from DBS samples by simply adding to 3 mm-discs 150 µL of acidified MeOH containing the ISt IMA-D8. The collected extract was then injected on a LC Nexera system in-house configured with a 2D chromatography for the on-line clean-up, coupled with an API-4000 QT. The chromatographic separation was conducted on a Synergi Fusion-RP column (4 µm, 2x50 mm) while the trapping column was a POROS R1/20 (20 µm, 2x30 mm). The total run time was 8.5 min. DBSs stored at RT in plastic envelopes containing a silica-gel drying bag were stable up to 16 months.

After the validation, this method was applied to quantify finger prick DBS samples from patients enrolled in a clinical study on going in the National Cancer Institute of Aviano (EudraCT N. 2017-002437-36, internal code: CRO-2017-19). Good agreement was obtained between IMA and norIMA

concentrations found in DBS and plasma samples (quantified exploiting the reference LC-MS/MS method, internally validated), collected at the same time from each patient, applying the Hct normalization. Furthermore, the possibility to avoid the Hct normalization, simply multiplying the DBS concentration with a correction factor, not only for IMA but also for norIMA was demonstrated. The correction factors applied were calculated on the basis of 55 patients' samples and successively tested in a set of additional 12 patients' samples. The statistical analyses demonstrated that the application of the correction factor even improved the agreement with the plasma concentrations, especially for IMA.

To conclude, the proposed LC-MS/MS method is the first analytical assay, fast and sensitive, for the simultaneous quantification of iMA and norIMA in finger-prick DBS samples. The cross-validation study demonstrated the possibility to obtain the drug plasma concentration simply from a drop of blood collected in a paper card and stored at room temperature. The hope is that, with the possibility to perform the quantification of these two analytes just having a finger prick DBS samples, this method could actually improve TDM application to clinical practice.

5.2 LC-MS/MS method for the quantification of RIBO, PALBO and LETRO in human plasma

The majority of patients with metastatic breast cancer have HR-positive and HER2-negative disease. In these cases, the key therapeutic option is represented by the endocrine therapy, which have been recently expanded with the introduction of CDKIs. In particular, PALBO and RIBO have been approved by the EMA for their application in concomitance with aromatase inhibitors, such as LETRO.

TDM recommendation for these drugs is currently only exploratory, based on limited exposure-response and -toxicity studies, but, in the prospective of a TDM application also for these drugs, it is necessary to have a method to perform their quantification.

Thus, the first LC-MS/MS method for the simultaneous quantification of PALBO, RIBO and LETRO in human plasma was developed and successfully validated according to FDA/EMA guidelines on bioanalytical method validation. The proposed method is suitable to be applied in clinical practice due to the simple and fast sample preparation based on protein precipitation, the low amount of

patient plasma necessary for the analysis (10 µL) and the total run time of 6.5 min. The linearity was assessed (R^2 within 0.9992-0.9983) over the concentration ranges of 0.3-250 ng/mL for PALBO, 10-10000 ng/mL for RIBO and 0.5-500 ng/mL for LETRO that properly cover the therapeutic plasma concentrations.

A specific strategy was put in place to reduce the carryover phenomenon, already known for these CDKIs, by introducing blank samples to be run with a precisely developed method.

Once concluded the validation, the method was applied to quantify the C_{min} of PALBO, RIBO and LETRO in patients' plasma samples enrolled in a clinical study ongoing at the National Cancer Institute in Aviano (prot. Code: CRO-2018-83). The same set of study samples was analysed twice in separate runs to assess the reproducibility of the method by means of the ISR. The percentage differences were always within ±10% for all the analytes and the R^2 of the correlation graph between the two quantifications was equal to 0.9994.

The ample calibration curve ranges allow the proposed method to be applied to evaluate also other pharmacokinetic parameters or clinical query: among the study samples analysed, PALBO was detected at the concentration of 1.6 ng/mL after 1 week off treatment and LETRO was detected (2.8 ng/mL) after 2 weeks from the last pill intake.

This simple and versatile analytical method could be a useful instrument to promote the personalization of anticancer therapy for these drugs.

5.3 Molecularly imprinted polymers

Despite LC-MS/MS is considered the election technique for TDM analysis, it is quite expensive and it needs trained personnel. Thus, the development of a point of care device usable at the patients' bed side by non-specialized personnel could represent a turning point to operate TDM of anticancer drugs, such as IMA.

With this purpose, the possibility to perform IMA quantification using a system based on a recognition phase and fluorescence detection was considered. Thus, the synthesis of MIPs (and the corresponding NIPs) was performed, exploiting the non-covalent approach and the HDRP (C_M=1%). The initiator (AIBN) concentration was fixed at 5%, the C_M at 1% (to avoid macrogelation phenomena) and the porogenic solvent (DMSO) was the 99% (in weight). The ratio between FM and IMA was fixed at 1:1.

In particular, polymers with MAA as FM were synthesized, and particles with nanometre size were obtained (confirmed by the DLS technique). The majority of the prepared MIPs showed no specificity (compared to the NIPs) except for two compositions, MIP4 (10% MAA, 30% AA, 60% MBA) and MIP8 (10% MAA, 70% AA, 20% PBA), that showed a good affinity for the target analyte and specificity (max IF_{MIP4}: 2.4 and IF_{MIP8}: 1.7). Moreover, these polymers showed a good selectivity when compared to other drugs such as PARA and SUNI.

To conclude, these two polymers, considering the good affinity for IMA, their specificity and selectivity, as future prospective should be tested in complex matrices, like plasma samples.

The most promising could be then be applied in a point of care device prototype.

REFERENCES

1. Yu H, Steeghs N, Nijenhuis CM, Schellens JHM, Beijnen JH, Huitema ADR (2014) Practical guidelines for therapeutic drug monitoring of anticancer tyrosine kinase inhibitors: focus on the pharmacokinetic targets. Clin Pharmacokinet 53:305–325 . https://doi.org/10.1007/s40262-014-0137-2

2. Spector R, Park GD, Johnson GF, Vesell ES (1988) Therapeutic drug monitoring. Clin Pharmacol Ther 43:345–353

3. Alnaim L (2007) Therapeutic drug monitoring of cancer chemotherapy. J Oncol Pharm Pract 13:207–221 . https://doi.org/10.1177/1078155207081133

4. Simsek C, Esin E, Yalcin S (2019) Metronomic Chemotherapy: A Systematic Review of the Literature and Clinical Experience. In: Journal of Oncology. https://www.hindawi.com/journals/jo/2019/5483791/. Accessed 5 Nov 2019

5. Therapeutic drug monitoring: which drugs, why, when and how to do it. In: NPS MedicineWise. https://www.nps.org.au/australian-prescriber/articles/therapeutic-drug-monitoring-which-drugs-why-when-and-how-to-do-it. Accessed 28 Jun 2019

6. Gross AS (2001) Best practice in therapeutic drug monitoring. Br J Clin Pharmacol 52:5S-10S . https://doi.org/10.1046/j.1365-2125.2001.0520s1005.x

7. Chatterjee K (2002) Congestive Heart Failure. Am J Cardiovasc Drugs 2:1–6 . https://doi.org/10.2165/00129784-200202010-00001

8. Sawyers C (2004) Targeted cancer therapy. Nature 432:294 . https://doi.org/10.1038/nature03095

9. Giamas G, Man YL, Hirner H, Bischof J, Kramer K, Khan K, Lavina Ahmed SS, Stebbing J, Knippschild U (2010) Kinases as targets in the treatment of solid tumors. Cellular Signalling 22:984–1002 . https://doi.org/10.1016/j.cellsig.2010.01.011

10. Widmer N, Bardin C, Chatelut E, Paci A, Beijnen J, Levêque D, Veal G, Astier A (2014) Review of therapeutic drug monitoring of anticancer drugs part two--targeted therapies. Eur J Cancer 50:2020–2036 . https://doi.org/10.1016/j.ejca.2014.04.015

11. Delbaldo C, Chatelut E, Ré M, Deroussent A, Séronie-Vivien S, Jambu A, Berthaud P, Le Cesne A, Blay J-Y, Vassal G (2006) Pharmacokinetic-pharmacodynamic relationships of imatinib and its main metabolite in patients with advanced gastrointestinal stromal tumors. Clin Cancer Res 12:6073–6078 . https://doi.org/10.1158/1078-0432.CCR-05-2596

12. von Mehren M, Widmer N (2011) Correlations between imatinib pharmacokinetics, pharmacodynamics, adherence, and clinical response in advanced metastatic gastrointestinal stromal tumor (GIST): an emerging role for drug blood level testing? Cancer Treat Rev 37:291–299 . https://doi.org/10.1016/j.ctrv.2010.10.001

13. Hughes T, Deininger M, Hochhaus A, Branford S, Radich J, Kaeda J, Baccarani M, Cortes J, Cross NCP, Druker BJ, Gabert J, Grimwade D, Hehlmann R, Kamel-Reid S, Lipton JH, Longtine J, Martinelli G, Saglio G, Soverini S, Stock W, Goldman JM (2006) Monitoring CML patients responding to treatment with tyrosine kinase inhibitors: review and recommendations for harmonizing current methodology for detecting BCR-ABL transcripts and kinase domain mutations and for expressing results. Blood 108:28–37 . https://doi.org/10.1182/blood-2006-01-0092

14. Klümpen H-J, Samer CF, Mathijssen RHJ, Schellens JHM, Gurney H (2011) Moving towards dose individualization of tyrosine kinase inhibitors. Cancer Treatment Reviews 37:251–260 . https://doi.org/10.1016/j.ctrv.2010.08.006

15. Wilkinson GR (2005) Drug Metabolism and Variability among Patients in Drug Response. New England Journal of Medicine 352:2211–2221 . https://doi.org/10.1056/NEJMra032424

16. Relling MV, Fairclough D, Ayers D, Crom WR, Rodman JH, Pui CH, Evans WE (1994) Patient characteristics associated with high-risk methotrexate concentrations and toxicity. J Clin Oncol 12:1667–1672 . https://doi.org/10.1200/JCO.1994.12.8.1667

17. Evans WE, Relling MV (1989) Clinical pharmacokinetics-pharmacodynamics of anticancer drugs. Clin Pharmacokinet 16:327–336 . https://doi.org/10.2165/00003088-198916060-00001

18. Moore MJ, Erlichman C (1987) Therapeutic drug monitoring in oncology. Problems and potential in antineoplastic therapy. Clin Pharmacokinet 13:205–227 . https://doi.org/10.2165/00003088-198713040-00001

19. Moore MJ, Erlichman C (1987) Therapeutic Drug Monitoring in Oncology. Clin-Pharmacokinet 13:205–227 . https://doi.org/10.2165/00003088-198713040-00001

20. MD VTDJ, PhD TSLM, PhD SARM, MD RAD, PhD RAW (2011) DeVita, Hellman, and Rosenberg's Cancer: Principles and Practice of Oncology, Ninth, North American edition. LWW, Philadelphia

21. Thomas-Schoemann A, Blanchet B, Bardin C, Noé G, Boudou-Rouquette P, Vidal M, Goldwasser F (2014) Drug interactions with solid tumour-targeted therapies. Critical Reviews in Oncology/Hematology 89:179–196 . https://doi.org/10.1016/j.critrevonc.2013.08.007

22. Gao B, Yeap S, Clements A, Balakrishnar B, Wong M, Gurney H (2012) Evidence for Therapeutic Drug Monitoring of Targeted Anticancer Therapies. JCO 30:4017–4025 . https://doi.org/10.1200/JCO.2012.43.5362

23. Reynolds DJ, Aronson JK (1993) ABC of monitoring drug therapy. Making the most of plasma drug concentration measurements. BMJ 306:48–51

24. Teng JFT, Mabasa VH, Ensom MHH (2012) The role of therapeutic drug monitoring of imatinib in patients with chronic myeloid leukemia and metastatic or unresectable gastrointestinal stromal tumors. Ther Drug Monit 34:85–97 . https://doi.org/10.1097/FTD.0b013e31823cdec9

25. Bardin C, Veal G, Paci A, Chatelut E, Astier A, Levêque D, Widmer N, Beijnen J (2014) Therapeutic drug monitoring in cancer – Are we missing a trick? European Journal of Cancer 50:2005–2009 . https://doi.org/10.1016/j.ejca.2014.04.013

26. Bray F, Ferlay J, Soerjomataram I, Siegel RL, Torre LA, Jemal A (2018) Global cancer statistics 2018: GLOBOCAN estimates of incidence and mortality worldwide for 36 cancers in 185 countries. CA: A Cancer Journal for Clinicians 68:394–424 . https://doi.org/10.3322/caac.21492

27. Doyle LA (2014) Sarcoma classification: An update based on the 2013 World Health Organization Classification of Tumors of Soft Tissue and Bone. Cancer 120:1763–1774 . https://doi.org/10.1002/cncr.28657

28. Miettinen M, Lasota J (2001) Gastrointestinal stromal tumors--definition, clinical, histological, immunohistochemical, and molecular genetic features and differential diagnosis. Virchows Arch 438:1–12

29. Lim KT, Tan KY (2017) Current research and treatment for gastrointestinal stromal tumors. World J Gastroenterol 23:4856–4866 . https://doi.org/10.3748/wjg.v23.i27.4856

30. Scherübl H, Faiss S, Knoefel W-T, Wardelmann E (2014) Management of early asymptomatic gastrointestinal stromal tumors of the stomach. World J Gastrointest Endosc 6:266–271 . https://doi.org/10.4253/wjge.v6.i7.266

31. Lim KT, Tan KY (2017) Current research and treatment for gastrointestinal stromal tumors. World J Gastroenterol 23:4856–4866 . https://doi.org/10.3748/wjg.v23.i27.4856

32. Nilsson B, Bümming P, Meis-Kindblom JM, Odén A, Dortok A, Gustavsson B, Sablinska K, Kindblom L-G (2005) Gastrointestinal stromal tumors: the incidence, prevalence, clinical course, and prognostication in the preimatinib mesylate era--a population-based study in western Sweden. Cancer 103:821–829 . https://doi.org/10.1002/cncr.20862

33. Demetri GD, von Mehren M, Antonescu CR, DeMatteo RP, Ganjoo KN, Maki RG, Pisters PWT, Raut CP, Riedel RF, Schuetze S, Sundar HM, Trent JC, Wayne JD (2010) NCCN Task Force report: update on the management of patients with gastrointestinal stromal tumors. J Natl Compr Canc Netw 8 Suppl 2:S1-41; quiz S42-44

34. Miettinen M, Lasota J (2006) Gastrointestinal stromal tumors: Pathology and prognosis at different sites. Seminars in Diagnostic Pathology 23:70–83 . https://doi.org/10.1053/j.semdp.2006.09.001

35. Tran T, Davila JA, El-Serag HB (2005) The epidemiology of malignant gastrointestinal stromal tumors: an analysis of 1,458 cases from 1992 to 2000. Am J Gastroenterol 100:162–168 . https://doi.org/10.1111/j.1572-0241.2005.40709.x

36. Keung EZ, Raut CP (2017) Management of Gastrointestinal Stromal Tumors. Surg Clin North Am 97:437–452 . https://doi.org/10.1016/j.suc.2016.12.001

37. Caterino S, Lorenzon L, Petrucciani N, Iannicelli E, Pilozzi E, Romiti A, Cavallini M, Ziparo V (2011) Gastrointestinal stromal tumors: correlation between symptoms at presentation, tumor location and prognostic factors in 47 consecutive patients. World J Surg Oncol 9:13 . https://doi.org/10.1186/1477-7819-9-13

38. Joensuu H, Hohenberger P, Corless CL (2013) Gastrointestinal stromal tumour. The Lancet 382:973–983 . https://doi.org/10.1016/S0140-6736(13)60106-3

39. DeMatteo RP, Lewis JJ, Leung D, Mudan SS, Woodruff JM, Brennan MF (2000) Two hundred gastrointestinal stromal tumors: recurrence patterns and prognostic factors for survival. Ann Surg 231:51–58

40. Franquemont DW (1995) Differentiation and Risk Assessment of Gastrointestinal Stromal Tumors. Am J Clin Pathol 103:41–47 . https://doi.org/10.1093/ajcp/103.1.41

41. Mazur MT, Clark HB (1983) Gastric stromal tumors. Reappraisal of histogenesis. Am J Surg Pathol 7:507–519

42. Corless CL, Fletcher JA, Heinrich MC (2004) Biology of gastrointestinal stromal tumors. J Clin Oncol 22:3813–3825 . https://doi.org/10.1200/JCO.2004.05.140

43. Miettinen M, Virolainen M, Maarit-Sarlomo-Rikala null (1995) Gastrointestinal stromal tumors--value of CD34 antigen in their identification and separation from true leiomyomas and schwannomas. Am J Surg Pathol 19:207–216

44. Isozaki K, Hirota S, Nakama A, Miyagawa J, Shinomura Y, Xu Z, Nomura S, Kitamura Y (1995) Disturbed intestinal movement, bile reflux to the stomach, and deficiency of c-kit-expressing cells in Ws/Ws mutant rats. Gastroenterology 109:456–464

45. Hirota S, Isozaki K, Moriyama Y, Hashimoto K, Nishida T, Ishiguro S, Kawano K, Hanada M, Kurata A, Takeda M, Muhammad Tunio G, Matsuzawa Y, Kanakura Y, Shinomura Y, Kitamura Y

(1998) Gain-of-function mutations of c-kit in human gastrointestinal stromal tumors. Science 279:577–580

46. Oppelt PJ, Hirbe AC, Van Tine BA (2017) Gastrointestinal stromal tumors (GISTs): point mutations matter in management, a review. J Gastrointest Oncol 8:466–473 . https://doi.org/10.21037/jgo.2016.09.15

47. Peng B, Lloyd P, Schran H (2005) Clinical pharmacokinetics of imatinib. Clin Pharmacokinet 44:879–894 . https://doi.org/10.2165/00003088-200544090-00001

48. Koh JS, Trent J, Chen L, El-Naggar A, Hunt K, Pollock R, Zhang W (2004) Gastrointestinal stromal tumors: overview of pathologic features, molecular biology, and therapy with imatinib mesylate. Histol Histopathol 19:565–574 . https://doi.org/10.14670/HH-19.565

49. Diagnosing GIST | GIST Support International. https://www.gistsupport.org/about-gist/for-new-gist-pages/understanding-your-pathology-report-for-gist/diagnosing-gist/. Accessed 12 Jul 2019

50. Lasota J, Miettinen M (2006) KIT and PDGFRA mutations in gastrointestinal stromal tumors (GISTs). Semin Diagn Pathol 23:91–102

51. ESMO/European Sarcoma Network Working Group (2014) Gastrointestinal stromal tumours: ESMO Clinical Practice Guidelines for diagnosis, treatment and follow-up. Ann Oncol 25 Suppl 3:iii21-26 . https://doi.org/10.1093/annonc/mdu255

52. Casali PG, Abecassis N, Bauer S, Biagini R, Bielack S, Bonvalot S, Boukovinas I, Bovee JVMG, Brodowicz T, Broto JM, Buonadonna A, De Álava E, Dei Tos AP, Del Muro XG, Dileo P, Eriksson M, Fedenko A, Ferraresi V, Ferrari A, Ferrari S, Frezza AM, Gasperoni S, Gelderblom H, Gil T, Grignani G, Gronchi A, Haas RL, Hannu A, Hassan B, Hohenberger P, Issels R, Joensuu H, Jones RL, Judson I, Jutte P, Kaal S, Kasper B, Kopeckova K, Krákorová DA, Le Cesne A, Lugowska I, Merimsky O, Montemurro M, Pantaleo MA, Piana R, Picci P, Piperno-Neumann S, Pousa AL, Reichardt P, Robinson MH, Rutkowski P, Safwat AA, Schöffski P, Sleijfer S, Stacchiotti S, Sundby Hall K, Unk M, Van Coevorden F, Van der Graaf W, Whelan J, Wardelmann E, Zaikova O, Blay JY (2018) Soft tissue and visceral sarcomas: ESMO–EURACAN Clinical Practice Guidelines for

diagnosis, treatment and follow-up. Ann Oncol 29:iv51–iv67 . https://doi.org/10.1093/annonc/mdy096

53. Langer C, Gunawan B, Schüler P, Huber W, Füzesi L, Becker H (2003) Prognostic factors influencing surgical management and outcome of gastrointestinal stromal tumours. Br J Surg 90:332–339 . https://doi.org/10.1002/bjs.4046

54. Blanke CD, Demetri GD, von Mehren M, Heinrich MC, Eisenberg B, Fletcher JA, Corless CL, Fletcher CDM, Roberts PJ, Heinz D, Wehre E, Nikolova Z, Joensuu H (2008) Long-term results from a randomized phase II trial of standard- versus higher-dose imatinib mesylate for patients with unresectable or metastatic gastrointestinal stromal tumors expressing KIT. J Clin Oncol 26:620–625 . https://doi.org/10.1200/JCO.2007.13.4403

55. Din OS, Woll PJ (2008) Treatment of gastrointestinal stromal tumor: focus on imatinib mesylate. Ther Clin Risk Manag 4:149–162

56. Heinrich MC, Griffith DJ, Druker BJ, Wait CL, Ott KA, Zigler AJ (2000) Inhibition of c-kit receptor tyrosine kinase activity by STI 571, a selective tyrosine kinase inhibitor. Blood 96:925–932

57. Demetri GD, von Mehren M, Blanke CD, Van den Abbeele AD, Eisenberg B, Roberts PJ, Heinrich MC, Tuveson DA, Singer S, Janicek M, Fletcher JA, Silverman SG, Silberman SL, Capdeville R, Kiese B, Peng B, Dimitrijevic S, Druker BJ, Corless C, Fletcher CDM, Joensuu H (2002) Efficacy and Safety of Imatinib Mesylate in Advanced Gastrointestinal Stromal Tumors. New England Journal of Medicine 347:472–480 . https://doi.org/10.1056/NEJMoa020461

58. van Oosterom AT, Judson I, Verweij J, Stroobants S, Donato di Paola E, Dimitrijevic S, Martens M, Webb A, Sciot R, Van Glabbeke M, Silberman S, Nielsen OS, European Organisation for Research and Treatment of Cancer Soft Tissue and Bone Sarcoma Group (2001) Safety and efficacy of imatinib (STI571) in metastatic gastrointestinal stromal tumours: a phase I study. Lancet 358:1421–1423

59. Gastrointestinal Stromal Tumor Meta-Analysis Group (MetaGIST) (2010) Comparison of two doses of imatinib for the treatment of unresectable or metastatic gastrointestinal stromal

tumors: a meta-analysis of 1,640 patients. J Clin Oncol 28:1247–1253 . https://doi.org/10.1200/JCO.2009.24.2099

60. van der Zwan SM, DeMatteo RP (2005) Gastrointestinal stromal tumor: 5 years later. Cancer 104:1781–1788 . https://doi.org/10.1002/cncr.21419

61. Gold JS, Dematteo RP (2006) Combined surgical and molecular therapy: the gastrointestinal stromal tumor model. Ann Surg 244:176–184 . https://doi.org/10.1097/01.sla.0000218080.94145.cf

62. Jeong W, Doroshow JH, Kummar S (2013) US FDA Approved Oral Kinase Inhibitors for the Treatment of Malignancies. Curr Probl Cancer 37:110–144 . https://doi.org/10.1016/j.currproblcancer.2013.06.001

63. D'Amato G, Steinert DM, McAuliffe JC, Trent JC (2005) Update on the biology and therapy of gastrointestinal stromal tumors. Cancer Control 12:44–56 . https://doi.org/10.1177/107327480501200106

64. Dutreix C, Peng B, Mehring G, Hayes M, Capdeville R, Pokorny R, Seiberling M (2004) Pharmacokinetic interaction between ketoconazole and imatinib mesylate (Glivec) in healthy subjects. Cancer Chemother Pharmacol 54:290–294 . https://doi.org/10.1007/s00280-004-0832-z

65. O'Brien SG, Meinhardt P, Bond E, Beck J, Peng B, Dutreix C, Mehring G, Milosavljev S, Huber C, Capdeville R, Fischer T (2003) Effects of imatinib mesylate (STI571, Glivec) on the pharmacokinetics of simvastatin, a cytochrome p450 3A4 substrate, in patients with chronic myeloid leukaemia. Br J Cancer 89:1855–1859 . https://doi.org/10.1038/sj.bjc.6601152

66. glivec-epar-product-information_it.pdf

67. Nikolova Z, Peng B, Hubert M, Sieberling M, Keller U, Ho Y-Y, Schran H, Capdeville R (2004) Bioequivalence, safety, and tolerability of imatinib tablets compared with capsules. Cancer Chemother Pharmacol 53:433–438 . https://doi.org/10.1007/s00280-003-0756-z

68. Nilsson B, Bümming P, Meis-Kindblom JM, Odén A, Dortok A, Gustavsson B, Sablinska K, Kindblom L-G (2005) Gastrointestinal stromal tumors: the incidence, prevalence, clinical course, and prognostication in the preimatinib mesylate era--a population-based study in western Sweden. Cancer 103:821–829 . https://doi.org/10.1002/cncr.20862

69. Jakhetiya A, Garg PK, Prakash G, Sharma J, Pandey R, Pandey D (2016) Targeted therapy of gastrointestinal stromal tumours. World J Gastrointest Surg 8:345–352 . https://doi.org/10.4240/wjgs.v8.i5.345

70. Giorgi UD, Verweij J (2005) Imatinib and gastrointestinal stromal tumors: Where do we go from here? Mol Cancer Ther 4:495–501 . https://doi.org/10.1158/1535-7163.MCT-04-0302

71. Zalcberg JR, Verweij J, Casali PG, Le Cesne A, Reichardt P, Blay J-Y, Schlemmer M, Van Glabbeke M, Brown M, Judson IR, EORTC Soft Tissue and Bone Sarcoma Group, the Italian Sarcoma Group, Australasian Gastrointestinal Trials Group (2005) Outcome of patients with advanced gastro-intestinal stromal tumours crossing over to a daily imatinib dose of 800 mg after progression on 400 mg. Eur J Cancer 41:1751–1757 . https://doi.org/10.1016/j.ejca.2005.04.034

72. Blanke CD, Rankin C, Demetri GD, Ryan CW, von Mehren M, Benjamin RS, Raymond AK, Bramwell VHC, Baker LH, Maki RG, Tanaka M, Hecht JR, Heinrich MC, Fletcher CDM, Crowley JJ, Borden EC (2008) Phase III randomized, intergroup trial assessing imatinib mesylate at two dose levels in patients with unresectable or metastatic gastrointestinal stromal tumors expressing the kit receptor tyrosine kinase: S0033. J Clin Oncol 26:626–632 . https://doi.org/10.1200/JCO.2007.13.4452

73. von Mehren M (2006) Beyond imatinib: second generation c-KIT inhibitors for the management of gastrointestinal stromal tumors. Clin Colorectal Cancer 6 Suppl 1:S30-34

74. Lopes LF, Bacchi CE (2010) Imatinib treatment for gastrointestinal stromal tumour (GIST). J Cell Mol Med 14:42–50 . https://doi.org/10.1111/j.1582-4934.2009.00983.x

75. Demetri GD, van Oosterom AT, Garrett CR, Blackstein ME, Shah MH, Verweij J, McArthur G, Judson IR, Heinrich MC, Morgan JA, Desai J, Fletcher CD, George S, Bello CL, Huang X, Baum

CM, Casali PG (2006) Efficacy and safety of sunitinib in patients with advanced gastrointestinal stromal tumour after failure of imatinib: a randomised controlled trial. Lancet 368:1329–1338 . https://doi.org/10.1016/S0140-6736(06)69446-4

76. Research C for DE and (2019) FDA approves sunitinib malate for adjuvant treatment of renal cell carcinoma. FDA

77. Ben-Ami E, Barysauskas CM, von Mehren M, Heinrich MC, Corless CL, Butrynski JE, Morgan JA, Wagner AJ, Choy E, Yap JT, Van den Abbeele AD, Solomon SM, Fletcher JA, Demetri GD, George S (2016) Long-term follow-up results of the multicenter phase II trial of regorafenib in patients with metastatic and/or unresectable GI stromal tumor after failure of standard tyrosine kinase inhibitor therapy. Ann Oncol 27:1794–1799 . https://doi.org/10.1093/annonc/mdw228

78. Home - ClinicalTrials.gov. https://www.clinicaltrials.gov/ct2/home. Accessed 5 Nov 2018

79. Lanke G, Lee JH (2017) How best to manage gastrointestinal stromal tumor. World J Clin Oncol 8:135–144 . https://doi.org/10.5306/wjco.v8.i2.135

80. Bolton AE, Peng B, Hubert M, Krebs-Brown A, Capdeville R, Keller U, Seiberling M (2004) Effect of rifampicin on the pharmacokinetics of imatinib mesylate (Gleevec, STI571) in healthy subjects. Cancer Chemother Pharmacol 53:102–106 . https://doi.org/10.1007/s00280-003-0722-9

81. Burger K, Nooter K (2004) Pharmacokinetic Resistance to Imatinib Mesylate: Role of the ABC Drug Pumps ABCG2 (BCRP) and ABCB1 (MDR1) in the Oral Bioavailability of Imatinib. Cell Cycle 3:1502–1505 . https://doi.org/10.4161/cc.3.12.1331

82. Widmer N, Decosterd LA, Csajka C, Leyvraz S, Duchosal MA, Rosselet A, Rochat B, Eap CB, Henry H, Biollaz J, Buclin T (2006) Population pharmacokinetics of imatinib and the role of α1-acid glycoprotein. British Journal of Clinical Pharmacology 62:97–112 . https://doi.org/10.1111/j.1365-2125.2006.02719.x

83. Yoo C, Ryu M-H, Kang BW, Yoon S-K, Ryoo B-Y, Chang H-M, Lee J-L, Beck MY, Kim TW, Kang Y-K (2010) Cross-sectional study of imatinib plasma trough levels in patients with advanced

gastrointestinal stromal tumors: impact of gastrointestinal resection on exposure to imatinib. J Clin Oncol 28:1554–1559 . https://doi.org/10.1200/JCO.2009.26.5785

84. Judson I, Ma P, Peng B, Verweij J, Racine A, di Paola ED, van Glabbeke M, Dimitrijevic S, Scurr M, Dumez H, van Oosterom A (2005) Imatinib pharmacokinetics in patients with gastrointestinal stromal tumour: a retrospective population pharmacokinetic study over time. EORTC Soft Tissue and Bone Sarcoma Group. Cancer Chemother Pharmacol 55:379–386 . https://doi.org/10.1007/s00280-004-0876-0

85. Gotta V, Widmer N, Montemurro M, Leyvraz S, Haouala A, Decosterd LA, Csajka C, Buclin T (2012) Therapeutic Drug Monitoring of Imatinib. Clin Pharmacokinet 51:187–201 . https://doi.org/10.2165/11596990-000000000-00000

86. Demetri GD, Wang Y, Wehrle E, Racine A, Nikolova Z, Blanke CD, Joensuu H, von Mehren M (2009) Imatinib plasma levels are correlated with clinical benefit in patients with unresectable/metastatic gastrointestinal stromal tumors. J Clin Oncol 27:3141–3147 . https://doi.org/10.1200/JCO.2008.20.4818

87. Eechoute K, Fransson MN, Reyners AK, de Jong FA, Sparreboom A, van der Graaf WTA, Friberg LE, Schiavon G, Wiemer EAC, Verweij J, Loos WJ, Mathijssen RHJ, De Giorgi U (2012) A long-term prospective population pharmacokinetic study on imatinib plasma concentrations in GIST patients. Clin Cancer Res 18:5780–5787 . https://doi.org/10.1158/1078-0432.CCR-12-0490

88. Bouchet S, Poulette S, Titier K, Moore N, Lassalle R, Abouelfath A, Italiano A, Chevreau C, Bompas E, Collard O, Duffaud F, Rios M, Cupissol D, Adenis A, Ray-Coquard I, Bouché O, Le Cesne A, Bui B, Blay J-Y, Molimard M (2016) Relationship between imatinib trough concentration and outcomes in the treatment of advanced gastrointestinal stromal tumours in a real-life setting. Eur J Cancer 57:31–38 . https://doi.org/10.1016/j.ejca.2015.12.029

89. Judson I (2012) Therapeutic drug monitoring of imatinib--new data strengthen the case. Clin Cancer Res 18:5517–5519 . https://doi.org/10.1158/1078-0432.CCR-12-2570

90. Farag S, Verheijen RB, Martijn JK, Cats A, Huitema AD, Steeghs N (2017) Imatinib Pharmacokinetics in a Large Observational Cohort of Gastrointestinal Stromal Tumour Patients. Clin Pharmacokinet 56:287–292 . https://doi.org/10.1007/s40262-016-0439-7

91. Lankheet N a. G, Desar IME, Mulder SF, Burger DM, Kweekel DM, Van CH, Van W der G, Van NE (2017) Optimizing the dose in cancer patients treated with imatinib, sunitinib and pazopanib. Br J Clin Pharmacol 83:2195–2204 . https://doi.org/10.1111/bcp.13327

92. Baccarani M, Pileri S, Steegmann J-L, Muller M, Soverini S, Dreyling M, ESMO Guidelines Working Group (2012) Chronic myeloid leukemia: ESMO Clinical Practice Guidelines for diagnosis, treatment and follow-up. Ann Oncol 23 Suppl 7:vii72-77 . https://doi.org/10.1093/annonc/mds228

93. Waks AG, Winer EP (2019) Breast Cancer Treatment: A Review. JAMA 321:288–300 . https://doi.org/10.1001/jama.2018.19323

94. Harbeck N, Gnant M (2017) Breast cancer. The Lancet 389:1134–1150 . https://doi.org/10.1016/S0140-6736(16)31891-8

95. Zujewski JA, Dvaladze AL, Ilbawi A, Anderson BO, Luciani S, Stevens L, Torode J (2017) Knowledge Summaries for Comprehensive Breast Cancer Control. JGO 1–7 . https://doi.org/10.1200/JGO.17.00141

96. Nounou MI, ElAmrawy F, Ahmed N, Abdelraouf K, Goda S, Syed-Sha-Qhattal H (2015) Breast Cancer: Conventional Diagnosis and Treatment Modalities and Recent Patents and Technologies. Breast Cancer : Basic and Clinical Research 9:17 . https://doi.org/10.4137/BCBCR.S29420

97. Polyak K (2011) Heterogeneity in breast cancer. J Clin Invest 121:3786–3788 . https://doi.org/10.1172/JCI60534

98. Holst F, Stahl PR, Ruiz C, Hellwinkel O, Jehan Z, Wendland M, Lebeau A, Terracciano L, Al-Kuraya K, Jänicke F, Sauter G, Simon R (2007) Estrogen receptor alpha (ESR1) gene amplification is frequent in breast cancer. Nat Genet 39:655–660 . https://doi.org/10.1038/ng2006

99. Ruddy KJ, Ganz PA (2019) Treatment of Nonmetastatic Breast Cancer. JAMA 321:1716–1717 . https://doi.org/10.1001/jama.2019.3927

100. Akram M, Iqbal M, Daniyal M, Khan AU (2017) Awareness and current knowledge of breast cancer. Biological Research 50: . https://doi.org/10.1186/s40659-017-0140-9

101. Shah R, Rosso K, Nathanson SD (2014) Pathogenesis, prevention, diagnosis and treatment of breast cancer. World J Clin Oncol 5:283–298 . https://doi.org/10.5306/wjco.v5.i3.283

102. Pernas S, Tolaney SM, Winer EP, Goel S (2018) CDK4/6 inhibition in breast cancer: current practice and future directions. Ther Adv Med Oncol 10: . https://doi.org/10.1177/1758835918786451

103. Sante GD, Pagé J, Jiao X, Nawab O, Cristofanilli M, Skordalakes E, Pestell RG (2019) Recent advances with cyclin-dependent kinase inhibitors: therapeutic agents for breast cancer and their role in immuno-oncology. Expert Review of Anticancer Therapy 19:569–587 . https://doi.org/10.1080/14737140.2019.1615889

104. Hortobagyi GN, Stemmer SM, Burris HA, Yap YS, Sonke GS, Paluch-Shimon S, Campone M, Petrakova K, Blackwell KL, Winer EP, Janni W, Verma S, Conte P, Arteaga CL, Cameron DA, Mondal S, Su F, Miller M, Elmeliegy M, Germa C, O'Shaughnessy J (2018) Updated results from MONALEESA-2, a phase III trial of first-line ribociclib plus letrozole versus placebo plus letrozole in hormone receptor-positive, HER2-negative advanced breast cancer. Ann Oncol 29:1541–1547 . https://doi.org/10.1093/annonc/mdy155

105. EMA ribociclib (2017) Kisqali | European Medicines Agency. https://www.ema.europa.eu/medicines/human/EPAR/kisqali#product-information-section. Accessed 2 Oct 2018

106. Finn RS, Martin M, Rugo HS, Jones S, Im S-A, Gelmon K, Harbeck N, Lipatov ON, Walshe JM, Moulder S, Gauthier E, Lu DR, Randolph S, Diéras V, Slamon DJ (2016) Palbociclib and Letrozole in Advanced Breast Cancer. New England Journal of Medicine 375:1925–1936 . https://doi.org/10.1056/NEJMoa1607303

107. Cristofanilli M, Turner NC, Bondarenko I, Ro J, Im S-A, Masuda N, Colleoni M, DeMichele A, Loi S, Verma S, Iwata H, Harbeck N, Zhang K, Theall KP, Jiang Y, Bartlett CH, Koehler M, Slamon D (2016) Fulvestrant plus palbociclib versus fulvestrant plus placebo for treatment of hormone-receptor-positive, HER2-negative metastatic breast cancer that progressed on previous endocrine therapy (PALOMA-3): final analysis of the multicentre, double-blind, phase 3 randomised controlled trial. The Lancet Oncology 17:425–439 . https://doi.org/10.1016/S1470-2045(15)00613-0

108. Food and Drug Administration (2014). Center for Drug Evaluationand Research. Palbociclib Clinical Pharmacology and Biopharmaceutics Review. Accessed 6 Aug 2019

109. Verheijen RB, Yu H, Schellens JHM, Beijnen JH, Steeghs N, Huitema ADR (2017) Practical Recommendations for Therapeutic Drug Monitoring of Kinase Inhibitors in Oncology. Clin Pharmacol Ther 102:765–776 . https://doi.org/10.1002/cpt.787

110. Spring LM, Zangardi ML, Moy B, Bardia A (2017) Clinical Management of Potential Toxicities and Drug Interactions Related to Cyclin-Dependent Kinase 4/6 Inhibitors in Breast Cancer: Practical Considerations and Recommendations. Oncologist 22:1039–1048 . https://doi.org/10.1634/theoncologist.2017-0142

111. Bakerian Lecture:—Rays of positive electricity | Proceedings of the Royal Society of London. Series A, Containing Papers of a Mathematical and Physical Character. https://royalsocietypublishing.org/doi/abs/10.1098/rspa.1913.0057. Accessed 27 Jun 2019

112. Electrospray ionization for mass spectrometry of large biomolecules. - PubMed - NCBI. https://www.ncbi.nlm.nih.gov/pubmed/2675315/. Accessed 27 Jun 2019

113. LC-MS/MS in the Clinical Laboratory – Where to From Here? https://www.ncbi.nlm.nih.gov/pmc/articles/PMC3052391/?report=classic. Accessed 27 Jun 2019

114. Soni NR Improve GC separations with derivatization for selective response and detection in novel matrices. 1:12

115. Nagy K, Vékey K (2008) Chapter 5 - Separation methods. In: Vékey K, Telekes A, Vertes A (eds) Medical Applications of Mass Spectrometry. Elsevier, Amsterdam, pp 61–92

116. Erni F, Frei RW (1978) Two-dimensional column liquid chromatographic technique for resolution of complex mixtures. Journal of Chromatography A 149:561–569 . https://doi.org/10.1016/S0021-9673(00)81011-0

117. Bushey MM, Jorgenson JW (1990) Automated instrumentation for comprehensive two-dimensional high-performance liquid chromatography of proteins. Anal Chem 62:161–167

118. Dülcks Th, Juraschek R (1999) ELECTROSPRAY AS AN IONISATION METHOD FOR MASS SPECTROMETRY. Journal of Aerosol Science 30:927–943 . https://doi.org/10.1016/S0021-8502(98)00781-2

119. F.R.S LR (1882) XX. On the equilibrium of liquid conducting masses charged with electricity. The London, Edinburgh, and Dublin Philosophical Magazine and Journal of Science 14:184–186 . https://doi.org/10.1080/14786448208628425

120. (2019) Electrospray ionization. Wikipedia

121. Stauffer E, Dolan JA, Newman R (2008) CHAPTER 8 - Gas Chromatography and Gas Chromatography—Mass Spectrometry. In: Stauffer E, Dolan JA, Newman R (eds) Fire Debris Analysis. Academic Press, Burlington, pp 235–293

122. Chace DH, Kalas TA, Naylor EW (2003) Use of tandem mass spectrometry for multianalyte screening of dried blood specimens from newborns. Clin Chem 49:1797–1817

123. Chace DH, Millington DS, Terada N, Kahler SG, Roe CR, Hofman LF (1993) Rapid diagnosis of phenylketonuria by quantitative analysis for phenylalanine and tyrosine in neonatal blood spots by tandem mass spectrometry. Clin Chem 39:66–71

124. Yang Z, Peng Y, Wang S (2005) Immunosuppressants: Pharmacokinetics, methods of monitoring and role of high performance liquid chromatography/mass spectrometry. Clinical and Applied Immunology Reviews 5:405–430 . https://doi.org/10.1016/j.cair.2005.12.001

125. Lennard L (2001) Therapeutic drug monitoring of cytotoxic drugs. Br J Clin Pharmacol 52 Suppl 1:75S-87S . https://doi.org/10.1046/j.1365-2125.2001.0520s1075.x

126. Gu J, Soldin SJ (2007) Modification of tandem mass spectrometric method to permit simultaneous quantification of 17 anti-HIV drugs which include atazanavir and tipranavir. Clin Chim Acta 378:222–224 . https://doi.org/10.1016/j.cca.2006.11.004

127. FDA (2018) Bioanalytical Method Validation Guidance for Industry. In: www.fda.gov

128. EMA (2011) guideline-bioanalytical-method-validation_en.pdf. In: www.ema.europa.eu. https://www.ema.europa.eu/en/documents/scientific-guideline/guideline-bioanalytical-method-validation_en.pdf. Accessed 14 Jun 2019

129. Adaway JE, Keevil BG (2012) Therapeutic drug monitoring and LC-MS/MS. J Chromatogr B Analyt Technol Biomed Life Sci 883–884:33–49 . https://doi.org/10.1016/j.jchromb.2011.09.041

130. Lakshmy R (2008) Analysis of the Use of Dried Blood Spot Measurements in Disease Screening. J Diabetes Sci Technol 2:242–243

131. Guthrie R, Susi A (1963) A Simple Phenylalanine Method for Detecting Phenylketonuria in Large Populations of Newborn Infants. Pediatrics 32:338–343

132. Zakaria R, Allen KJ, Koplin JJ, Roche P, Greaves RF (2016) Advantages and Challenges of Dried Blood Spot Analysis by Mass Spectrometry Across the Total Testing Process. EJIFCC 27:288–317

133. Chace DH, Spitzer AR, Jesús VRD (2014) Applications of Dried Blood Spots in Newborn and Metabolic Screening. In: Dried Blood Spots. John Wiley & Sons, Ltd, pp 53–75

134. Lehmann S, Delaby C, Vialaret J, Ducos J, Hirtz C (2013) Current and future use of “dried blood spot” analyses in clinical chemistry. Clin Chem Lab Med 51:1897–1909 . https://doi.org/10.1515/cclm-2013-0228

135. Stove CP, Ingels A-SME, De Kesel PMM, Lambert WE (2012) Dried blood spots in toxicology: from the cradle to the grave? Crit Rev Toxicol 42:230–243 . https://doi.org/10.3109/10408444.2011.650790

136. McDade TW, Williams S, Snodgrass JJ (2007) What a drop can do: dried blood spots as a minimally invasive method for integrating biomarkers into population-based research. Demography 44:899–925 . https://doi.org/10.1353/dem.2007.0038

137. Brindle E, O'Connor KA, Garrett DA (2014) Applications of Dried Blood Spots in General Human Health Studies. In: Dried Blood Spots. John Wiley & Sons, Ltd, pp 114–129

138. Parker SP, Cubitt WD (1999) The use of the dried blood spot sample in epidemiological studies. Journal of Clinical Pathology 52:633–639 . https://doi.org/10.1136/jcp.52.9.633

139. D'Arienzo CJ, Ji QC, Discenza L, Cornelius G, Hynes J, Cornelius L, Santella JB, Olah T (2010) DBS sampling can be used to stabilize prodrugs in drug discovery rodent studies without the addition of esterase inhibitors. Bioanalysis 2:1415–1422 . https://doi.org/10.4155/bio.10.94

140. Li W, Zhang J, Tse FLS (2011) Strategies in quantitative LC-MS/MS analysis of unstable small molecules in biological matrices. Biomed Chromatogr 25:258–277 . https://doi.org/10.1002/bmc.1572

141. Sagendorph WK (2017) Shipping Guidelines for Dried-Blood Spot Specimens

142. Timmerman P, White S, Globig S, Lüdtke S, Brunet L, Smeraglia J (2011) EBF recommendation on the validation of bioanalytical methods for dried blood spots. Bioanalysis 3:1567–1575 . https://doi.org/10.4155/bio.11.132

143. Wilhelm AJ, den Burger JCG, Swart EL (2014) Therapeutic Drug Monitoring by Dried Blood Spot: Progress to Date and Future Directions. Clinical Pharmacokinetics 53:961–973 . https://doi.org/10.1007/s40262-014-0177-7

144. Kralj E, Trontelj J, Paji T, Kristl A (2012) Simultaneous measurement of imatinib, nilotinib and dasatinib in dried blood spot by ultra high performance liquid chromatography tandem mass

spectrometry. Journal of Chromatography B 903:150–156 . https://doi.org/10.1016/j.jchromb.2012.07.011

145. Antunes MV, Raymundo S, Wagner SC, Mattevi VS, Vieira N, Leite R, Reginato F, Capra MZ, Fogliatto L, Linden R (2015) DBS sampling in imatinib therapeutic drug monitoring: from method development to clinical application. Bioanalysis 7:2105–2117 . https://doi.org/10.4155/bio.15.101

146. Clark LC, Lyons C (1962) Electrode Systems for Continuous Monitoring in Cardiovascular Surgery. Annals of the New York Academy of Sciences 102:29–45 . https://doi.org/10.1111/j.1749-6632.1962.tb13623.x

147. Fracchiolla NS, Artuso S, Cortelezzi A (2013) Biosensors in Clinical Practice: Focus on Oncohematology. Sensors (Basel) 13:6423–6447 . https://doi.org/10.3390/s130506423

148. (2018) Biosensors Market Study By Advanced Technology [Thermal,. https://www.openpr.com/news/1329883/biosensors-market-study-by-advanced-technology-thermal-electrochemical-optical-top-competitors-analysis-abbott-laboratories-lifescan-siemens-healthcare-agamatrix-nova-biomedical-corporation-bayer-medtronic.html. Accessed 3 Oct 2019

149. Bohunicky B, Mousa SA (2010) Biosensors: the new wave in cancer diagnosis. Nanotechnol Sci Appl 4:1–10 . https://doi.org/10.2147/NSA.S13465

150. Wang J (1998) DNA biosensors based on peptide nucleic acid (PNA) recognition layers. A review. Biosens Bioelectron 13:757–762

151. Haupt K, Mosbach K (2000) Molecularly Imprinted Polymers and Their Use in Biomimetic Sensors. Chem Rev 100:2495–2504 . https://doi.org/10.1021/cr990099w

152. Andersson HS, Nicholls IA (2001) Chapter 1 - A historical perspective of the development of molecular imprinting. In: Sellergren B (ed) Techniques and Instrumentation in Analytical Chemistry. Elsevier, pp 1–19

153. Mujahid A, Dickert FL (2016) 5 - Molecularly Imprinted Polymers: Principle, Design, and Enzyme-Like Catalysis. In: Li S, Cao S, Piletsky SA, Turner APF (eds) Molecularly Imprinted Catalysts. Elsevier, Amsterdam, pp 79–101

154. Vasapollo G, Sole RD, Mergola L, Lazzoi MR, Scardino A, Scorrano S, Mele G (2011) Molecularly Imprinted Polymers: Present and Future Prospective. Int J Mol Sci 12:5908–5945 . https://doi.org/10.3390/ijms12095908

155. Lotierzo M, Henry OYF, Piletsky S, Tothill I, Cullen D, Kania M, Hock B, Turner APF (2004) Surface plasmon resonance sensor for domoic acid based on grafted imprinted polymer. Biosensors and Bioelectronics 20:145–152 . https://doi.org/10.1016/j.bios.2004.01.032

156. Tan Y, Zhou Z, Wang P, Nie L, Yao S (2001) A study of a bio-mimetic recognition material for the BAW sensor by molecular imprinting and its application for the determination of paracetamol in the human serum and urine. Talanta 55:337–347 . https://doi.org/10.1016/S0039-9140(01)00442-8

157. Rachkov A, McNiven S, El'skaya A, Yano K, Karube I (2000) Fluorescence detection of β-estradiol using a molecularly imprinted polymer. Analytica Chimica Acta 405:23–29 . https://doi.org/10.1016/S0003-2670(99)00743-6

158. Ansari S, Masoum S (2019) Molecularly imprinted polymers for capturing and sensing proteins: Current progress and future implications. TrAC Trends in Analytical Chemistry 114:29–47 . https://doi.org/10.1016/j.trac.2019.02.008

159. Luliński P (2017) Molecularly imprinted polymers based drug delivery devices: a way to application in modern pharmacotherapy. A review. Materials Science and Engineering: C 76:1344–1353 . https://doi.org/10.1016/j.msec.2017.02.138

160. Recent advances in molecularly imprinted polymers in food analysis - Song - 2014 - Journal of Applied Polymer Science - Wiley Online Library. https://onlinelibrary.wiley.com/doi/full/10.1002/app.40766. Accessed 3 Oct 2019

161. Piletsky SA, Turner NW, Laitenberger P (2006) Molecularly imprinted polymers in clinical diagnostics—Future potential and existing problems. Medical Engineering & Physics 28:971–977 . https://doi.org/10.1016/j.medengphy.2006.05.004

162. Haupt K, Linares AV, Bompart M, Bui BTS (2012) Molecularly imprinted polymers. Top Curr Chem 325:1–28 . https://doi.org/10.1007/128_2011_307

163. Mosbach K (1994) Molecular imprinting. Trends in Biochemical Sciences 19:9–14 . https://doi.org/10.1016/0968-0004(94)90166-X

164. Umpleby RJ, Baxter SC, Chen Y, Shah RN, Shimizu KD (2001) Characterization of molecularly imprinted polymers with the Langmuir-Freundlich isotherm. Anal Chem 73:4584–4591 . https://doi.org/10.1021/ac0105686

165. Sellergren B (1999) Polymer- and template-related factors influencing the efficiency in molecularly imprinted solid-phase extractions. TrAC Trends in Analytical Chemistry 18:164–174 . https://doi.org/10.1016/S0165-9936(98)00117-4

166. Mohamed MH, Wilson LD (2012) Porous Copolymer Resins: Tuning Pore Structure and Surface Area with Non Reactive Porogens. Nanomaterials (Basel) 2:163–186 . https://doi.org/10.3390/nano2020163

167. POROS™ R1 10 µm Column, Stainless Steel, 2.1 x 100 mm, 0.3 mL. https://www.thermofisher.com/order/catalog/product/1101416#/1101416. Accessed 3 Oct 2019

168. Whelan TJ, Gray MJ, Slonecker PJ, Shalliker RA, Wilson MA (2005) Study of the selectivity of reversed-phase columns for the separation of polycarboxylic acids and polyphenol compounds. Journal of Chromatography A 1097:148–156 . https://doi.org/10.1016/j.chroma.2005.08.026

169. Lim MD (2018) Dried Blood Spots for Global Health Diagnostics and Surveillance: Opportunities and Challenges. Am J Trop Med Hyg 99:256–265 . https://doi.org/10.4269/ajtmh.17-0889

170. Mei JV, Alexander JR, Adam BW, Hannon WH (2001) Use of Filter Paper for the Collection and Analysis of Human Whole Blood Specimens. J Nutr 131:1631S-1636S . https://doi.org/10.1093/jn/131.5.1631S

171. Vu DH, Koster RA, Alffenaar JWC, Brouwers JRBJ, Uges DRA (2011) Determination of moxifloxacin in dried blood spots using LC–MS/MS and the impact of the hematocrit and blood volume. Journal of Chromatography B 879:1063–1070 . https://doi.org/10.1016/j.jchromb.2011.03.017

172. Wong P, James CA (2014) Punching and Extraction Techniques for Dried Blood Spot Sample Analysis. In: Dried Blood Spots. John Wiley & Sons, Ltd, pp 160–167

173. Antunes MV, Charão MF, Linden R (2016) Dried blood spots analysis with mass spectrometry: Potentials and pitfalls in therapeutic drug monitoring. Clinical Biochemistry 49:1035–1046 . https://doi.org/10.1016/j.clinbiochem.2016.05.004

174. Tang N, Pahalawatta V, Frank A, Bagley Z, Viana R, Lampinen J, Leckie G, Huang S, Abravaya K, Wallis CL (2017) HIV-1 viral load measurement in venous blood and fingerprick blood using Abbott RealTime HIV-1 DBS assay. J Clin Virol 92:56–61 . https://doi.org/10.1016/j.jcv.2017.05.002

175. Abu-Rabie P, Denniff P, Spooner N, Brynjolffssen J, Galluzzo P, Sanders G (2011) Method of Applying Internal Standard to Dried Matrix Spot Samples for Use in Quantitative Bioanalysis. Anal Chem 83:8779–8786 . https://doi.org/10.1021/ac202321q

176. (2018) Bioanalytical Method Validation Guidance for Industry. 44

177. Mei H, Hsieh Y, Nardo C, Xu X, Wang S, Ng K, Korfmacher WA (2003) Investigation of matrix effects in bioanalytical high-performance liquid chromatography/tandem mass spectrometric assays: application to drug discovery. Rapid Commun Mass Spectrom 17:97–103 . https://doi.org/10.1002/rcm.876

178. González O, Blanco ME, Iriarte G, Bartolomé L, Maguregui MI, Alonso RM (2014) Bioanalytical chromatographic method validation according to current regulations, with a special focus on

the non-well defined parameters limit of quantification, robustness and matrix effect. J Chromatogr A 1353:10–27 . https://doi.org/10.1016/j.chroma.2014.03.077

179. Bowen CL, Volpatti J, Cades J, Licea-Perez H, Evans CA (2012) Evaluation of glucuronide metabolite stability in dried blood spots. Bioanalysis 4:2823–2832 . https://doi.org/10.4155/bio.12.269

180. Fast DM, Kelley M, Viswanathan CT, O'Shaughnessy J, King SP, Chaudhary A, Weiner R, DeStefano AJ, Tang D (2009) Workshop report and follow-up--AAPS Workshop on current topics in GLP bioanalysis: Assay reproducibility for incurred samples--implications of Crystal City recommendations. AAPS J 11:238–241 . https://doi.org/10.1208/s12248-009-9100-9

181. Rhoden L, Antunes MV, Hidalgo P, Silva CÁ da, Linden R (2014) Simple procedure for determination of valproic acid in dried blood spots by gas chromatography–mass spectrometry. Journal of Pharmaceutical and Biomedical Analysis 96:207–212 . https://doi.org/10.1016/j.jpba.2014.03.044

182. Food and Drug Administration Center for Drug Evaluation and Research (CDER) (2018) Bioanalytical Method Validation Guidance for Industry. https://www.fda.gov/regulatory-information/search-fda-guidance-documents/bioanalytical-method-validation-guidance-industry. Accessed 26th June

183. European Medicines Agency (2011) Guideline on bioanalytical method validation. https://www.ema.europa.eu/en/documents/scientific-guideline/guideline-bioanalytical-method-validation_en.pdf. Accessed 26th June

184. Martínez-Chávez A, Rosing H, Hillebrand M, Tibben M, Schinkel AH, Beijnen JH (2019) Development and validation of a bioanalytical method for the quantification of the CDK4/6 inhibitors abemaciclib, palbociclib, and ribociclib in human and mouse matrices using liquid chromatography-tandem mass spectrometry. Anal Bioanal Chem. https://doi.org/10.1007/s00216-019-01932-w

185. Kala A, Patel YT, Davis A, Stewart CF (2017) Development and validation of LC-MS/MS methods for the measurement of ribociclib, a CDK4/6 inhibitor, in mouse plasma and Ringer's solution

and its application to a cerebral microdialysis study. J Chromatogr B Analyt Technol Biomed Life Sci 1057:110–117 . https://doi.org/10.1016/j.jchromb.2017.05.002

186. EMA palbociclib (2018) Ibrance | European Medicines Agency. https://www.ema.europa.eu/medicines/human/EPAR/ibrance. Accessed 2 Oct 2018

187. Svenson J, Karlsson JG, Nicholls IA (2004) 1H Nuclear magnetic resonance study of the molecular imprinting of (−)-nicotine: template self-association, a molecular basis for cooperative ligand binding. Journal of Chromatography A 1024:39–44 . https://doi.org/10.1016/j.chroma.2003.09.064

188. Athikomrattanakul U, Katterle M, Gajovic-Eichelmann N, Scheller FW (2009) Development of molecularly imprinted polymers for the binding of nitrofurantoin. Biosens Bioelectron 25:82–87 . https://doi.org/10.1016/j.bios.2009.06.003

189. Carboni D, Flavin K, Servant A, Gouverneur V, Resmini M (2008) The first example of molecularly imprinted nanogels with aldolase type I activity. Chemistry 14:7059–7065 . https://doi.org/10.1002/chem.200800675

190. Malvern (2011) Dynamic light scattering common terms defined. 6

191. Wu L, Sun B, Li Y, Chang W (2003) Study properties of molecular imprinting polymer using a computational approach. Analyst 128:944–949 . https://doi.org/10.1039/B212731H

192. Nantasenamat C, Isarankura-Na-Ayudhya C, Naenna T, Prachayasittikul V (2007) Quantitative structure-imprinting factor relationship of molecularly imprinted polymers. Biosensors and Bioelectronics 22:3309–3317 . https://doi.org/10.1016/j.bios.2007.01.017

193. Rowland M, Emmons GT (2010) Use of Dried Blood Spots in Drug Development: Pharmacokinetic Considerations. AAPS J 12:290–293 . https://doi.org/10.1208/s12248-010-9188-y

194. Antunes MV, Charão MF, Linden R (2016) Dried blood spots analysis with mass spectrometry: Potentials and pitfalls in therapeutic drug monitoring. Clin Biochem 49:1035–1046 . https://doi.org/10.1016/j.clinbiochem.2016.05.004

195. von Mehren M, Widmer N (2011) Correlations between imatinib pharmacokinetics, pharmacodynamics, adherence, and clinical response in advanced metastatic gastrointestinal stromal tumor (GIST): An emerging role for drug blood level testing? Cancer Treatment Reviews 37:291–299 . https://doi.org/10.1016/j.ctrv.2010.10.001

196. Chavan BB, Tiwari S, G S, Nimbalkar RD, Garg P, R S, Talluri MVNK (2018) In vitro and in vivo metabolic investigation of the Palbociclib by UHPLC-Q-TOF/MS/MS and in silico toxicity studies of its metabolites. J Pharm Biomed Anal 157:59–74 . https://doi.org/10.1016/j.jpba.2018.05.008

197. Shao R, Yu L, Lou H, Ruan Z, Jiang B, Chen J (2016) Development and validation of a rapid LC-MS/MS method to quantify letrozole in human plasma and its application to therapeutic drug monitoring. Biomed Chromatogr 30:632–637 . https://doi.org/10.1002/bmc.3607

198. Williams JS, Donahue SH, Gao H, Brummel CL (2012) Universal LC-MS method for minimized carryover in a discovery bioanalytical setting. Bioanalysis 4:1025–1037 . https://doi.org/10.4155/bio.12.76

199. Verheijen RB, Yu H, Schellens JHM, Beijnen JH, Steeghs N, Huitema ADR (2017) Practical Recommendations for Therapeutic Drug Monitoring of Kinase Inhibitors in Oncology. Clin Pharmacol Ther 102:765–776 . https://doi.org/10.1002/cpt.787

200. Samant TS, Dhuria S, Lu Y, Laisney M, Yang S, Grandeury A, Mueller-Zsigmondy M, Umehara K, Huth F, Miller M, Germa C, Elmeliegy M (2018) Ribociclib Bioavailability Is Not Affected by Gastric pH Changes or Food Intake: In Silico and Clinical Evaluations. Clin Pharmacol Ther 104:374–383 . https://doi.org/10.1002/cpt.940

201. Beer B, Schubert B, Oberguggenberger A, Meraner V, Hubalek M, Oberacher H (2010) Development and validation of a liquid chromatography-tandem mass spectrometry method for the simultaneous quantification of tamoxifen, anastrozole, and letrozole in human plasma and its application to a clinical study. Anal Bioanal Chem 398:1791–1800 . https://doi.org/10.1007/s00216-010-4075-z

202. Mioduszewska K, Dołżonek J, Wyrzykowski D, Kubik Ł, Wiczling P, Sikorska C, Toński M, Kaczyński Z, Stepnowski P, Białk-Bielińska A (2017) Overview of experimental and computational methods for the determination of the pKa values of 5-fluorouracil, cyclophosphamide, ifosfamide, imatinib and methotrexate. TrAC Trends in Analytical Chemistry 97:283–296 . https://doi.org/10.1016/j.trac.2017.09.009

203. McNicol ED, Strassels S, Goudas L, Lau J, Carr DB (2005) NSAIDS or paracetamol, alone or combined with opioids, for cancer pain. Cochrane Database of Systematic Reviews. https://doi.org/10.1002/14651858.CD005180